CONSTRAINTS ON SUBDUCTION GEODYNAMICS FROM SEISMIC ANISOTROPY

Maureen D. Long[1]

[1] Much progress has been made over the past several decades in delineating the structure of subducting slabs, but several key aspects of their dynamics remain poorly constrained. Major unsolved problems in subduction geodynamics include those related to mantle wedge viscosity and rheology, slab hydration and dehydration, mechanical coupling between slabs and the ambient mantle, the geometry of mantle flow above and beneath slabs, and the interactions between slabs and deep discontinuities such as the core-mantle boundary. Observations of seismic anisotropy can provide relatively direct constraints on mantle dynamics because of the link between deformation and the resulting anisotropy: when mantle rocks are deformed, a preferred orientation of individual mineral crystals or materials such as partial melt often develops, resulting in the directional dependence of seismic wave speeds. Measurements of seismic anisotropy thus represent a powerful tool for probing mantle dynamics in subduction systems. Here I review the observational constraints on seismic anisotropy in subduction zones and discuss how seismic data can place constraints on wedge, slab, and sub-slab anisotropy. I also discuss constraints from mineral physics investigations and geodynamical modeling studies and how they inform our interpretation of observations. I evaluate different models in light of constraints from seismology, geodynamics, and mineral physics. Finally, I discuss some of the major unsolved problems related to the dynamics of subduction systems and how ongoing and future work on the characterization and interpretation of seismic anisotropy can lead to progress, particularly in frontier areas such as understanding slab dynamics in the deep mantle.

1. INTRODUCTION

[2] The recycling of oceanic lithosphere back into the mantle via subduction is a key aspect of the Earth's plate tectonic system and represents one of the most important processes taking place in our planet's interior. Subducting slabs represent the main driving mechanism for plate motion and, as downwelling limbs of the mantle's convective system, drive the secular cooling of the Earth. Subduction zones also represent prime sites for natural hazards such as earthquakes, volcanoes, and tsunamis and as such represent the most important tectonic setting at the Earth's surface. Understanding how slabs sink from the surface to the base of the mantle—and how they interact with the mantle around them–is crucial for understanding the mantle as a dynamic system. However, major questions relating to subduction geodynamics remain unanswered; in particular, the pattern of flow and deformation in the ambient mantle around subducting slabs remains poorly understood.

[3] Observations of seismic anisotropy represent a powerful tool for probing mantle dynamics, because there is a relatively direct link between mantle deformation and macroscopic seismic anisotropy. (In contrast, inferences on mantle dynamics from other observations can be somewhat indirect. For example, seismic tomography provides a snapshot of present-day mantle structure but does not directly constrain ongoing dynamic processes.) When mantle material is subjected to deformation, it may develop a lattice or crystallographic preferred orientation (LPO or CPO) of intrinsically anisotropic minerals (in the upper mantle, primarily olivine) or a shape preferred orientation (SPO) of elastically distinct materials such as partial melt. If the relationship between the geometry of deformation and the resulting anisotropy is known (or inferred), then observations of seismic anisotropy—that is, the directional dependence of seismic wave speeds—can yield constraints on mantle dynamics. Anisotropy may manifest itself in seismic wave propagation in many ways, including in the birefringence or splitting of shear waves, the directional dependence of P wave travel times, the character of P-to-S conversions, the splitting of normal modes, and the difference

[1]Department of Geology and Geophysics, Yale University, New Haven, Connecticut, USA.

Corresponding author: Maureen D. Long, Department of Geology and Geophysics, Yale University, PO Box 208109, New Haven, CT 06520, USA. (maureen.long@yale.edu)

between the propagation of Love and Rayleigh surface waves, among others. The most popular tool to study anisotropy, particularly in subduction zones, is shear wave splitting, which has emerged as a standard part of the seismological toolkit over the past several decades.

[4] The shear wave splitting analysis method has been widely applied in subduction settings. A surprising finding from these studies is that splitting observations usually do not conform to the predictions made by the simplest models. The classical model for the subduction zone flow field is two-dimensional, with viscous coupling between the downgoing slab and the ambient mantle resulting in corner flow in the mantle wedge above the slab and entrained flow beneath the slab. If anisotropy in these regions of the mantle develops in a manner consistent with the simplest olivine LPO relationships, in which the fast axes of olivine tend to align in the direction of maximum finite extension, then this simple flow model would predict fast splitting orientations that are roughly parallel to the motion of the downgoing plate (generally, roughly perpendicular to the trench). In fact, observations from nearly all subduction zones deviate from this simple prediction; in the sub-slab mantle, the majority of measured fast splitting directions are trench-parallel, while in the mantle wedge, most subduction zones exhibit a complicated mix of fast splitting directions.

[5] This deviation of upper mantle anisotropy observations from the predictions of the simplest geodynamic and mineral physics models represents a challenge for interpretation, but it also represents a prime opportunity to explore key questions relating to the dynamics of subducting slabs. Additionally, while most studies of seismic anisotropy and mantle flow near slabs have focused on the upper mantle, tantalizing recent results on anisotropic structure in the mid-mantle (transition zone and uppermost lower mantle) and in the D″ layer at the base of the mantle suggest that slabs likely play a major role in deforming the material around them in the deeper parts of the mantle as well. These recent observations of upper-mantle, mid-mantle, and lowermost-mantle anisotropy in the vicinity of subducting slabs have highlighted a host of major unsolved problems related to subduction geodynamics—and mantle dynamics more generally—that can potentially be addressed, and perhaps resolved, by studying the anisotropic signature of the mantle. For example, do slabs entrain large amounts of material with them as they descend through the upper mantle? Is there a component of three-dimensional mantle flow beneath slabs? Is there significant transport of mantle material along strike in the mantle wedge? How does any along-strike flow affect the generation, transport, and extraction of melt from the wedge? What is the nature and extent of slab hydration when slabs begin their descent into the mantle, and how is that hydration accomplished? How and where is water transported into the mantle wedge? How does the ambient mantle flow affect the morphology of trenches and subducting slabs, and vice versa? Does background mantle flow play a role in slab flattening, steepening, and rollback? How do subducting slabs deform (and/or are deformed by) the ambient mantle when they impact the viscosity jump at the 660 km discontinuity and

possibly the core-mantle boundary (CMB)? Does the aniso-tropic structure of subducting slabs reflect past deformation processes in the oceanic lithosphere? What does seismic anisotropy beneath subducting slabs tell us about the nature of the suboceanic asthenosphere?

[6] Understanding subduction zone geodynamics and the links between mantle deformation and seismic anisotropy in subduction systems requires the integration of constraints from seismology, geodynamics, and mineral physics. In this paper, I will review the constraints on subduction zone anisotropy gleaned from each of these disciplines, with a particular focus on the seismologic observations. My intent is not to provide a historical overview of the subject but rather to highlight the observations, models, and experiments that provide us with the most direct information on anisotropy in subduction systems, with an emphasis on the rapid progress that has been made over the last 5–10 years. I will discuss the various conceptual models for mantle flow and deformation in subduction systems that have been proposed to explain the observations and evaluate each in light of experimental and observational constraints. Much of this paper focuses on understanding upper mantle anisot-ropy, but I will also discuss investigations of transition zone and D″ anisotropy as a frontier area for understanding the dynamic behavior of slabs in the deep mantle. Finally, I will return to the list of critical unsolved problems mentioned above and will explore how constraints from seismic anisot-ropy can be used to make progress on each.

2. SEISMOLOGICAL TOOLS AND OBSERVATIONS

2.1. Analysis Techniques and Tools

2.1.1. Shear Wave Splitting Analysis

[7] The measurement of shear wave splitting has emerged as the most popular tool for characterizing anisotropy in the mantle [e.g., *Vinnik et al.*, 1989; *Silver and Chan*, 1991], and it is routinely applied to data from subduction systems as well as other tectonic settings. Here I briefly describe the principles behind the method; for additional details, I refer the reader to reviews of the technique and its applications [e.g., *Silver*, 1996; *Savage*, 1999; *Vecsey et al.*, 2008; *Long and Becker*, 2010] and to global and regional databases of splitting measurements from the literature [e.g., *Liu*, 2009; *Wüstefeld et al.*, 2009]. The shear wave splitting technique relies upon the following principle: when a shear wave propagates through an anisotropic medium, it is split into two components (quasi-*S* waves) that have different polari-zations and travel at different speeds. In the Earth's mantle, the polarizations of the two quasi-*S* waves will be nearly orthogonal, with their directions controlled by the elastic properties of the anisotropic medium. The shear wave splitting technique is very often applied to *SKS* phases, which are converted from a *P* wave in the liquid outer core to an *S* wave at the core-mantle boundary. From a ray theoretical point of view, the splitting of an *SKS* phase may reflect anisotropy anywhere along the raypath from the CMB to the surface. *SKS* splitting, however, is nearly always interpreted in terms of upper mantle anisotropy [e.g., *Long and Becker*, 2010],

with a few exceptions [e.g., *Long*, 2009]. As discussed in section 3 below, constraints from experimental mineral physics and from petrographic examination of mantle rocks are used to interpret shear wave splitting in terms of the geometry of mantle deformation.

[8] Although it is straightforward in theory, the actual measurement of shear wave splitting parameters (fast polarization direction, ϕ, and delay time between the fast and slow arrivals, δt) from real data is not trivial, particularly in the noisy environments that characterize many stations in subduction settings. A variety of measurement methods [see, e.g., *Wüstefeld et al.*, 2008; *Vecsey et al.*, 2008; *Monteiller and Chevrot*, 2010] have been developed to extract splitting parameters from seismograms as accurately as possible for the scenario in which the delay time δt is much smaller than the characteristic period of the wave, which is the case for most measurements of mantle anisotropy. Accurate measurements are particularly difficult for the case in which the initial polarization of the shear phase is close to either a fast or slow direction of the medium. Even if well-constrained estimates of (ϕ, δt) can be obtained from a single seismogram, the presence of complex anisotropy (such as multiple anisotropic layers) along a raypath can result in very complicated patterns of shear wave splitting [e.g., *Silver and Savage*, 1994] and in additional complications such as a dependence of splitting parameters on the frequency content of the wave under study [e.g., *Wirth and Long*, 2010].

[9] The shear wave splitting technique has been extensively applied in subduction systems, beginning with the early studies of *Ando et al.* [1980] and *Ando et al.* [1983], usually utilizing data from stations that are deployed on the overriding plate above the slab. A variety of raypath combinations may be used to interrogate anisotropy in various parts of the subduction system, as shown in Figure 1. Most splitting studies in subduction zones utilize *SKS* phases [e.g., *Anderson et al.*, 2004; *Baccheschi et al.*, 2007; *Christensen and Abers*, 2010; *Hanna and Long*, 2012], which are sensitive to anisotropy in the sub-slab mantle, slab, and mantle wedge (and may also carry a small signal from anisotropy in the overriding plate). Phases such as teleseismic *S* originating from deep earthquakes [e.g., *Marson-Pidgeon and Savage*, 1997; *Long and van der Hilst*, 2005] or *ScS* at regional distances [e.g., *Tono et al.*, 2009] can also be used; these are particularly useful because they cover a different incidence angle range than SKS, but any contribution to splitting from anisotropy near the earthquake source must be ruled out. Local *S* phases originating from slab earthquakes [e.g., *Smith et al.*, 2001; *Pozgay et al.*, 2007; *Abt et al.*, 2009; *Wirth and Long*, 2010], which mainly sample wedge anisotropy, are also commonly used, and some studies use a combination of the two [e.g., *Fouch and Fischer*, 1998; *Léon Soto et al.*, 2009; *Abt et al.*, 2010].

[10] A slightly different observational strategy involves so-called source-side shear wave splitting, which utilizes teleseismic *S* phases originating from earthquakes in the subducting slab measured at distant stations (Figure 1a). As long as the signal from anisotropy beneath the receiver
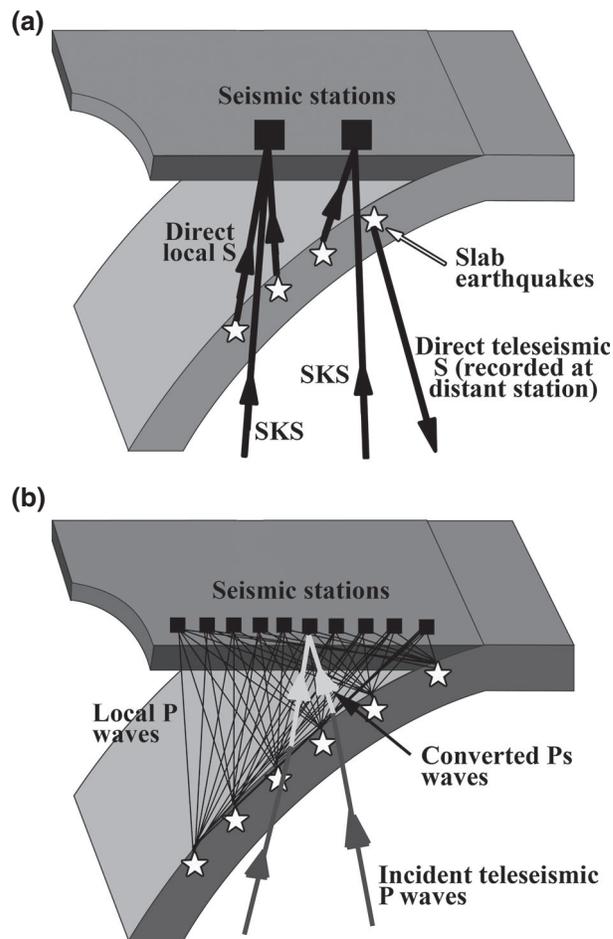

Figure 1. (a) Sketch of seismic raypaths commonly used in shear wave splitting studies to probe different parts of subduction systems, including local *S* phases, *SKS* phases, and direct teleseismic *S*, after *Long and Silver* [2009]. (b) Sketch of seismic raypaths commonly used in receiver function and *P* tomography studies to probe anisotropy in the mantle wedge and slab.

is accounted for, this technique can isolate the signal from anisotropy beneath the slab. It was initially applied to data from South America [*Russo and Silver*, 1994] and has recently been applied to a number of subduction systems [e.g., *Russo*, 2009; *Russo et al.*, 2010; *Foley and Long*, 2011; *Di Leo et al.*, 2012a; *Lynner and Long*, 2013].

[11] Shear wave splitting has both advantages and disadvantages as an observational technique in subduction zones. On the positive side, it is an unambiguous indicator of anisotropy and does not trade off with other medium characteristics such as isotropic heterogeneity. The measurement itself is straightforward in theory (if markedly more difficult in practice) and does not require the inversion of large amounts of data. The splitting technique can be used to place some depth constraints on anisotropy if multiple phases are used; for example, measurements of *SKS* splitting can be combined with local *S* measurements to estimate the likely splitting signal from the sub-slab mantle. A disadvantage of the technique, however, is that it remains a path-integrated measurement, and constraints on the depth

of anisotropy are weak even when multiple phases are used. Estimates of sub-slab splitting from combining *SKS* and local *S* phases have large errors, because local *S* splitting data sets tend to be complex and corrections for the effect of wedge anisotropy on *SKS* phases are necessarily imperfect. This is particularly true when splitting depends on frequency [e.g., *Marson-Pidgeon and Savage*, 1997], since local *S* and *SKS* usually have very different frequency contents.

[12] A further uncertainly with the use of *SKS* phases to characterize upper mantle anisotropy is the possibility that there may be a contribution to splitting from the lower mantle and/or from the crust. There is mounting observational evidence that anisotropy in the lowermost mantle can make a locally significant contribution to the splitting of *SK(K)S* phases [e.g., *Niu and Perez*, 2004; *Restivo and Helffrich*, 2006; *Long*, 2009; *He and Long*, 2011; *Lynner and Long*, 2012]. If these contributions are carefully characterized and accounted for, they can be exploited to study the dynamics of the lowermost mantle, as discussed further in section 6. If not, they may represent a source of contamination of the upper mantle anisotropy signal. There are, however, several lines of evidence that suggest that upper mantle anisotropy makes the primary contribution to *SK(K)S* splitting globally [e.g., *Lynner and Long*, 2012]. The most persuasive of these comes from global comparisons between models of azimuthal anisotropy derived from surface waves, which are not sensitive to the lowermost mantle, and SKS splitting measurements. Such comparisons are generally successful, although they may fail in specific regions [e.g., *Wüstefeld et al.*, 2009; *Becker et al.*, 2012]. Similarly, while crustal anisotropy is generally thought to be too small to make a primary contribution to *SKS* splitting, it may locally modify the splitting signal [e.g., *Kaviani et al.*, 2011] and must be considered as a potential contaminant of estimates of upper mantle anisotropy.

2.1.2. Anisotropic Receiver Function Analysis

[13] Receiver function (RF) analysis can place constraints on anisotropic structure that are complementary to those obtained via shear wave splitting analysis. Receiver function analysis is designed to isolate the signal from waves converted at interfaces within the Earth and thus contains information about sharp contrasts in seismic properties at depth. RF analysis for anisotropic structure usually focuses on teleseismic *P*-to-*S* conversions (see raypath diagram in Figure 1b). For the simple case of a flat interface with a contrast in isotropic velocity, a *P*-to-*S* conversion will result in energy only on the radial component receiver function (that is, the horizontal component that lies in the vertical plane containing the source and the receiver). For the case of either a dipping interface [e.g., *Bostock*, 1998] or a contrast in anisotropic properties [e.g, *Levin and Park*, 1998], there will also be converted *S* energy on the transverse component receiver function (that is, the horizontal component perpendicular to the radial component), with the amplitude of the arrival depending on the propagation direction of the wave (and the contrast in elastic properties). Anisotropic receiver function analysis, therefore, involves the computation of transverse component RFs for events

arriving from a range of back azimuths. The character of converted arrivals on the transverse RFs, and specifically how the amplitudes of *P*-to-*S* conversions vary with direction, can yield information about the geometry of anisotropic layers and/or dipping interfaces at depth. This technique has been applied to study anisotropy in subducting slabs and in the mantle wedge in several subduction zones, including Cascadia [*Park et al.*, 2004; *Nikulin et al.*, 2009; *Audet*, 2013], Mexico [*Song and Kim*, 2012a, 2012b; *Audet*, 2013], Japan [*Wirth and Long*, 2012; *Audet*, 2013], and Hikurangi [*Savage*, 1998; *Savage et al.*, 2007].

[14] A key advantage of the anisotropic RF technique is that it has excellent depth resolution; so long as the (isotropic) velocity structure of the region is well known, the timing of converted *P*-to-*S* phases can be used to constrain the depth to contrasts in anisotropic properties. Because it provides constraints on sharp discontinuities in anisotropy, it can provide information about the anisotropic medium that is complementary to that provided by path-integrated shear wave splitting measurements. Because conversions on transverse component RFs can be due to factors other than anisotropy, however, rigorous examination of RFs must be done in order to conclusively identify a signature from anisotropic structure, and good back azimuthal coverage is typically needed. Because a large number of parameters are needed to describe the characteristics of the anisotropic interfaces, it is typically necessary to carry out extensive forward modeling in order to constrain the geometry of anisotropy [e.g., *Nikulin et al.*, 2009; *Wirth and Long*, 2012], and there are usually strong tradeoffs among different parameters (for example, those describing the strength and geometry of anisotropy).

2.1.3. Anisotropic *P* Wave Tomography

[15] A third technique that can be used to place constraints on anisotropy in subduction systems is the implementation of *P* wave traveltime tomography schemes that include parameters describing anisotropy (usually the orientation and dip of the fast axis and the anisotropic strength) in the inversions. This technique requires good raypath coverage in the part of the subduction system that is being imaged (Figure 1b), with rays arriving from a variety of back azimuths and incidence angles. The successful application of the technique in subduction settings thus depends on the spatial distribution of sources (usually earthquakes in the subducting slab) and receivers (usually located on the overriding plate; a few studies have also incorporated data from ocean bottom seismometers located offshore, such as *Koulakov et al.* [2009]). As the name suggests, *P* wave tomography constrains the directional dependence of *P* wave speeds, in contrast to *S* wave splitting. Because of the raypath coverage achievable, *P* tomography is usually used to study anisotropy in the mantle wedge and (perhaps) within the subducting slab and has been applied in subduction systems including Hikurangi [*Eberhart-Phillips and Reyners*, 2009], Japan [*Wang and Zhao*, 2012], Java [*Koulakov et al.*, 2009], and Alaska [*Tian and Zhao*, 2012]. A key advantage of the technique is that it can resolve variations in anisotropic geometry both laterally and with depth; a disadvantage, however, is that anisotropic
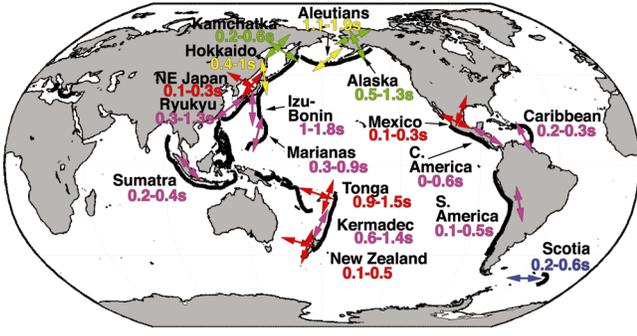
Figure 2. Summary map of first-order observations of local *S* splitting due to wedge anisotropy in subduction zones worldwide, from *Long and Wirth* [2013]. Arrows indicate the first-order patterns in average fast direction; where multiple arrows are present, this indicates a spatial transition in observed ϕ. Arrows are color coded by fast direction observations; magenta arrows indicate dominantly trench-parallel ϕ, blue arrows indicate dominantly trench-perpendicular ϕ, yellow arrows indicate complex and variable ϕ, red arrows indicate a transition from trench-parallel ϕ close to the trench to trench-perpendicular ϕ farther away, and green arrows indicate the opposite transition (from trench-perpendicular ϕ close to the trench to trench-parallel ϕ farther away). The range of observed delay times is indicated beneath the name of each subduction zone. References for individual studies are listed in Table 1.

parameters trade off with isotropic ones in the inversion framework. Additionally, the introduction of anisotropy into tomographic inversions increases the number of free parameters, and higher levels of damping and smoothing may be needed to stabilize the inversions.

2.2. Observations of Anisotropy in Subduction Systems
2.2.1. The Mantle Wedge

[16] *Long and Wirth* [2013] recently compiled observations of wedge anisotropy in subduction zones worldwide.

Here I briefly describe these observational constraints, based on *Long and Wirth* [2013], to which I refer readers who are interested in a more extensive discussion. A cartoon sketch in map view of first-order patterns of wedge anisotropy inferred from shear wave splitting is shown in Figure 2, and these first-order observations are shown in table form in Table 1.

[17] In general, shear wave splitting patterns in most mantle wedges worldwide are complex, with pronounced spatial variations, large variations in splitting delay times (from ~0.1 s to ~1.5 s) both within and among individual subduction zones, and apparent splitting parameters that vary with raypath geometry and frequency content [*Long and Wirth*, 2013]. To illustrate this variability, in Figure 3, I show representative splitting patterns from four different local *S* splitting studies in Kamchatka, Japan, Central America, and the Marianas [from *Levin et al.*, 2004; *Wirth and Long*, 2010; *Abt et al.*, 2009; *Pozgay et al.*, 2007]. The studies from which these examples are drawn generally have relatively good station coverage at the surface and thus good raypath coverage. However, many studies of wedge anisotropy are limited to only a few stations, commonly located on arc islands [e.g., *Long and Silver*, 2008; *Müller*, 2001; *Piñero-Felicangeli and Kendall*, 2008], and the interpretation of sparse data sets can be difficult and non-unique. Many subduction systems appear to be dominated by either trench-parallel fast directions (e.g., central Tonga-Kermadec, *Long and Silver* [2008]; Caribbean, *Piñero-Felicangeli and Kendall* [2008]; Java-Sumatra, *Hammond et al.* [2010]) or trench-perpendicular fast directions (e.g., Scotia, *Müller* [2001]), but for many of these studies the raypath coverage is quite limited.

[18] A commonly observed spatial pattern in fast splitting directions is trench-parallel ϕ measured at stations located relatively close to the trench in the forearc and arc region, with a transition to trench-perpendicular ϕ farther from the trench. Such a pattern is observed in several subduction

TABLE 1. Summary of Wedge Splitting[a]

Subduction Zone	Wedge δt (s)	Wedge ϕ	Event Depths (km)	Frequency Range (Hz)	Primary source(s)
Tonga	1.2 ± 0.3	Trench-$\parallel$ to trench-$\perp$	100–600	~0.3	*Smith et al.* [2001]
Kermadec	1.0 ± 0.4	Trench-$\parallel$	~235	0.02–0.125	*Long and Silver* [2008]
Hikurangi	0.3 ± 0.2	Trench-$\parallel$ to trench-$\perp$	57–293	0.5–3.0	*Morley et al.* [2006]
Sumatra	0.3 ± 0.1	Trench-$\parallel$	100–200	0.1–1.0	*Hammond et al.* [2010]
Marianas	0.6 ± 0.3	Trench-$\parallel$	80–250	0.3–0.7	*Pozgay et al.* [2007]
Izu-Bonin	1.4 ± 0.4	Trench-$\parallel$	370–502	0.02–0.125	*Wirth and Long* [2010]
Ryukyu	0.8 ± 0.5	Trench-$\parallel$	80–272	0.1–1.0	*Long and van der Hilst* [2006]
NE Japan	0.2 ± 0.1	Trench-$\parallel$ to trench-$\perp$	75–150	0.125–0.5	*Huang et al.* [2011b]
Hokkaido	0.7 ± 0.3	Variable	86–474	0.125–0.5	*Wirth and Long* [2010]
Kamchatka	0.4 ± 0.2	Trench-$\perp$ to trench-$\parallel$	25–150	0.5–2.0	*Levin et al.* [2004]
Aleutians	1.5 ± 0.4	Trench-$\parallel$ or oblique	~100 km	0.02–0.125	*Long and Silver* [2008]
Alaska	0.9 ± 0.4	Trench-$\perp$ to trench-$\parallel$	Not reported	Not reported	*Christensen et al.* [2003]
Caribbean	0.27 ± 0.03	Trench-$\parallel$	128	1.0–3.0	*Piñero-Felicangeli and Kendall* [2008]
Middle America	0.3 ± 0.3	Trench-$\parallel$	30–220	0.01–2.0	*Abt et al.* [2009]
Mexico	0.2 ± 0.1	Trench-$\parallel$ to trench-$\perp$	60–106	0.5–2.0	*Léon Soto et al.* [2009]
South America	0.3 ± 0.2	Trench-$\parallel$	50–350	0.01–1.0	*Polet et al.* [2000]
Scotia	0.4 ± 0.2	Trench-$\perp$	100–170	0.05–0.5	*Müller* [2001]

[a]Table of constraints on shear wave splitting in the mantle wedge from the published literature. The most relevant citations are listed in the table, with additional relevant studies discussed in *Long and Wirth* [2013]. For each subduction zone, we list the local *S* splitting delay times and fast directions, along with the range of event depths and the frequency band used to filter the data (and/or the characteristic frequency estimated from sample waveforms). Fast directions that include more than one orientation describe how the orientation changes moving from the forearc into the backarc. From *Long and Wirth* [2013].
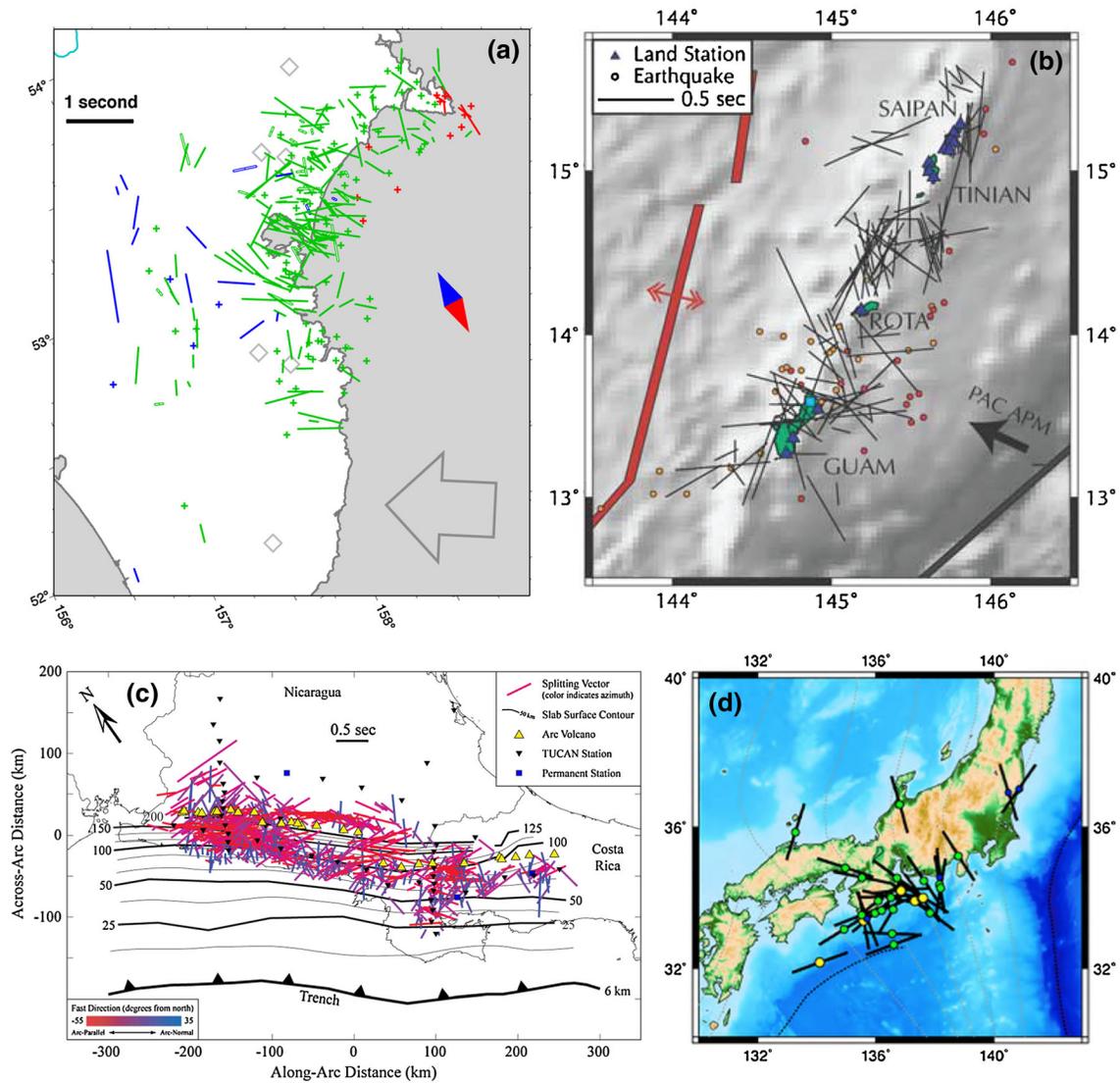$\parallel$ = parallel; $\perp$ = perpendicular.

Figure 3. Examples of local *S* splitting patterns due to wedge anisotropy beneath (a) Kamchatka, (b) the Marianas, (c) Central America, and (d) southwest Japan. In each map, measurements are plotted at the midpoint between the station and earthquake location, with the orientation of the bar indicating the fast direction and the delay time indicated by either the length of the bar (in Figures 3a–3c) or the color of the symbol (in Figure 3d). Figure 3a shows measurements beneath southernmost Kamchatka. Crosses show null measurements. Color indicates depth of the ray midpoint: red above 30 km, blue below 100 km, green between 100, and 300 km. Open diamonds show locations of active volcanoes; large arrow shows subduction direction of the Pacific Plate. Figure from *Levin et al.* [2004]. Figure 3b shows measurements beneath the southern Marianas. Thick red lines denote the backarc spreading center; thick gray line indicates the trench location; black arrow indicates the subduction direction of the Pacific Plate. Figure from *Pozgay et al.* [2007]. Figure 3c shows measurements beneath Costa Rica and Nicaragua. Measurements are color coded by orientation, with blue indicating trench-normal fast directions and red indicating trench-parallel. Figure from *Abt et al.* [2009]. Figure 3d shows measurements from southwest Japan. Delay times are indicated by the symbol color, ranging from less than 0.4 s (blue) to 0.4–0.8 s (green) to greater than 0.8 s (yellow). Figure from *Wirth and Long* [2010].

systems, including Tonga [*Smith et al.*, 2001], Ryukyu [*Long and van der Hilst*, 2006], Central America [*Abt et al.*, 2009], northeastern Japan [*Nakajima and Hasegawa*, 2004; *Wirth and Long*, 2010], and the Marianas [*Pozgay et al.*, 2007] (Figure 3). For mantle wedges that exhibit this pattern, there is some variability in the location of the transition; in some systems, the transition from trench-parallel to trench-perpendicular ϕ occurs at or near the arc [e.g., *Nakajima*

and Hasegawa, 2004; *Long and van der Hilst*, 2006], while in other regions it occurs farther in the backarc [e.g., *Smith et al.*, 2001]. An additional complication is that some subduction systems exhibit the opposite spatial trend in ϕ. For example, in Kamchatka, stations located in the forearc exhibit trench-perpendicular fast directions, with a transition to trench-parallel ϕ in the backarc [*Levin et al.*, 2004] (Figure 3).

(a)

Station: DBO
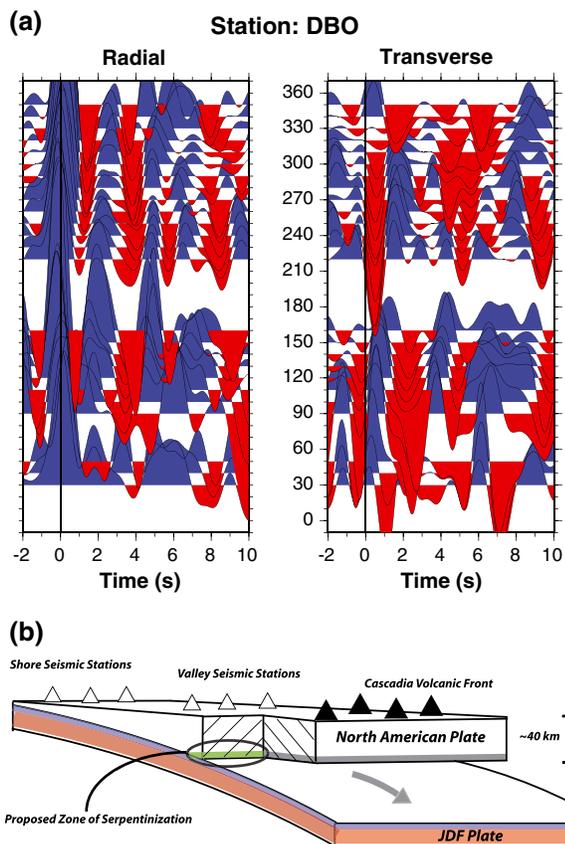
Radial

Transverse

Figure 4. An example from an anisotropic receiver function study in a subduction system. (a) Example of an RF gather, plotted as a function of event back azimuth, for a seismic station (DBO) located in the Cascadia subduction zone, located approximately 40 km above the subducting slab. Left panel presents radial component RFs; the large positive pulse at zero time indicates the direct *P* wave arrival. Right panel presents transverse component RFs; signal on these traces is due to the presence of anisotropy. The polarity reversal at a back azimuth of 270° at a time of ~5 s is interpreted as due to a layer of anisotropy directly beneath the slab. (b) Cartoon sketch of the interpretation of the RF gather shown in Figure 4a. The major feature is the thin anisotropic layer directly above the slab, interpreted as serpentinized mantle, beneath the valley stations, including DBO. Figure from *Nikulin et al.* [2009].

[19] Anisotropic RF analysis has been applied to study wedge anisotropy in a few subduction systems. Examples of anisotropic RF analysis from two different studies [*Nikulin et al.*, 2009; *Wirth and Long*, 2012] are illustrated in Figures 4 and 5. The technique has mainly been applied to study the character of seismic anisotropy directly above or beneath the slab interface, although some studies have also attempted to place constraints on anisotropy within the main volume of the wedge and compare these constraints to those obtained from local *S* splitting studies. Several authors have argued for the presence of a relatively thin, highly anisotropic layer directly above the subducting slab, which has been interpreted as possible evidence for the presence of serpentinized minerals such as antigorite [e.g., *Park et al.*, 2004; *Nikulin et al.*, 2009; *McCormack et al.*, 2013],

based on the inference of strong anisotropy with a slow axis of hexagonal symmetry [*Mainprice and Ildefonse*, 2009]. Such a layer directly above subducting slabs does not appear to be a ubiquitous feature, however; for example, it is only intermittently observed in Cascadia [*Nikulin et al.*, 2009]. *Wirth and Long* [2012] inferred relatively weak anisotropy beneath northeastern Japan within the wedge itself that generally exhibits fast directions perpendicular to the trench (parallel to the motion of the slab) (Figure 5). In contrast, *McCormack et al.* [2013] applied identical analysis techniques to stations from the Ryukyu arc and found evidence for a layer within the mantle wedge with an anisotropic fast axis that is parallel to the trench, consistent with fast splitting directions [*Long and van der Hilst*, 2006].

[20] Anisotropic *P* wave tomography of the mantle wedge has been applied to several different subduction systems, yielding good constraints on the three-dimensional pattern and strength (generally less than ~5%) of *P* anisotropy in mantle wedges. An example of an anisotropic *P* wave model for Alaska [*Tian and Zhao*, 2012] is shown in Figure 6. In general, *P* wave tomographic models tend to show evidence for trench-parallel fast velocity directions in the shallow forearc portion of the mantle wedge [e.g., *Koulakov et al.*, 2009], often in good agreement with splitting measurements in the same region [e.g., *Wang and Zhao*, 2008]. In some regions, however, the anisotropic geometry inferred from *P* tomography is somewhat different from that inferred from shear wave splitting [e.g., Alaska; *Tian and Zhao*, 2012]. *Wang and Zhao* [2012] documented complex and spatially varying wedge anisotropy beneath southwestern Japan, with trench-normal fast velocity directions in the backarc beneath Kyushu, again in good agreement with constraints from splitting.

2.2.2. The Subducting Slab

[21] Constraints on anisotropy within the slab itself are sparser than constraints on anisotropy within the mantle wedge or the sub-slab mantle. A global comparison between *SKS* fast splitting directions (which are mostly trench-parallel) and fossil spreading directions in the subducting lithosphere yielded no obvious agreement [*Long and Silver*, 2009]. This suggests that while *SKS* phases surely are sensitive to anisotropic structure within the slab, anisotropy that is frozen into oceanic lithosphere during lithospheric formation does not represent the primary contribution to *SKS* splitting. The global pattern of fast *SKS* splitting directions was used by *Faccenda et al.* [2008] to argue that *SKS* splitting may primarily reflect anisotropy in the shallow part of the slab due to aligned serpentinized cracks, but because *SKS* phases sample many parts of the subduction system including the wedge and the sub-slab mantle, arguments based on *SKS* phases are somewhat indirect.

[22] Recently, more direct constraints on anisotropy within the slab have come from anisotropic RF studies, *P* wave tomography models, and local *S* splitting studies that take advantage of different raypath combinations to isolate certain parts of the subduction system. *Song and Kim* [2012a] used RF analysis to argue for the presence of clay minerals such as talc in the uppermost part of the slab, coinciding
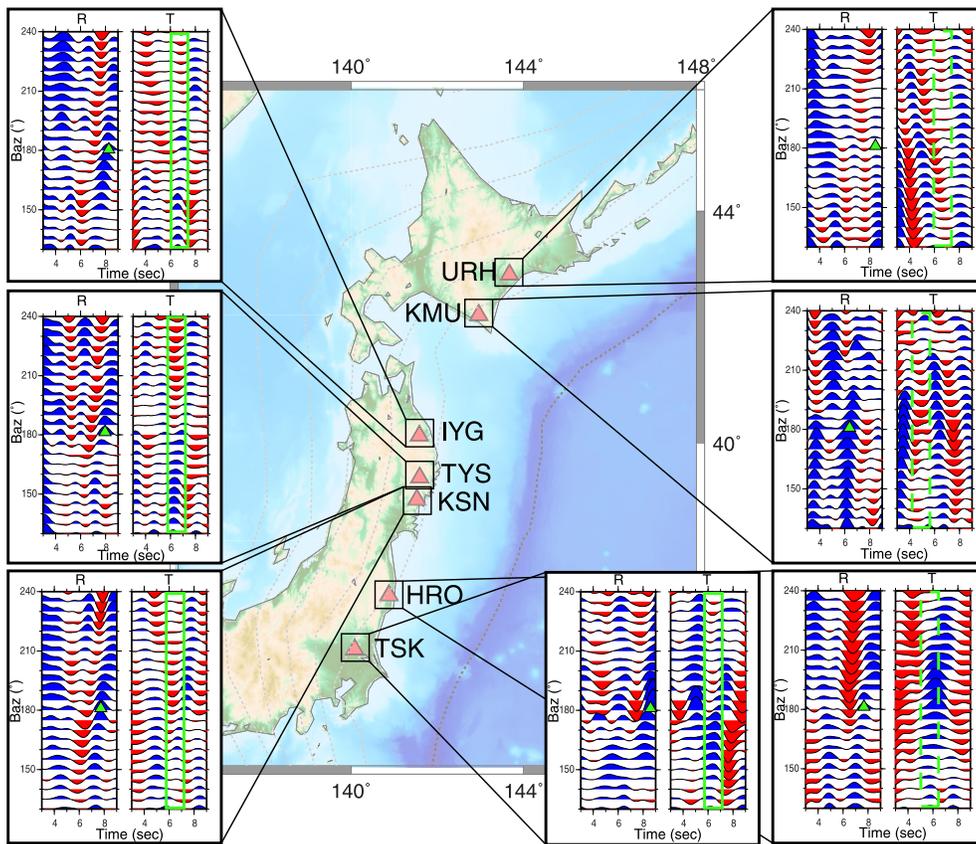
Figure 5. An example of lateral variability in anisotropic structure of the mantle wedge in a single subduction system inferred from anisotropic RF analysis. Each individual panel indicates RF results (radial RFs, left; transverse RFs, right) for a single station from a select group of back azimuths, focusing on a narrow time window in which we would expect to see *P*-to-*S* conversions from structure in the wedge. Green triangles on the radial components indicate the pulse associated with the subducting oceanic Moho. Green boxes on the transverse components indicate the time window associated with structure immediately above the slab. Stations IYG, TYS, KSN, and TSK show a clear polarity flip at a back azimuth near 180° associated with anisotropy above the slab (solid green boxes), while stations HRO, KMU, and URH do not (dashed green boxes). Transverse component receiver function gathers for all back azimuths (not shown; see Figures 4–10 of *Wirth and Long* [2012]) exhibit a four-lobed polarity flip (every 90°) at stations IYG, TYS, KSN, and TSK in this time range, which is characteristic of an anisotropic layer. In contrast, a dipping interface would predict a two-lobed polarity flip (every 180°). Figure from (*Wirth and Long*, 2012).

geographically with the region where slow slip events occur. A companion study [*Song and Kim*, 2012b] used the same data set to argue for frozen lithospheric anisotropy in the uppermost mantle of the downgoing slab and correlated the geometry and strength (~7%) of this inferred anisotropy with the spreading direction and rate at the nearby East Pacific Rise. Similar results have recently been obtained in other subduction zones [*Audet*, 2013]. There is corroborating evidence for lithospheric anisotropy within subducting slabs from *P* wave tomography models; for example, *Wang and Zhao* [2008, 2012] and *Tian and Zhao* [2012] have suggested that the slabs beneath northwest Japan, southwest Japan, and Alaska, respectively, exhibit anisotropy with a typical strength up to ~5–7% and geometries that correlate well with the fossil spreading directions for the slab. Given the evidence from both RF and tomography studies for significant (~5–7%) fossil anisotropy in the downgoing lithosphere of subducting slabs, it is somewhat surprising that there is no unambiguous

evidence for a signature of this anisotropy in *SKS* splitting measurements [*Long and Silver*, 2009].

[23] It remains a difficult task to extract direct information about slab anisotropy from splitting measurements, but a recent study by *Huang et al.* [2011a] exploited the dense station coverage and high-resolution seismicity catalog available in northeastern Japan to measure the differential splitting of local *S* phases originating in the upper and lower plane of seismicity (Figure 1). Northeastern Japan has perhaps the best-defined double Wadati-Benioff zone of any subduction system worldwide [e.g., *Brudzinski et al.*, 2007], and differences in splitting between *S* phases from lower and upper plane earthquakes reflect the anisotropic signature of the shallow (~40–50 km) part of the subducting slab. They identified a splitting signature from the shallow slab with a roughly N-S fast direction, consistent with previous *P* wave tomography [*Wang and Zhao*, 2008], and a delay time on the order of ~0.1 s [*Huang et al.*, 2011a].
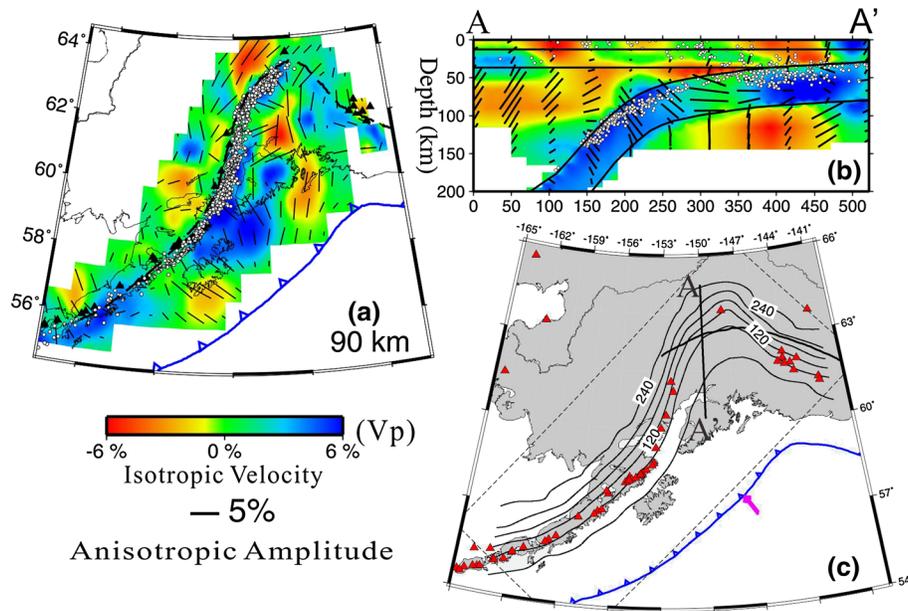
Figure 6. Example of an anisotropic *P* wave tomography model of wedge and slab anisotropy beneath southern Alaska, after (*Tian and Zhao*, 2012). (a) Map view of a horizontal slice through the model at a depth of 90 km. Background colors indicate isotropic *P* wave speed anomalies (see color scale in legend) The dashed black line indicates the inferred upper boundary of the Pacific slab; gray dots indicate earthquake locations. Orientation and length of the black bars indicate the fast velocity direction and anisotropic amplitude, respectively (see length scale in legend). (b) Vertical cross-section through the model (cross-section location shown in Figure 6c). Orientation and length of the black bars indicate the horizontal azimuth of fast velocity direction (vertical bars represent N-S direction, horizontal bars indicate E-W direction) and the strength of anisotropy, respectively. (c) Tectonic setting and location of cross-section. Blue sawtoothed line indicates the location of the trench; red triangles denote active arc volcanoes. Black lines indicate slab depth contours. Pink arrow indicates direction of motion of the subducting Pacific plate.

2.2.3. The Sub-slab Mantle

[24] Constraints on the anisotropic structure of the sub-slab mantle come almost exclusively from splitting studies, and in general splitting patterns in the sub-slab mantle tend to be considerably simpler than those in the mantle wedge [e.g., *Long and Silver*, 2008]. There are two different splitting measurement techniques that can be used to isolate the signal from sub-slab anisotropy (Figure 1), both of which involve a correction for anisotropy elsewhere along the raypath. *SKS* phases with long path lengths in the sub-slab mantle can be corrected for the effect of wedge anisotropy, or direct teleseismic *S* phases originating from slab earthquakes can be corrected for the effect of anisotropy directly beneath the receiver. Neither measurement technique is free from possible errors introduced by imperfect corrections, but because of the complexity of wedge splitting patterns, source-side splitting measurements made at stations where the receiver-side anisotropy is simple and well known likely provide the most accurate estimates [*Lynner and Long*, 2013]. Measurements of sub-slab anisotropy from subduction zones worldwide were compiled by *Long and Silver* [2008, 2009] and updated by *Paczkowski* [2012]; first-order estimates of sub-slab splitting in various regions from the most recent version of this compilation is shown in map view in Figure 7 and in table form in Table 2.

[25] Most subduction systems exhibit sub-slab fast splitting directions that are either dominantly trench-perpendicular or dominantly trench-parallel. Trench-parallel ϕ, which were first documented beneath South America by *Russo and Silver* [1994], make up the majority of the global data set (Figure 7), but there are several important exceptions, including Cascadia [*Currie et al.*, 2004; *Russo*, 2009], Greece [*Olive et al.*, 2011],
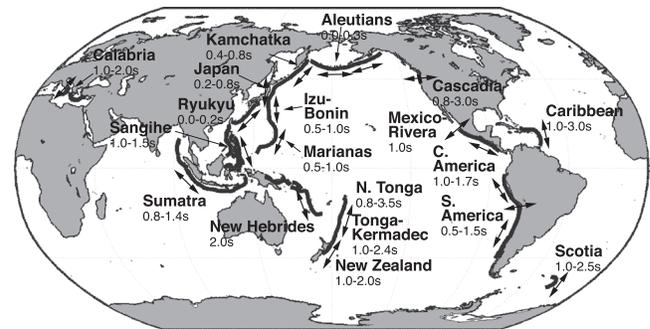

Figure 7. Summary map of sub-slab anisotropy worldwide, updated from the compilations of *Long and Silver* [2009] and *Paczkowski* [2012]. Arrows indicate the dominant sub-slab fast direction (either trench-parallel or trench-perpendicular). The range of observed delay times is indicated beneath the name of each subduction zone. References for individual studies are in Table 2.

TABLE 2. Summary of Sub-slab Shear Wave Splitting[a]

Subduction Zone	Type of Data	Sub-wedge δt	Sub-wedge ϕ	Sub-wedge Path Lengths in Upper Mantle	# of Stations (Events)	Primary Source(s)
Northern Tonga	Source-side S	~0.8–3.5 s	Trench-||	~400 km	(~50)	Foley and Long [2011]
Tonga-Kermadec	SKS, local S	~1.0–2.4 s	Trench-||	~300 km	1	Long and Silver [2008]
Hikurangi	SKS, local S	~1.0–2.0 s	Trench-||	~360 km	2	Audoine et al. [2004]
Sumatra/Indonesia	SKS, local S	~0.8–1.4 s	Trench-||, oblique	~200 km for PSI; large range for other stations	~20	Long and Silver [2008]; Hammond et al. [2010]
Sangihe	SKS, local S, Source-side S	~1.0–1.5 s	Trench-||	~300 km	2 (7)	Di Leo et al. [2012a]; Di Leo et al. [2012b]
New Hebrides	SKS	~2.0 s	Trench-||	~300 km	3	Király et al. [2012]
Izu-Bonin	SKS	~0.5–1.0 s	Trench-||, some oblique; splitting patterns complex	~300 km	4	Wirth and Long [2008]
Marianas	Source-side S	~0.5–1.0 s	Trench-||	~200 km	(2)	Wookey et al. [2005]
Ryukyu	SKS, local S	~0.0–0.2 s	Trench-||, if any	~280–350 km	8	Long and van der Hilst [2005]; Long and van der Hilst [2006]
Japan (N. Honshu, Hokkaido)	SKS, local S	~0.2–0.8 s	Oblique, some trench-||; splitting patterns complex	~200–320 km	~20	Long and van der Hilst [2005]; Nakajima and Hasegawa [2004]; Wirth and Long [2010]
Kamchatka	SKS, local S	~0.4–0.8 s	Trench-||	~200–340 km	~5	Peyton et al. [2001]; Levin et al. [2004]
Aleutians	SKS, local S	~0.0–0.3 s	Trench-||, if any	~300 km	3	Long and Silver [2008]
Cascadia	SKS, Source-side S	~0.8–3.0 s	Trench-perp (SKS), complex (source-side)	~300 km	~5 (3)	Currie et al. [2004]; Russo [2009]
Mexico-Rivera	SKS, local S	~1.0 s	Trench-perp	~300 km	50	Leon Soto et al. [2009]
Caribbean	SKS, limited local S, Source-side S	~1.0–3.0 s	Trench-||	~300 km	~7 (~25)	Piñero-Felicangeli and Kendall [2008]; Lynner and Long [2013]
Calabria	SKS	~1.0–2.0	Trench-||	~200–350 km	~30	Baccheschi et al. [2007]
Middle America	SKS, local S	~1.0–1.7 s	Trench-||	~250–360 km	~20	Abt et al. [2009]
South America	SKS, local S, source-side S	~0.5–1.5 s	Variable, but mostly trench-||	~0–200 km (source-side), ~100–300 (SKS)	~20 (~10)	Rokosky et al. [2006] (source-side); Polet et al. [2000] (SKS, local S); Russo and Silver [1994] (all types)
Scotia	Source-side S	~1.0–2.5	Trench-||	~125–390 km	(~20–30)	Müller [2001]; Lynner and Long [2013]

[a]Table of constraints on sub-slab shear wave splitting from the published literature, updated from *Long and Silver* [2009]. The most relevant citations are listed in the table, with additional relevant studies discussed in *Long and Silver* [2009]. For each subduction zone, the range of delay times and fast directions allowed by the data are listed, along with the approximate number of stations (or events for source-side splitting) used to obtain the estimate. The range of path lengths were estimated by assuming that the depth of the bottom of the anisotropic layer is at ~400 km and taking into consideration the depth to the slab beneath the stations used (for SKS/local S studies) and/or the depth of the earthquakes used (for source-side studies).
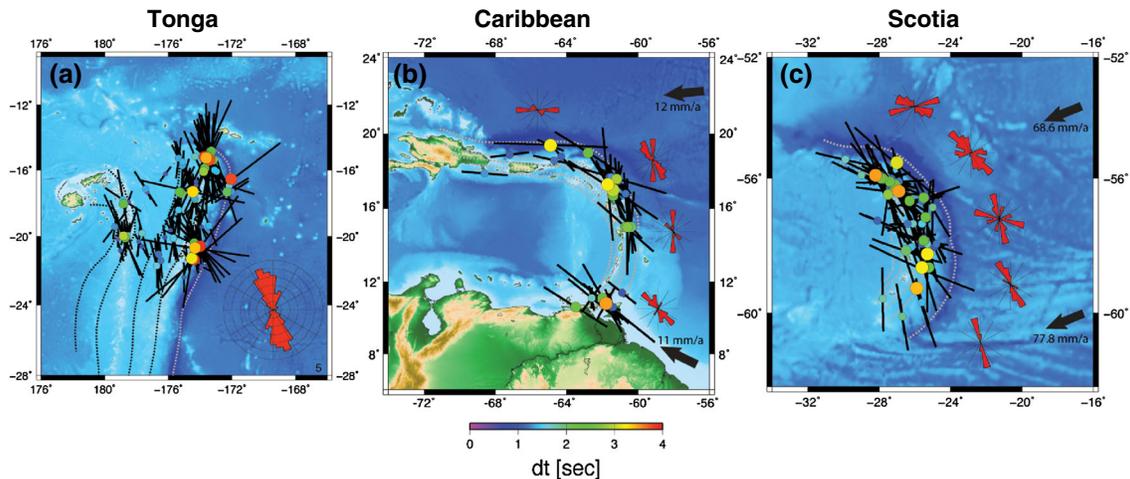|| = parallel.

85

Figure 8. Examples of source-side splitting measurements which reflect anisotropy beneath the subducting (a) Tonga, (b) Caribbean, and (c) Scotia slabs. Orientation and lengths of the bars indicate fast splitting directions and delay times, respectively; symbol colors also indicate delay time. Measurements are plotted in horizontal projection at the earthquake location, and measured fast directions have been reflected over the back azimuth to transform ϕ into the reference frame of the downgoing ray. Circular histograms indicate the fast direction distribution for different trench segments. Dashed lines indicate contours of the slabs at depth, from *Gudmundsson and Sambridge* [1998]. For Tonga, the 100, 300, 500, and 700 km contours are shown; for Scotia and the Caribbean, the contour interval is 50 km. Figures from *Foley and Long* [2011] (Figure 8a) and *Lynner and Long* [2013] (Figures 8b and 8c).

and Mexico [*Léon Soto et al.*, 2009]. There is a large range in average sub-slab delay times for the global data set, with some systems exhibiting relatively weak sub-slab anisotropy [e.g., Ryukyu; *Long and Silver*, 2008] and others exhibiting delay times up to ~2 s or more [e.g., Tonga; *Foley and Long*, 2011].

[26] It is difficult to place precise constraints on the depth distribution of anisotropy beneath subducting slabs using *SKS* phases. Recently, however, the source-side splitting technique has been more commonly applied to data sets from subduction systems [e.g., *Müller et al.*, 2008; *Russo et al.*, 2010; *Foley and Long*, 2011; *Di Leo et al.*, 2012a; *Lynner and Long*, 2013], yielding stronger constraints on the depth distribution of anisotropy beneath subducting slabs. Figure 8 shows examples from such recent studies for the northern Tonga [*Foley and Long*, 2011], Caribbean [*Lynner and Long*, 2013], and Scotia [*Lynner and Long*, 2013] subduction systems. As is typical of subduction zones worldwide, trench-parallel sub-slab fast splitting directions dominate in all three of these systems. Tonga exhibits a particularly well-developed pattern of trench-parallel ϕ (Figure 8) with a weak trend of decreasing δt with event depth for upper mantle events [*Foley and Long*, 2011], providing support for the interpretation that the splitting primarily reflects upper mantle anisotropy beneath the slab. *Foley and Long* [2011] also documented splitting due to anisotropy in the transition zone or uppermost lower mantle, discussed further in section 6. *Lynner and Long* [2013] compared source-side splitting for the Caribbean and Scotia regions (Figure 8), which exhibit similar slab morphologies but different slab kinematics. They documented dominantly trench-parallel fast directions, which closely follow the slab curvature throughout most parts of the subduction system,

but both regions exhibit a transition to dominantly trench-perpendicular or oblique ϕ at the southern ends of the subduction zones. This pattern of dominantly trench-parallel ϕ, along with a significant minority of exceptions to the trench-parallel rule, mimics the pattern documented in subduction zones worldwide (Figure 7) [*Long and Silver*, 2009].

3. MINERAL PHYSICS CONSTRAINTS

3.1. Olivine Fabrics

[27] Seismic anisotropy in the upper mantle is nearly always interpreted as being due to the lattice or crystallographic preferred orientation of intrinsically anisotropic minerals. LPO will develop when mantle materials are deformed in the dislocation creep regime, which corresponds to a non-Newtonian rheology. Because olivine is the primary constituent of the upper mantle and has a large (~18%) intrinsic shear wave anisotropy, olivine LPO is thought to make the primary contribution to anisotropy observations. In certain regions of the upper mantle, including the mantle wedge of subduction zones, there may be a contribution from other factors such as the shape preferred orientation of partial melt [e.g., *Ando et al.* [1980]; *Zimmerman et al.*, 1999; *Vauchez et al.*, 2000]. The literature on fabric development in upper mantle minerals, based on both experimental studies and on the petrographic examination of mantle-derived rocks, has been extensively reviewed elsewhere [e.g., *Mainprice*, 2007; *Karato et al.*, 2008], and I refer the reader to these papers for an exhaustive discussion. Here I provide only a brief explanation of recent developments in the study of olivine fabric types that are relevant to the study of anisotropy in the subduction systems, based in part on the discussions found in *Mainprice* [2007] and *Karato et al.* [2008].
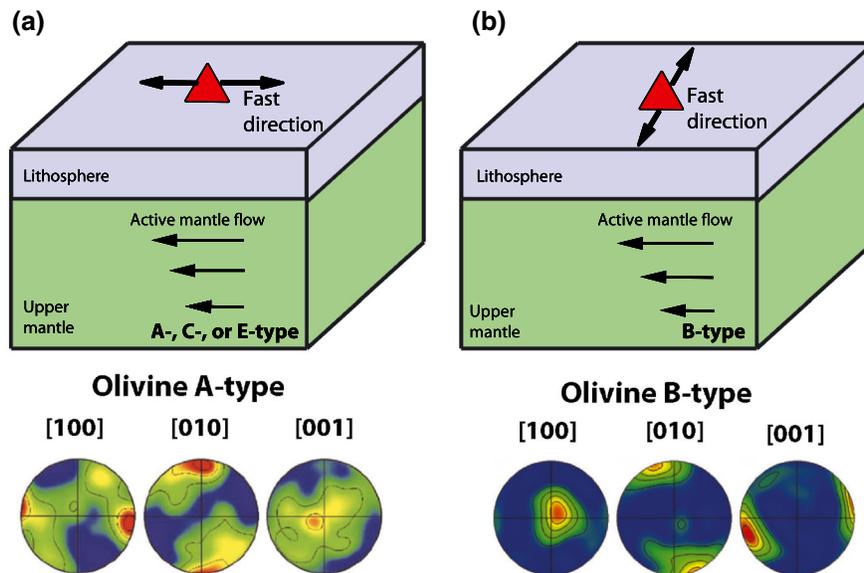
Figure 9. Cartoon sketch of the effect of B-type olivine fabric on the interpretation of shear wave splitting measurements in terms of mantle flow, from *Long and Becker* [2010]. (a) In most regions of the asthenosphere, likely including much of the mantle wedge and the sub-slab mantle, olivine fabric is expected to be A-, C-, or E-type, resulting in a fast axis of anisotropy (black arrow) that is parallel to the (horizontal) flow direction beneath a seismic station (red triangle). Typical examples of pole figures for an experimentally deformed olivine aggregate are shown; the statistical distribution of the [100], [010], and [001] crystallographic axes are shown as stereographic plots with respect to the deformation geometry (horizontal line represents the shear plate), with red colors indicating higher orientation density. (b) For the case of B-type olivine fabric, which may be present in the cold, shallow corner of the mantle wedge, the same flow direction would result in an observed fast direction that is different by 90°. Typical pole figures for B-type olivine are shown. All pole figures are from *Karato et al.* [2008], after *Jung et al.* [2006].

[28] Early deformation experiments on olivine aggregates carried out in a simple shear geometry by *Zhang and Karato* [1995] are often cited by seismologists as the basis for the commonly used rule of thumb that fast shear wave splitting directions generally reflect the direction of horizontal mantle flow beneath a seismic station. This interpretation relies on the assumption of a vertical gradient in horizontal mantle velocity, which results in shear strain. For A-type olivine fabric, which prevails at relatively low stresses, high temperatures, and low water contents [*Karato et al.*, 2008], an olivine aggregate deformed in simple shear to high strains (> ~100–150%) will develop an LPO pattern in which the fast axes of individual olivine crystals tend to align in the direction of shear. For the simple geodynamic case of horizontal flow with a vertical gradient in velocity (Figure 9), the fast axis of anisotropy will thus tend to align with the flow direction. This rule of thumb is very commonly applied in subduction systems, despite the fact that even in the simplest two-dimensional flow models the flow (and thus anisotropy) patterns are expected to be substantially more complicated than in the case of horizontal simple shear [e.g., *Chastel et al.*, 1993; *Levin et al.*, 2007]. Additionally, the complicated strain history and time lag between changes in flow geometry and changes in olivine LPO means that even for simple, A-type olivine LPO, one might expect complications in subduction zone anisotropy patterns [e.g., *Kaminski and Ribe*, 2002].

[29] A-type olivine LPO is sometimes further simplified by seismologists who use an approximation of hexagonal anisotropy with a fast direction that is parallel to horizontal mantle flow (assuming a vertical gradient in flow velocity and large strain) [e.g., *Russo and Silver*, 1994] or to the long axis of the finite strain ellipse [e.g., *Hall et al.*, 2000]. The validity of the assumption of hexagonal symmetry to represent olivine LPO was recently evaluated by *Becker et al.* [2006], who predicted olivine LPO for a global mantle circulation model and found that the best fitting hexagonal anisotropy generally does a good job of representing the elastic tensor. There is a great deal of uncertainty about the strength of anisotropy in deformed mantle aggregates; there is a large range of S anisotropy strengths in natural peridotite rocks, up to ~10–15%, but many samples show modest anisotropy of a few percent [e.g., *Ben Ismail and Mainprice*, 1998].

[30] While the A-type olivine rule of thumb remains a commonly used framework for seismologists who interpret measurements of anisotropy in terms of mantle flow patterns, recent results have demonstrated that olivine LPO geometries may be affected by factors such as water content, (deviatoric) stress, temperature, pressure, and the presence of melt, and many of these complications are likely relevant for subduction systems. The effect of water on olivine fabric development was emphasized by *Jung and Karato* [2001], who demonstrated the development of B-type olivine fabric in water-rich samples deformed in simple shear. Subsequent

work on delineating the B-type olivine fabric regime showed that stress and temperature also play a role, with B-type fabric dominating at relatively low temperatures, high stresses, and high water contents [e.g., *Jung et al.*, 2006; *Karato et al.*, 2008]. B-type fabrics have been identified in natural peridotite rocks [e.g., *Mizukami et al.*, 2004; *Skemer et al.*, 2006; *Tasaka et al.*, 2008]. Other types of olivine fabric, including C-, D-, and E-type fabric, have also been identified by a series of experimental studies [*Katayama et al.*, 2004; *Katayama and Karato*, 2006; *Jung et al.*, 2006] and documented in natural rock samples [e.g., *Mehl et al.*, 2003; *Tommasi et al.*, 2006; *Michibayashi et al.*, 2006; *Mainprice*, 2007; *Jung*, 2009], with the dominant fabric type being determined by the stress, temperature, and water content conditions (perhaps among other variables) during deformation.

[31] One of the other variables that may be important in controlling olivine fabric geometry is pressure; several recent experimental studies have suggested that there may be a transition in olivine fabric at increasing pressures [*Couvy et al.*, 2004; *Mainprice et al.*, 2005; *Raterron et al.*, 2007; *Jung et al.*, 2009]. Specifically, *Couvy et al.* [2004] and *Mainprice et al.* [2005] suggest a pressure-induced transition to C-type olivine fabric at a pressure of 11 GPa or less, while *Jung et al.* [2009] propose a pressure-induced transition to B-type olivine fabric at a significantly lower pressure (around 3 GPa). A possible transition in olivine fabric types at high pressure is significant for the interpretation of anisotropy measurements, particularly in the deep mantle beneath subducting slabs. (As argued by *Karato et al.* [2008], however, uncertainties remain about whether the transitions in olivine fabric attributed to pressure may in fact be due to the effect of stress on LPO. Additionally, there are some arguments against a pressure-induced transition based on evidence from deep xenoliths [*Karato et al.*, 2008].) The presence of partial melt may also affect the geometry of olivine LPO; a series of experiments by *Holtzman et al.* [2003] provided evidence that the fast axes of olivine crystals align 90° from the shear direction when partial melt is present in the samples. There is, however, some debate about the applicability of the experimental geometry used by *Holtzman et al.* [2003] to the Earth's mantle [*Karato et al.*, 2008].

[32] It is important to consider the possible consequences of different olivine fabric types on the interpretation of measurements of anisotropy in subduction systems. The importance of B-type fabric is clear; as the fast axes of olivine tend to align in the shear plane but 90° away from the shear direction, it thus changes by 90° the relationship between the fast splitting direction and the inferred flow direction [*Jung and Karato*, 2001] (Figure 9). For C- or E-type fabric, which may be the most likely candidates to dominate most parts of the wedge (away from the low-temperature, high-stress forearc mantle; *Kneller et al.* [2005]) as well as the sub-slab mantle [*Karato et al.*, 2008], the difference with A-type fabric is far more subtle. As shown in Figure 2 of *Karato et al.* [2008], there is no difference between the expected shear wave splitting signature of A-, C-, and E-type olivine fabric for the case of horizontal

shear. For the case of vertical planar flow, A- and E-type fabric will result in only small splitting, while C-type fabric will yield fast splitting directions normal to the shear plane, 90° away from the fast direction expected for B-type fabric. For the intermediate case of a dipping layer of olivine (as might be expected directly above or beneath a subducting slab), the differences in splitting behavior between A-, C-, or E-type fabric are subtle and will depend on the exact geometry of the slab as well as complications in deformation history and/or fabric transitions that any given piece of mantle may have undergone [e.g., *Skemer et al.*, 2012].

3.2. Elasticity and Fabric Development in Hydrous Phases

[33] While olivine LPO patterns provide the interpretive framework for seismic anisotropy in nearly all regions of the upper mantle, there is a crucial aspect of subduction systems that necessitates the consideration of other types of minerals: the presence of water. The shallow part of subducting slabs is likely hydrated through processes such as lithospheric formation at mid-ocean ridges, hydrothermal circulation in oceanic crust, and bending-induced faulting at the outer rise [e.g., *Johnson and Prius*, 2003; *Ranero et al.*, 2003]. A large array of hydrous minerals may therefore be present in subducting slabs, and as these minerals become unstable at high pressures and temperatures, water is released into the wedge [e.g., *Cagnioncle et al.*, 2007], provoking melting [e.g., *Grove et al.*, 2009] and perhaps serpentinizing the wedge mantle [e.g., *Bostock et al.*, 2002; *Hyndman and Peacock*, 2003; *Reynard et al.*, 2007; *Hilairet and Reynard*, 2008]. Our knowledge of the single-crystal elasticity of hydrous minerals at the relevant pressure and temperature conditions remains incomplete, but *Mainprice and Ildefonse* [2009] provide a recent overview of the elasticity of hydrous phases and their applicability to seismic studies of subduction systems. In particular, *Mainprice and Ildefonse* [2009] argue that most hydrous minerals relevant for subduction zones have single-crystal anisotropies that are as strong as or stronger than that of olivine, including antigorite (shear wave anisotropy AVs = 68% in the compilation of *Mainprice and Ildefonse* [2009]), talc (AVs = 68%), chlorite (AVs = 76%), hornblende (AVs = 31%), brucite (AVs = 31%), and phase A (AVs = 18%).

[34] For the shallow part of the mantle wedge, serpentine minerals such as antigorite are probably relevant to our understanding of seismological indicators of anisotropy, as they have strong intrinsic single-crystal anisotropies [e.g., *Kern*, 1993; *Mainprice and Ildefonse*, 2009; *Mookherjee and Capitani*, 2011]. Until recently, little was known about fabric development in serpentinite minerals, but recent work on serpentinite LPO from both experiments [e.g., *Katayama et al.*, 2009] and petrographic examination of natural samples [e.g., *van de Moortèle et al.*, 2010; *Bezacier et al.*, 2010; *Nishii et al.*, 2011; *Jung*, 2011] has begun to suggest relationships between deformation geometry and the resulting seismic anisotropy. Because of the strong single-crystal anisotropy of antigorite and other serpentinite minerals, even if serpentinite is only present in relatively thin layers
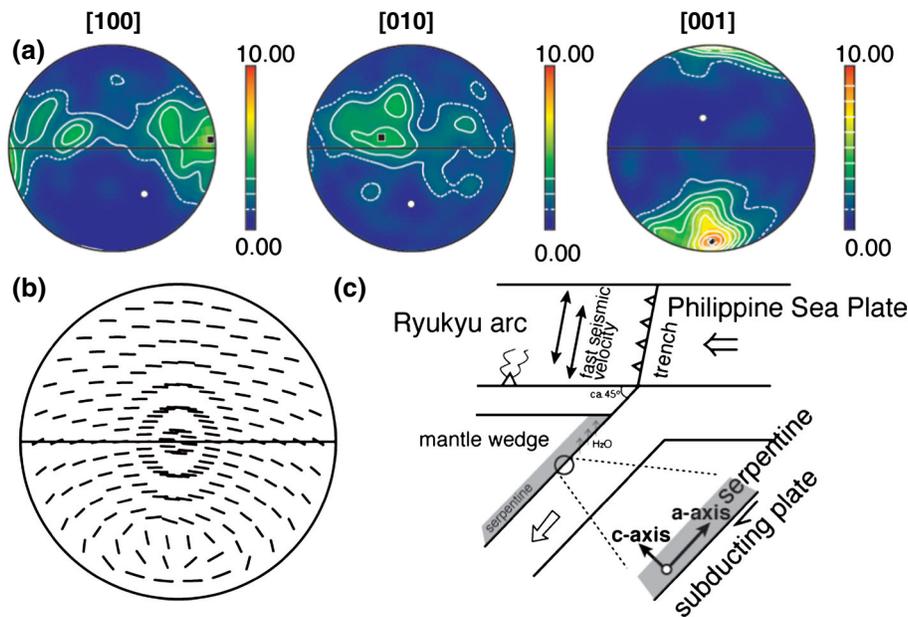
Figure 10. Illustration of the possible effect of serpentinite LPO on subduction zone anisotropy. (a) Pole figures (equal-area lower-hemisphere projections) of crystallographic orientation of deformed antigorite for a sample deformed at 300°C to 200% strain. Horizontal line corresponds to the (dextral) shear direction. There is a strong concentration of [001] axes normal to the shear plane and a relatively weak concentration of [100] axes subparallel to the shear direction (the [001] axis of single-crystal antigorite is much slower than the [100] (fast) and [010] (intermediate) axes, leading to a maximum single-crystal shear wave anisotropy of 68% [*Mainprice and Ildefonse*, 2009]). (b) Predicted patterns of shear wave splitting for the experimentally determined LPO shown in Figure 10a. The predicted polarization of the fast shear wave for each possible wave propagation direction is shown. (c) Schematic cartoon of proposed contribution from antigorite anisotropy beneath the Ryukyu arc. Deformation of serpentine is concentrated in a relatively thin layer above the subducting plate, with the seismically slow axis (c axis) aligning normal to the plate interface. This results in a strong anisotropy with trench-parallel fast direction in the forearc wedge. Figures from *Katayama et al*. [2009].

in the mantle, it may make a significant contribution to the observed anisotropy [e.g., *Katayama et al*., 2009; *Bezacier et al*., 2010]. In a series of experiments on serpentinite samples, *Katayama et al*. [2009] found that deformed aggregates exhibit an overall anisotropy with a slow axis aligned perpendicular to the shear plane and suggested that shear in a serpentinized layer directly above the dipping slab would result in trench-parallel fast splitting directions (Figure 10). Slightly different fabric geometries have been suggested based on natural samples; for example, *Jung* [2011] argued that horizontal shear of serpentine, rather than a dipping layer, provides a better match to seismological observations. More work is required to elucidate the relationships between deformation geometry and the resulting anisotropy in serpentine aggregates and to understand why deformation experiments and natural samples sometimes yield different views of the active slip systems in minerals such as antigorite [e.g., *Jung*, 2011]. It is clearly important, however, to consider the potential contributions of hydrous minerals such as antigorite to the anisotropic signature of subduction systems, given the large single-crystal anisotropies of many hydrous phases [e.g., *Mainprice and Ildefonse*, 2009] and the independent observational evidence for mantle wedge serpentinization [e.g., *Bostock et al*., 2002].

4. GEODYNAMICAL MODELING CONSTRAINTS

[35] As with the mineral physics aspects of subduction zone anisotropy, there is a huge body of literature on the geodynamic modeling of mantle flow in subduction systems, and a comprehensive review of this area is beyond the scope of this paper. Here I highlight a relatively small collection of (mostly recent) geodynamical modeling papers that have explicitly addressed the problem of modeling seismic anisotropy observations in subduction systems. For more comprehensive papers reviewing the state of the art in geodynamic modeling of subduction processes, I refer the reader to recent work by *Billen* [2008] and *Gerya* [2011].

4.1. Tools for Modeling and Linking Geodynamical Models to Seismological Observations

[36] A variety of numerical and laboratory modeling tools have been developed to simulate the process of subduction and gain insight into subduction geodynamics. Models of subduction (both numerical and analog) fall into two broad categories: fully dynamic models, in which the slab sinks under its own weight and undergoes deformation, and kinematic-dynamic models, in which the slab geometry and motion are defined in the model and the dynamic response of the surrounding mantle to the kinematic forcing

of the slab is examined. Each modeling approach has distinct strengths [*Billen*, 2008]: a fully dynamic model contains more realistic physics, and if no kinematic boundary conditions are applied, then no assumption must be made about the consistency between buoyancy-driven flow and flow induced by imposed boundary conditions. On the other hand, coupled kinematic-dynamic models have the advantage of being able to study local processes in greater detail than for fully dynamic models and easily incorporate realistic slab morphologies and kinematics. Such models cannot be used to study slab dynamics per se; however, they are useful for exploring the likely flow patterns in the wedge and sub-slab mantle that result from plate forcings such as downdip slab motion and trench migration.

[37] A crucial consideration in geodynamical modeling studies is the treatment of rheology. Many of the published studies that attempt to simulate the development of anisotropy due to mantle flow use a simplified Newtonian rheology, in which viscosity and stress (or strain rate) are linearly related. Such a rheology, which corresponds to deformation in the diffusion creep regime, is easier to implement in a numerical modeling code, but it represents a significant simplification for anisotropy studies. In order for LPO to develop, the deformation must be accommodated via dislocation creep, which implies a non-Newtonian, nonlinear viscosity with a stress exponent of $n \approx 3$. The use of a simplified Newtonian viscosity law in a flow model, therefore, does not correctly capture the rheology associated with dislocation creep and may not correctly predict some important aspects of subduction dynamics [e.g., *Billen*, 2008].

[38] Given the increasing interest in using geodyamical modeling frameworks to investigate the formation and evolution of anisotropic structure, many tools are available to predict seismological observables, such as shear wave splitting from the velocity fields produced in geodynamical models, and thus relate models to observations. A common simplified approach has been to calculate streamlines through a (usually instantaneous) velocity model and to compute the finite strain evolution along each streamline [*McKenzie*, 1979]. The relationship between finite strain and anisotropy is then approximated by locally applying an appropriate elastic tensor (based on olivine LPO studies) and assuming a fixed geometrical relationship between the finite strain axis and the elastic tensor. This approach has been applied in several different subduction zone modeling studies [e.g., *Fischer et al.*, 2000; *Hall et al.*, 2000; *Long et al.*, 2007]. Other methods for representing anisotropy based on simplifications of the full elastic tensor, such as the use of "directors" which indicate the easy glide plane of deformation, have also been investigated [*Lev and Hager*, 2008].

[39] A more complete way of simulating the development of the LPO of olivine (or other minerals) involves a statistical model of how the orientations of individual grains evolve with deformation. One such model, called D-Rex [*Kaminski et al.*, 2004], incorporates the effects of plastic deformation and dynamic recrystallization and is available as a software package that can be easily incorporated into numerical geodynamic models. Programs that explicitly model

texture development have some key advantages over simplified methods, including the ability to take into account any preexisting texture and the ability to accurately model the time-dependent evolution of LPO [e.g., *Kaminski and Ribe*, 2002]. (In contrast, simplified models based on the finite strain distribution assume that LPO adjusts instantaneously to changes in the strain geometry.) D-Rex has been applied by several different workers to model texture development in subduction systems [e.g., *Lassak et al.*, 2006; *Conder and Wiens*, 2007; *Morishige and Honda*, 2011; *Faccenda and Capitanio*, 2012, 2013]. Once a scheme has been used to predict elastic constants at different points in the model, various seismologic modeling tools can be applied to predict observable quantities such as shear wave splitting. These range from relatively simple raytracing schemes that progressively solve the Christoffel equation along the raypath [e.g., *Fischer et al.*, 2000; *Abt and Fischer*, 2008] to the computation of synthetic seismograms via reflectivity [e.g., *Becker et al.*, 2006] or pseudospectral [e.g., *Fischer et al.*, 2005] methods to the use of three-dimensional, finite-frequency splitting sensitivity kernels [e.g., *Favier and Chevrot*, 2003; *Chevrot*, 2006; *Long et al.*, 2008].

4.2. Two-Dimensional and 2.5-D Numerical Modeling Studies

[40] Simple two-dimensional flow patterns have been explored via numerical models by several workers, often in studies that were designed to reproduce specific regional splitting data sets. For example, *Fischer et al.* [2000] carried out a series of 2-D numerical models designed to mimic the geometry and kinematics of the Tonga subduction system, finding that the finite strain distribution predicted by a 2-D flow pattern was able to reproduce measurements of splitting well when combined with realistic parameters describing olivine LPO over the upper 410 km of the mantle. In a similar study, *Long et al.* [2007] modeled simple 2-D flow induced by a kinematically defined subducting slab with a geometry appropriate for the Ryukyu subduction system. Their study found that variations in wedge structure—for example, the inclusion of a low-viscosity region in the wedge corner—have a subtle effect on the predicted shear wave splitting patterns that is likely only detectable in regions with dense station coverage on the overriding plate.

[41] Another class of 2-D numerical models includes those that explicitly include the effect of olivine fabric transitions, in particular B-type olivine fabric, in the modeling framework. For example, *Long et al.* [2007] found that a region of B-type fabric in the wedge corner was needed to successfully match the observation of trench-parallel fast splitting directions observed in the Ryukyu forearc with a transition to trench-perpendicular ϕ in the backarc. In this study, however, the transition from A-type to B-type fabric was imposed in the model in a region chosen to maximize the fit between the model predictions and splitting observations. The effect of a transition to B-type fabric was systematically explored in the context of a

2-D corner flow by *Lassak et al.* [2006], who predicted splitting patterns at hypothetical station locations on the overriding plate for a generic subduction geometry with a B-type fabric transition imposed at different locations from the trench. The main goal of this study was to ascertain whether a B-type fabric transition could actually be detected using shear wave splitting data; *Lassak et al.* [2006] concluded that for regions with dense raypath sampling in the wedge mantle, such a fabric transition can indeed be resolved. A series of papers by *Kneller et al.* [2005, 2007, 2008], which also used 2-D models for wedge flow, introduced a more sophisticated treatment of olivine fabric that implemented a non-Newtonian rheology and predicted what regions of the wedge should be dominated by B-type fabric based on the stress, temperature, and hydration conditions. The work of *Kneller et al.* [2005, 2007] demonstrated that B-type fabric may indeed dominate in the shallow part of the wedge corner, where temperatures are low, stresses are high, water is present, and flow is more sluggish than elsewhere in the wedge. Even with the lower strain rates in the cold forearc corner of the wedge, the models of *Kneller et al.* [2005, 2007] predict sufficient strains (~100–300%) to produce detectable splitting with a trench-parallel fast direction in the forearc mantle. In a regionally specific model for the Ryukyu subduction system, *Kneller et al.* [2008] found that a 2-D model incorporating B-type fabric (Figure 11) successfully predicted observed patterns of shear wave splitting beneath Ryukyu, although they also suggested that a contribution from serpentinite anisotropy may be needed to explain the large delay times.

[42] Two-dimensional numerical models are more computationally efficient than fully three-dimensional models, but they involve assumptions that are often too reductive for realistic slab morphologies and kinematics. An interesting middle ground is the use of so-called 2.5-D models, in which a component of along-strike flow (that is, in the third dimension of the model) is permitted, but the model parameters and geometry are not permitted to vary along strike. Recent examples of this type of modeling approach that have been applied to study mantle flow and anisotropy in subduction systems include work by *Hall et al.* [2000] to explore the effect of overriding plate motion on mantle wedge flow and a study by *Conder and Wiens* [2007] which investigated the possibility of along-strike mantle flow in the mantle wedge beneath Tonga. In particular, *Conder and Wiens* [2007] (Figure 11) found that models with a low-viscosity region in the wedge and an imposed along-strike pressure gradient predicted rapid, channelized along-strike flow. Comparison between predicted and observed splitting patterns in the *Conder and Wiens* [2007] study revealed that the best fitting model involved very rapid trench-parallel mantle flow velocities (~50 cm/yr), considerably faster than plate-motion velocities. It is important to recognize, however, that this modeling study did not take into account the effects of 3-D flow around slab edges, and that the along-strike pressure gradient was imposed as an a priori constraint and did not arise naturally from the dynamics of the system.

4.3. Three-Dimensional Numerical Modeling Studies

[43] Fully three-dimensional numerical models, while computationally expensive, have the advantage of being able to explore the possibility of 3-D flow patterns in subduction systems. The possibility of toroidal flow around subducting slabs associated with retreating trenches has been investigated by many 3-D numerical modeling studies [e.g., *Stegman et al.*, 2006; *Piromallo et al.*, 2006; *Schellart et al.*, 2007; *Becker and Faccenna*, 2009; *Faccenda and Capitanio*, 2012, 2013] and a subset of these have directly addressed the anisotropic signature that likely results from such flow. For example, *Becker and Faccenna* [2009] explored the implications of a dynamic subduction model from *Becker and Faccenna* [2010] for mantle flow and anisotropy beneath subducting slabs, highlighting the strong component of trench-parallel flow beneath a retreating slab. A more recent modeling study by *Faccenda and Capitanio* [2012] (Figure 12) predicted finite strain and SKS splitting behavior for a fully dynamic retreating slab model; this study found that toroidal flow at a slab edge induces a deep layer of strong trench-parallel strain beneath a layer of entrained flow plate-motion-parallel strain immediately beneath the slab. These authors found that such an anisotropy configuration would result in ~0.5–1.3 s of *SKS* splitting with trench-parallel fast directions.

[44] Several different workers have implemented particularly high-resolution 3-D numerical models that are designed to explore the dynamics of individual subduction systems. For example, *Jadamec and Billen* [2010, 2012] implemented a series of fully dynamic models of flow at the corner of the eastern Alaska subduction system in which the shape of the slab was prescribed based on tomography and seismicity (Figure 13). They found that models with a non-Newtonian rheology predicted rapid toroidal flow around the edge of the slab that is efficiently decoupled from the plate driving forces. Predictions of finite strain distribution for their preferred Alaska flow model [*Jadamec and Billen*, 2010] compare well with observations of SKS splitting in the region. *Kneller and van Keken* [2007] carried out 3-D kinematic-dynamic slab models with slab morphologies appropriate for modeling the Mariana and southern Andean systems and found that lateral variations in slab dip can induce local trench-parallel stretching in the mantle wedge for systems where the slab motion is purely downdip. They generalized this result to other slab morphologies in a subsequent paper [*Kneller and van Keken*, 2008], concluding that layers of trench-parallel stretching of thickness 20–60 km can be created in the mantle wedge for complex slab morphologies (Figure 13). They also found evidence for strong toroidal flow at the slab edges that produces a component of trench-parallel wedge flow, but this effect is localized to within 50–100 km of the slab edge.

[45] Most three-dimensional numerical models of mantle flow in subduction systems have focused either on the wedge mantle [e.g., *Kneller and van Keken*, 2007, 2008] or on slab edges [e.g., *Jadamec and Billen*, 2010, 2012; *Faccenda and Capitanio*, 2012]. Recent work by *Paczkowski* [2012] was aimed at modeling mantle flow beneath subduction systems, with a focus on understanding what conditions might induce
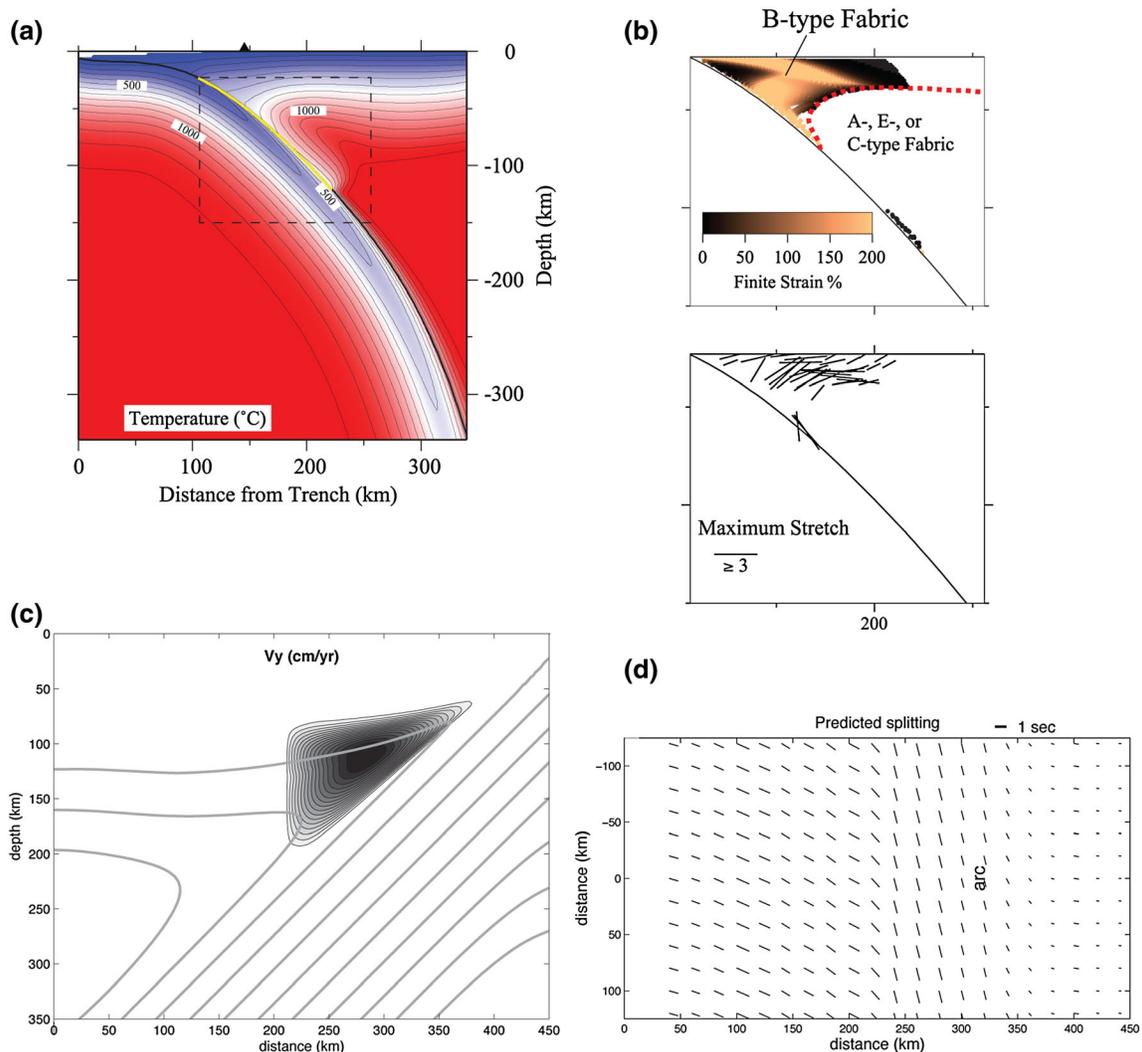
(a)

(b) B-type Fabric

(c)

(d)

Figure 11. Examples of 2-D or 2.5-D flow modeling studies for the mantle wedge. (a and b) Results from a model of B-type olivine fabric in the Ryukyu subduction zone (*Kneller et al.*, 2008). Figure 11a shows steady state thermal structure of a representative model; the temperature at which the transition to B-type fabric takes place is approximately 800°C. Figure 11b shows development of B-type fabric in the wedge corner. Top panel shows the amount of finite strain developing in the B-type region, with the dashed red line indicating the transition between B-type and A-, C-, or E-type fabric. Bottom panel shows the geometric distribution of finite strain axes in the part of the wedge dominated by B-type fabric. Figures from *Kneller et al.* [2008]. (c and d) Results from a 2.5-D model of along-strike mantle wedge flow in the Tonga subduction zone (*Conder and Wiens*, 2007). Figure 11c shows along-strike flow calculated for a model with an imposed low-viscosity channel beneath the arc and a trench-parallel pressure gradient of 4 kPa/km. Grayscale with contour lines indicate arc-parallel flow velocities (maximum value is 48 cm/yr). Figure 11d shows predicted fast splitting directions from the flow model for local *S* phases (originating in the subducting slab) at the surface, with the orientation and length of the bars indicating the fast direction and magnitude, respectively. Figures from *Conder and Wiens* [2007].

a strong component of trench-parallel flow beneath subducting slabs. Her modeling approach used a kinematically defined slab and took into account the background mantle flow (as described by a global convection model) to investigate the interactions among slabs, background flow, and trench migration. She found that slabs may deflect mantle flow beneath them, inducing a strong component of trench-parallel subslab flow, for cases with little or no coupling between the slab and the subjacent mantle. She further found that trench-parallel flow beneath slabs is enhanced for systems with steep slab dips and suppressed for systems with shallowly dipping slabs or slabs that do not reach into the mid-mantle.

[46] Three-dimensional numerical modeling has also been used to investigate the possibility of small-scale convection processes in subduction systems, particularly in the mantle wedge. For example, *Behn et al.* [2007] used a numerical model to investigate a scenario in which dense lower crustal material beneath volcanic arcs periodically becomes gravitationally unstable and founders, resulting in complicated small-scale variability in the flow field (Figure 13). These
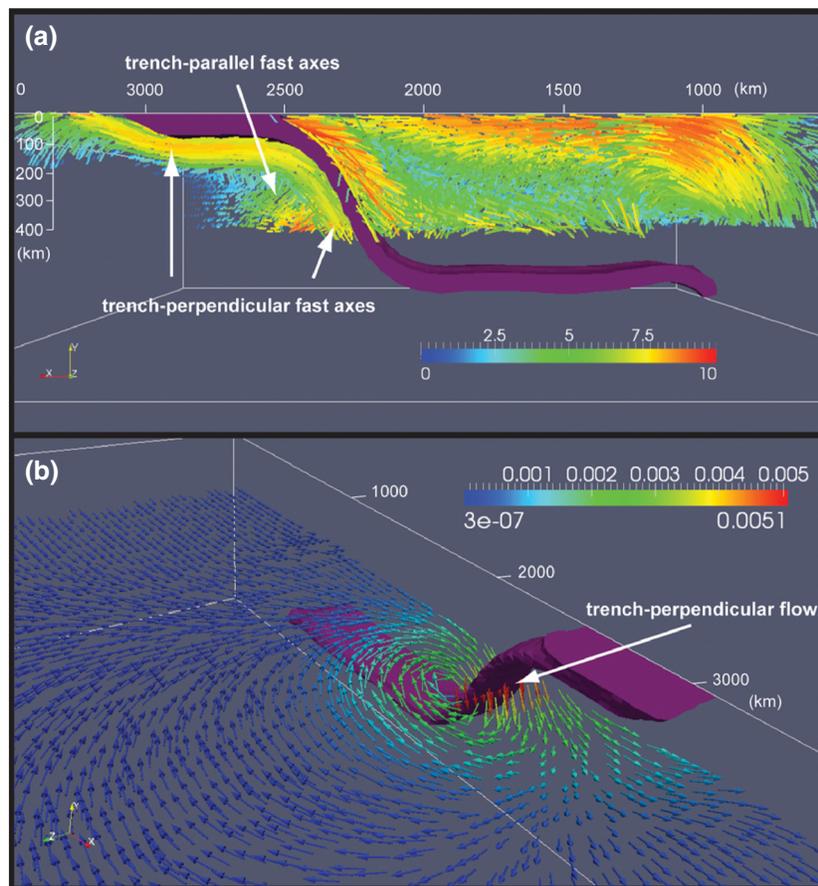
Figure 12. Example from a 3-D numerical modeling study of the sub-slab mantle, from *Faccenda and Capitanio* [2012]. (a) Side view of the model showing the development of seismic anisotropy (colored bars). Purple surface is the contour of the density field around the subducting plate. Bars represent the orientation of the symmetry axis of anisotropy (based on a hexagonal symmetry class); length and color are proportional to the amount of anisotropy. White arrows indicate a layer of trench-perpendicular fast axes directly beneath the subducting slab (due to entrained flow) and a deep zone of trench-parallel fast axes beneath this layer (due to toroidal flow). (b) Oblique view of the velocity field at 300 km depth associated with this model. Figures from *Faccenda and Capitanio* [2012].

authors found that crustal foundering will result in predominantly trench-parallel stretching beneath the arc and proposed that this mechanism may explain the complex and variable splitting patterns observed in many mantle wedges.

4.4. Laboratory Experimental Studies

[47] Experimental studies of subduction dynamics, which simulate the motions of the mantle using analog materials in a laboratory setting, provide a good complement to numerical modeling studies. Laboratory experiments do not suffer from some of the problems of numerical models, such as limited spatial resolution, challenges in creating a suitable mesh on which to solve physical equations, and numerical noise or dispersion. Studies that have sought to create laboratory subduction models include those that use a kinematically defined, rigid slab [e.g., *Kincaid and Griffiths*, 2003, 2004] and those that use a dynamic slab [e.g., *Schellart*, 2004; *Funiciello et al.*, 2004, 2006]. Only a few laboratory studies have specifically sought to model the development of seismic anisotropy in subduction systems [*Buttles and Olson*, 1998; *Druken et al.*, 2011].

A key aspect of this work is establishing an observable that contains information about anisotropy development in the deforming fluid. One strategy is to seed the mantle analog fluid with small whiskers that have nearly neutral buoyancy and a large aspect ratio. Whiskers in a glucose syrup "mantle" will locally align with the finite strain field and can thus be used as a proxy for anisotropic geometry [*Buttles and Olson*, 1998].

[48] An early laboratory study of anisotropy development in subduction systems was carried out by *Buttles and Olson* [1998] using a kinematic-dynamic slab model that investigated the effect of trench rollback (of a vertical plate) and downdip motion of the slab separately. This study investigated anisotropy development in both the wedge and the sub-slab mantle. For the slab rollback model, *Buttles and Olson* [1998] found efficient trench-parallel alignment of finite strain directions beneath the slab due to toroidal sub-slab flow. The downdip slab model produced a wedge anisotropy field characterized by a horizontal layer of plate-motion-parallel finite strain directly beneath the overriding plate, a slab-parallel layer directly above the slab,
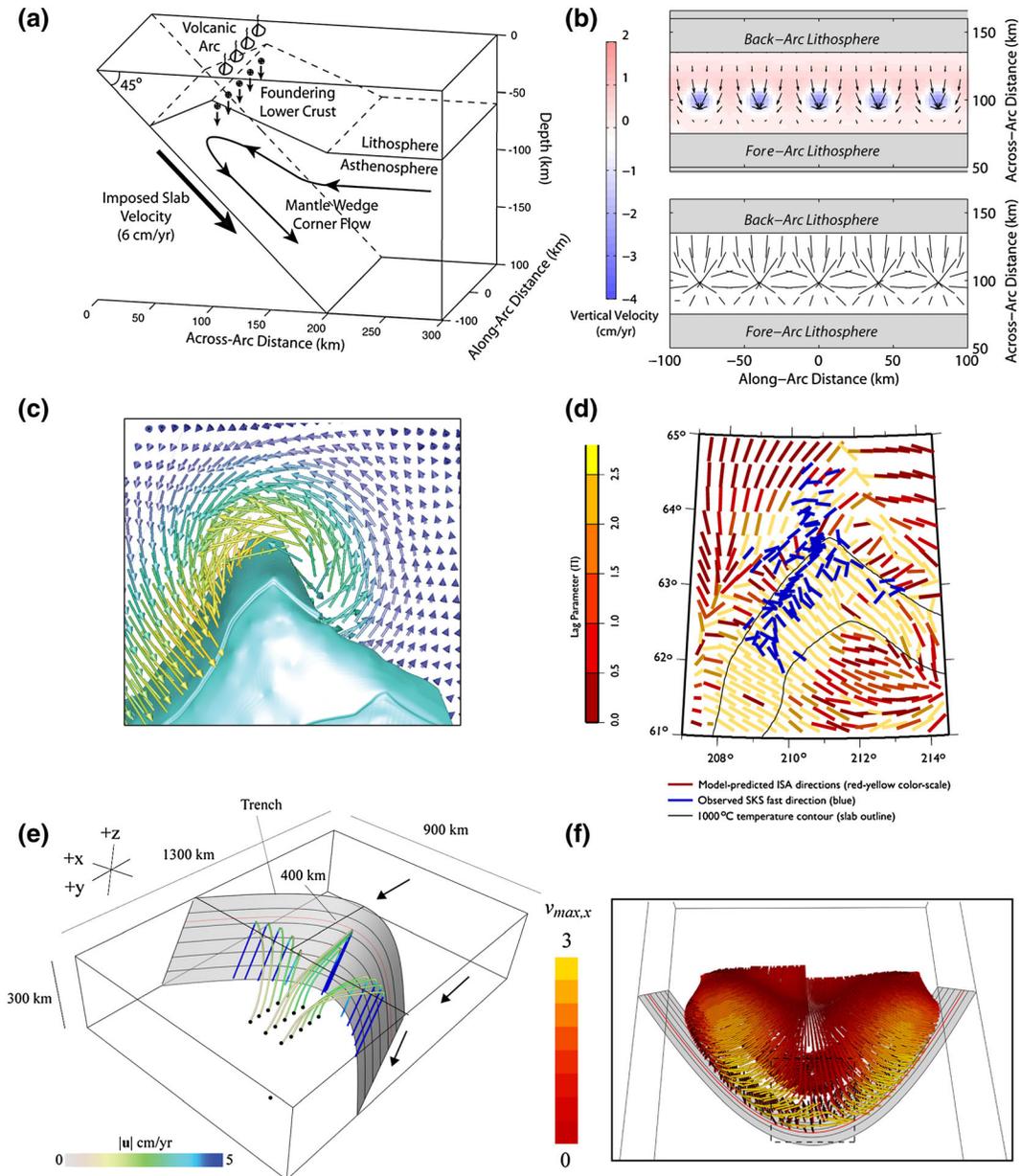
Figure 13. Examples from three-dimensional flow modeling studies of wedge anisotropy. (a and b) Results for the crustal foundering model of *Behn et al.* [2007]. In Figure 13a, schematic diagram of model setup is shown. In Figure 13b, map view of predicted anisotropy signature from crustal foundering is shown. Top panel shows the orientation of the (horizontal components of) mantle velocities; bottom panel shows the orientation and length of the long axis of the finite strain-rate ellipsoid. Foundering produces 3-D flow in the mantle wedge and coherent regions of trench-parallel shear beneath the volcanic arc. Figures from *Behn et al.* [2007]. (c and d) Results from a model of flow around the corner of the Alaska slab [*Jadamec and Billen*, 2010]. Figure 13c is a map view of horizontal velocity vectors (arrows, color coded by velocity magnitude), clearly showing anticlockwise toroidal flow around the edge of the slab (blue surface). Figure 13d is the predicted infinite strain axes (ISA) (red-yellow bars) for the flow model shown in Figure 13c. Bars are oriented in the direction of the ISA and colored by the value of the lag parameter *Π* [*Kaminski and Ribe*, 2002], an indication of how quickly olivine LPO is expected to adjust to changes in the flow field. When *Π* < 1 (red values), the ISA orientation provides a good estimate of seismic anisotropy orientation. Blue bars indicate observed SKS fast directions. Figures from *Jadamec and Billen* [2010]. (e and f) Results from a model investigating the effect of slab morphology on wedge flow (*Kneller and van Keken*, 2008). Figure 13e is an oblique view of slab geometry and flow lines for a curved slab model. Lines indicate flow trajectories, with the absolute value of velocity indicated with the color (maximum value 5 cm/yr). Figure 13f is a map view of finite strain accumulation in the wedge for this model after 17 Ma of (steady state) deformation; bars indicate the local orientation of the finite strain axis, colored by the magnitude of the maximum stretch. There is a zone of strong trench-parallel stretching in the wedge corner (yellow region). Figures from *Kneller and van Keken* [2008].

and a region in the core of the wedge with nearly randomly oriented finite strain markers. *Buttles and Olson* [1998] carried out one hybrid experiment with both downdip motion and rollback, finding that this configuration was much less efficient at generating trench-parallel sub-slab finite strain alignments than rollback motion alone. A more recent study by *Druken et al.* [2011] carried out a systematic study of finite strain alignment in the wedge for models with both downdip motion and slab rollback, finding that models with rollback and accompanying modest extension in the overriding plate resulted in enhanced rollback-parallel (that is, trench-perpendicular) finite strain alignment in the central part of the backarc region. Such a model may explain the strong trench-perpendicular *SKS* splitting observed in the backarc of the Cascadia subduction system [*Druken et al.*, 2011].

5. CONCEPTUAL MODELS FOR SUBDUCTION ZONE ANISOTROPY AND MANTLE FLOW

[49] The seismologic observations, geodynamic modeling experiments, and mineral physics constraints described above have been synthesized into a large number of conceptual models for upper mantle seismic anisotropy in various parts of subduction systems (the wedge, slab, and sub-slab mantle). Here I provide a brief overview of the many conceptual models that have been proposed to explain subduction zone anisotropy and discuss each in light of the integrated constraints provided by various disciplines.

5.1. Models for the Sub-slab Mantle

[50] As discussed in section 2.2.3, observations of shear wave splitting beneath subducting slabs are considerably simpler than those in the mantle wedge, with the majority of subduction systems exhibiting trench-parallel sub-slab fast directions. Three different conceptual models have been proposed that may explain both the dominantly trench-parallel ϕ beneath slabs as well as the occasional exceptions: the trench-parallel flow model, the B-type olivine fabric model, and the strong radial anisotropy model of entrained asthenosphere.

[51] The trench-parallel flow model was first proposed by *Russo and Silver* [1994] to explain trench-parallel sub-slab splitting beneath South America. It has subsequently been invoked in several individual subduction systems [e.g., Kamchatka, *Peyton et al.*, 2001; Calabria, *Civello and Margheriti*, 2004; *Baccheschi et al.*, 2007; Caribbean, *Piñero-Felicangeli and Kendall*, 2008; Scotia, *Müller et al.*, 2008; Hikurangi, *Marson-Pidgeon and Savage*, 1997] and generalized to explain the global sub-slab splitting data set [*Long and Silver*, 2008, 2009]. *Long and Silver* [2008] documented a correlation between the strength of sub-slab splitting delay times—taken to be a proxy for the strength and coherence of the sub-slab flow field—and the absolute value of trench migration rates in a Pacific hotspot reference frame. This correlation was interpreted to support a model in which slabs that are migrating rapidly induce a strong toroidal component to the mantle flow field that results in a strong component of trench-parallel flow directly beneath

the slab, while subduction systems with nearly stationary trenches tend to have weaker anisotropy.

[52] An important caveat to this conceptual model of dominantly trench-parallel flow beneath subducting slabs is that it is the geometry of finite strain, rather than flow velocity direction per se, that controls the geometry of anisotropy. As originally envisioned by *Russo and Silver* [1994], the dominantly trench-parallel horizontal mantle flow velocities beneath the slab must be accompanied by vertical gradients in flow velocity in order to produce trench-parallel strain. Subsequent numerical modeling work has specifically addressed the finite strain distribution in the sub-slab mantle for models that exhibit dominantly trench-parallel sub-slab flow. Specifically, *Paczkowski* [2012] calculated the finite strain field for models in which background mantle flow is deflected by a subducting slab and is forced to flow laterally beneath the slab; in these types of models, the finite strain directions align efficiently in a trench-parallel direction, very close to the average sub-slab mantle flow velocity.

[53] The trench-parallel sub-slab flow model requires a high degree of mechanical decoupling between the slab and the subjacent mantle as well as a barrier to entrained mantle flow at depth, likely associated with the 660 km discontinuity [*Russo and Silver*, 1994; *Long and Silver*, 2008; *Paczkowski*, 2012]. In the context of this conceptual model, exceptions to the trench-parallel rule can be interpreted as either reflecting 2-D entrained flow enabled by enhanced local sub-slab coupling (perhaps correlated with young slab age) [*Long and Silver*, 2009] or as being due to the slab geometry. The geodynamical plausibility of the trench-parallel sub-slab flow model was recently tested by *Paczkowski* [2012], who found that trench-parallel flow should dominate in many subduction systems as long as slabs are efficiently decoupled from the mantle beneath them. A recent numerical modeling study by *Faccenda and Capitanio* [2012] that implemented a fully dynamic subduction zone model with full mechanical coupling (and a non-Newtonian rheology) found that toroidal flow around the slab edge results in a deep anisotropic layer with trench-parallel fast directions beneath a layer of entrained sub-slab flow. Such a view of three-dimensional flow beneath a retreating slab is conceptually similar to the models of *Russo and Silver* [1994] and *Long and Silver* [2009], although different in its details. This model may explain trench-parallel *SKS* splitting near the edges of retreating slabs, but it may have difficulty matching the observations in systems such as Tonga that exhibit large delay times (~2–3 s). Specifically, if a thick (~100 km) layer of anisotropy with a fast direction parallel to the downgoing plate motion were present directly beneath the Tonga slab, then unreasonably strong anisotropy in the deeper layer would be needed to overcome the splitting contributed by the sub-slab layer and produce 2–3 s of splitting with a trench-parallel ϕ.

[54] The pressure-induced B-type fabric model was proposed by *Jung et al.* [2009] as an alternative to the trench-parallel flow model. Taken at face value, the experimental

results of *Jung et al.* [2009] suggest that the upper mantle should be dominated by B-type fabric at depths greater than ~90 km, rather than the more commonly assumed A-type. As pointed out by *Jung et al.* [2009], one of the major implications of the work is that if B-type fabric dominates beneath subducting slabs, then two-dimensional entrained flow would result in trench-parallel sub-slab fast splitting directions. In the context of this model, exceptional subduction systems that exhibit trench-normal fast directions might reflect local trench-parallel flow.

[55] Recently, *Song and Kawakatsu* [2012] proposed another explanation for trench-parallel sub-slab splitting, which invokes a layer of suboceanic asthenosphere entrained beneath subducting slabs. This model requires that the suboceanic asthenosphere is everywhere characterized by both strong radial anisotropy (that is, with $V_{SH} > V_{SV}$, or horizontally polarized shear waves traveling faster than vertically polarized ones) and relatively weaker azimuthal anisotropy. Upper mantle anisotropy has often been approximated in terms of hexagonal symmetry; for the case of hexagonal anisotropy with a horizontal symmetry axis, one would expect to observe modest $V_{SH} > V_{SV}$ radial anisotropy with stronger azimuthal anisotropy [e.g., *Karato et al.*, 2008]. *Song and Kawakatsu* [2012] argue that the oceanic asthenosphere is instead characterized by orthorhombic anisotropy with a strong radial component and weaker azimuthal component, which may require the presence of horizontally aligned sheets of melt (the so-called "millefeuille" asthenosphere model) [*Kawakatsu et al.*, 2009]. If such anisotropy is translated to depth beneath a subducting slab, then vertically propagating shear phases would undergo splitting with a trench-parallel fast direction as long as the dip of the slab was large enough (greater than about 25°) [*Song and Kawakatsu*, 2012]. For shallower slabs, the *Song and Kawakatsu* [2012] model would predict trench-normal *SKS* fast directions, which are in fact observed in several systems with shallowly dipping slabs [e.g., Mexico, *Léon Soto et al.*, 2009; Cascadia, *Currie et al.*, 2004].

[56] Which of these models correctly describes seismic anisotropy and mantle flow beneath slabs? Each of these models has strengths and weaknesses, but to first order, each is able to correctly predict both the global preponderance of trench-parallel sub-slab fast splitting directions and the substantial minority of subduction systems that exhibit trench-normal ϕ. Arguments against the *Jung et al.* [2009] model come mainly from the rock record and from observations of seismic anisotropy beneath ocean basins. Specifically, azimuthal anisotropy beneath ocean basins is generally consistent with the predictions from simple geodynamical models (which mainly invoke plate-driven shear in the asthenosphere) combined with A-type or similar olivine fabric [e.g., *Becker et al.*, 2003; *Conrad et al.*, 2007]. This simple framework would be completely inconsistent with the presence of B-type fabric, which suggests that B-type fabric is not ubiquitous in the mantle at depths greater than ~90 km. Additionally, petrographic investigation of mantle-derived rocks reveals that the vast majority of samples exhibit A-type

(or similar) fabric, rather than B-type [e.g., *Ben Ismail and Mainprice*, 1998; *Karato et al.*, 2008]. Therefore, the pressure-induced B-type fabric model must be validated with additional experiments (particularly to rule out whether variations in stress, rather than pressure, might have produced the observed fabric transition) and reconciled with seismologic and petrographic observations in order to be considered a viable model for sub-slab anisotropy.

[57] The trench-parallel sub-slab flow model and the entrained oceanic asthenosphere model (Figure 14) remain viable explanations for the global patterns of sub-slab shear wave splitting, and discriminating between these models is a task with immediate importance (and consequential implications) for researchers who observe and/or model sub-slab anisotropy. One frustrating difficulty in discriminating between the models is that they both make similar predictions for sub-slab splitting for steeply dipping versus shallowly dipping slabs: both models would predict trench-parallel ϕ for steep slab dips and trench-normal ϕ for shallow dips [*Song and Kawakatsu*, 2012; *Paczkowski*, 2012]. A second challenge is that for most subduction zones, constraints on sub-slab splitting come mainly from *SKS* phases with nearly vertically propagating ray paths that have been (imperfectly) corrected for the effect of the mantle wedge [*Long and Silver*, 2009]. A key prediction of the *Song and Kawakatsu* [2012] model is that striking variations in measured splitting parameters for different propagation paths through the sub-slab region (that is, different incidence angles and back azimuths) should be observed. This prediction is somewhat difficult to test with *SKS* data sets only, but phases such as *S* or *ScS* at teleseismic distances can increase the coverage in incidence angle and initial polarization direction, as long as any contribution from anisotropy near the source is ruled out. Another promising approach is to construct detailed datasets of sub-slab splitting parameters for a variety of source depths and propagation directions from source-side splitting studies [e.g., *Foley and Long*, 2011; *Lynner and Long*, 2013]. In a recent study, *Lynner and Long* [2013] argued that source-side splitting measurements beneath the Scotia and Caribbean subduction zones were more consistent with along-strike sub-slab mantle flow than with the entrained asthenosphere model. However, this result is far from universal, and future studies that quantitatively test the predictions of the two models in different regions will be crucial in resolving this important question.

[58] Another possibility is that none of the conceptual models proposed so far correctly describes the pattern of mantle flow beneath slabs. In particular, a great deal of work remains to be done to explore what types of three-dimensional flow patterns can produce distributions of finite strain beneath slabs that are consistent with observations of trench-parallel fast splitting directions. Anisotropy is a consequence of finite strain, so flow patterns that include a gradient in flow velocity along strike will produce some component of trench-parallel strain. The simplest 2-D models of entrained flow beneath slabs do not include such a gradient, so a significant component of along-strike (that is, toroidal) mantle flow is likely needed to produce
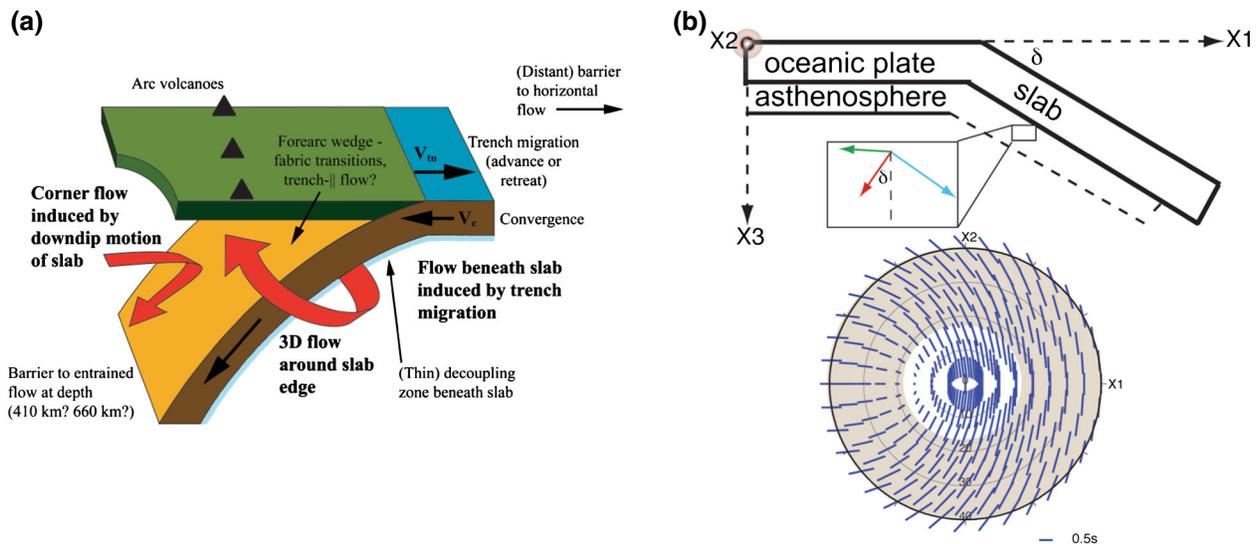
Figure 14. Cartoon sketch of two plausible models for sub-slab mantle flow and the resulting anisotropy. (a) The trench-migration-controlled model of *Long and Silver* [2008], in which sub-slab flow is primarily trench-parallel. This flow field is enabled by a thin decoupling zone beneath the subducting slab, a barrier to entrained flow at depth (which may correspond to the viscosity jump at the 660 km discontinuity), and a distant lateral barrier to horizontal flow. This model would predict trench-parallel stretching beneath the slab for relatively steeply dipping slabs (Paczkowski, 2012) and may thus explain trench-parallel sub-slab fast directions. Figure from *Long and Silver* [2008]. (b) The model of *Song and Kawakatsu* [2012] (top panel) proposes an effective orthorhombic symmetry (represented by the blue, red, and green arrows) for the oceanic asthenosphere, which is translated to depth beneath the subducting slab. Predictions of shear wave splitting (bottom panel) are shown, as stereo plots for a model with a slab dipping at 40° are plotted with blue bars representing the fast axis and delay time for a range of incidence angles and back azimuths. X_2 represents the orientation of the trench. The direction of the bar represents the polarization of the fast wave projected on the horizontal plane. The range of incidence angles for *SKS* phases are shown with white background colors; for direct *S* phases, the incidence angle range is shown with gray background colors. The plot goes out to an incidence angle of 40°. Figures from *Song and Kawakatsu* [2012].

significant trench-parallel stretching. One way to produce trench-parallel finite strain is via dominantly trench-parallel sub-slab flow [e.g., *Paczkowski*, 2012], but other flow scenarios are certainly possible. Much more geodynamical modeling work must be done to answer the question of how strong the along-strike gradients in sub-slab flow need to be in order to produce dominantly trench-parallel finite strain beneath subducting slabs and to match the splitting observations.

5.2. Models for Slab Anisotropy

[59] Seismic anisotropy within the slab itself is a potentially important contributor to the anisotropic signature of subduction systems, but it typically receives less attention than the wedge or the sub-slab mantle. Despite the observational difficulties described in section 2.2.2, the slab remains an important part of subduction systems to understand from an anisotropy point of view. There are two major classes of models for anisotropy within subducting slabs: those that invoke frozen-in anisotropic structure in the oceanic lithosphere and those that invoke anisotropy due to faulting and hydration in the shallow part of the slab.

[60] The "frozen lithospheric anisotropy" model follows from the predictions of the classical model for anisotropy in the oceanic lithosphere-asthenosphere system. In this view, anisotropic structure is created in the asthenosphere

due to (roughly) horizontal shear created as the lithosphere moves over the asthenosphere. As the lithosphere moves away from spreading centers and cools, it becomes mechanically rigid and hard to deform, and anisotropic structure from past deformation is "frozen" into the plate [e.g., *Forsyth*, 1975; *Nishamura and Forsyth*, 1989]. If this view of anisotropy within the oceanic lithosphere is correct, then it suggests that subducting slabs ought to have frozen anisotropy with a geometry that reflects the fossil spreading direction at the time the lithosphere was formed. For the case where the oceanic lithosphere has experienced changes in plate motions over its history, the resulting structure will reflect multiple layers of anisotropy, and this represents a potential complication in the interpretation of slab anisotropy.

[61] As an alternative to this model, *Faccenda et al.* [2008] proposed that the anisotropic structure of slabs might be modified by hydration and faulting. Specifically, this model invokes widespread hydration of faults in the downgoing slab that result from bending at the outer rise (or other mechanisms). These faults may penetrate relatively deeply (up to tens of kilometers) and are likely pervasively serpentinized [*Faccenda et al.*, 2008; *Healy et al.*, 2009]. *Faccenda et al.* [2008] propose that a combination of LPO and SPO of highly anisotropic serpentinite minerals may produce effective anisotropy with a trench-parallel fast axis

and may cause large (up to ~1 s or more) splitting of vertically propagating *SKS* phases measured at forearc stations.

[62] Given the sparse constraints on slab anisotropy, it is somewhat difficult to discriminate between these two models. One of the few direct observations of fossil anisotropy in a subducting slab comes from the work of *Song and Kim* [2012b] and *Audet* [2013], who found evidence for anisotropy in the downgoing Cocos slab [*Song and Kim*, 2012b] as well as in other regions [*Audet*, 2013]. *Song and Kim* [2012b] further suggested that fossil lithospheric anisotropy may be a ubiquitous feature in the subducting oceanic mantle and that the strength of this anisotropy might contain information about past spreading rates at mid-ocean ridges. More work is needed, however, to test whether this prediction is borne out in other subduction systems.

[63] The serpentinized fault model of *Faccenda et al.* [2008] was originally proposed as an explanation for *SKS* fast splitting directions, but other workers have argued that it may be difficult to produce large delay times via anisotropy in a small region of the subducting slab [*Long and Silver*, 2009]. *Foley and Long* [2011] explicitly considered the possibility that serpentinized faults might be contributing to a source-side splitting data set but found significant splitting from events originating beneath the serpentinite stability field, which ruled out this mechanism as the primary contributor to their data set. One of the very few datasets which has been able to place tight constraints on the magnitude of anisotropy in the shallow part of the slab is that of *Huang et al.* [2011a], who found only a modest contribution to splitting from the shallow part of the slab, with delay times of a few tenths of a second. While aligned serpentinized cracks is a likely explanation for the observed anisotropy [*Huang et al.*, 2011a], this study would seem to rule out a large contribution (~1–2 s delay times) to *SKS* splitting from such a mechanism, at least in this region.

5.3. Models for the Mantle Wedge

[64] A very large number of conceptual models have been proposed to explain observations of seismic anisotropy in the mantle wedge, in part due to the complexity in shear wave splitting patterns and other observations of wedge anisotropy. The discussion of different models for wedge anisotropy presented here is based on the more comprehensive treatment contained in *Long and Wirth* [2013], and I refer the reader to this paper for additional details.

[65] The classical 2-D corner flow model for the mantle wedge [*McKenzie*, 1969] should result in generally convergence-parallel fast splitting directions throughout the wedge for simple LPO scenarios [e.g., *Hall et al.*, 2000; *Long et al.*, 2007]. The observation of dominantly trench-parallel ϕ in many subduction zone wedges has led to many alternative models for wedge anisotropy that variously invoke variations in fabric or mineralogy, the presence of trench-parallel flow, small-scale convective processes, or other mechanisms.

[66] The observation that changes in deformation conditions lead to changes in the resulting olivine LPO geometry [*Jung and Karato*, 2001; *Jung et al.*, 2006; *Katayama and Karato*, 2006] led to the B-type fabric model for wedge anisotropy. This invokes the presence of B-type olivine fabric as an explanation for the common observation of trench-parallel fast directions in the forearc part of the wedge [e.g., *Jung and Karato*, 2001; *Nakajima and Hasegawa*, 2004; *Long and van der Hilst*, 2006; *Kneller et al.*, 2008]. Another related model invokes the presence of deformed, aligned serpentinite minerals such as antigorite in the shallow part of the mantle wedge as a possible explanation for trench-parallel fast directions and large delay times in the forearc mantle [e.g., *Kneller et al.*, 2008; *Katayama et al.*, 2009; *Jung*, 2011; *Mookherjee and Capitani*, 2011].

[67] Another class of model that has been proposed to explain patterns of wedge anisotropy involves the concept of trench-parallel mantle flow in wedge systems. Models that invoke along-strike mantle flow may explain observations of trench-parallel ϕ in the backarc portion of the mantle wedge [e.g., *Smith et al.*, 2001; *Pozgay et al.*, 2007; *Abt et al.*, 2009], where the conditions needed for B-type or serpentinite LPO are unlikely to occur. Geodynamical modeling studies of trench-parallel flow have invoked along-strike pressure gradients due to effects such as trench migration [e.g., *Conder and Wiens*, 2007], rapid flow around a slab edge facilitated by a non-Newtonian rheology [e.g., *Jadamec and Billen*, 2010, 2012], or complex slab morphology [*Kneller and van Keken*, 2007, 2008]. Oblique subduction may also play a role in transporting material in an along-strike direction in mantle wedges [e.g., *Nakajima et al.*, 2006; *Bengtson and van Keken*, 2012] and may result in transpressive deformation in the shallow part of the mantle wedge [e.g., *Mehl et al.*, 2003].

[68] Yet another class of model for mantle wedge flow invokes the presence of small-scale convective processes as a perturbation to the corner flow field. The lower crustal foundering model of *Behn et al.* [2007] would predict a mantle wedge flow field that is dominated by small-scale downwellings. Small-scale convection, which is thought to be present beneath old oceanic lithosphere, may be present in some mantle wedges [e.g., *Honda and Yoshida*, 2005; *Honda*, 2011; *Wirth and Korenaga*, 2012], although the presence of small-scale convection likely requires relatively low wedge viscosities [*Wirth and Korenaga*, 2012]. Small-scale convection, whether controlled by the wedge viscosity structure and/or by the presence of gravitationally unstable lower crust, is likely to result in a very complicated pattern of anisotropy in the mantle wedge [e.g., *Behn et al.*, 2007; *Morishege and Honda*, 2011].

[69] *Long and Silver* [2008] proposed a hybrid model that incorporates aspects of both the classical 2-D corner flow scenario and trench-parallel flow induced by trench migration. In this view, flow in the mantle wedge is controlled by a competition by the 2-D flow field, induced by downdip motion of the slab, and along-strike flow, induced by pressure gradients that result from trench migration. As with all models that invoke a component of along-strike flow, the details of the wedge viscosity structure are crucial to this model, and a low-viscosity region is likely necessary for trench migration to successfully drive along-strike wedge

flow [e.g., *Conder and Wiens*, 2007]. For the case of an isoviscous wedge, trench rollback will actually tend to enhance trench-perpendicular flow throughout most of the wedge volume, except for localized regions at the slab edges [*Druken et al.*, 2011].

[70] While the classical model for wedge anisotropy invokes solid-state deformation and LPO of olivine or other minerals, it is certainly possible that there may be a shape preferred orientation contribution to anisotropy as well. In particular, the presence of arc volcanism at the surface in most subduction systems suggests that partial melt must be present somewhere in the mantle wedge. If this melt is aligned by deformation, the bulk medium may have an effective anisotropy on a length scale relevant to seismic waves [e.g., *Zimmerman et al.*, 1999; *Vauchez et al.*, 2000; *Holtzman and Kendall*, 2010]. The presence of partial melt may also affect the geometry of olivine LPO in the surrounding matrix, in addition to providing an SPO effect [*Holtzman et al.*, 2003].

[71] The recent work of *Long and Wirth* [2013] directly tested the predictions made by the many conceptual models for wedge anisotropy against observations. We concluded that none of the models that have been proposed to explain anisotropy in the mantle wedge matches all of the available observations globally. Some models cannot be discarded completely but can be ruled out as first-order explanations in most subduction systems. For example, the major prediction of the melt SPO model—the observation of a sharp, localized signal from melt-related anisotropy directly beneath the arc—has only rarely been observed. A sharp change in splitting at the volcanic front has been documented in New Zealand and attributed to melt SPO [*Greve et al.*, 2008], although other studies invoke olivine LPO as the wedge as the explanation for the splitting pattern [*Morley et al.*, 2006], and an unambiguous signal from melt SPO beneath the volcanic front has not been identified in other regions.

[72] In general, models that seem to be the most plausible explanation for the anisotropic signal in a particular subduction system often do not do a good job of explaining observations in other regions. For example, the presence of serpentinite LPO is a leading candidate explanation for the strong splitting with trench-parallel ϕ observed in the Ryukyu forearc [e.g., *Kneller et al.*, 2008; *Katayama et al.*, 2009], and studies of anisotropy at the slab-wedge interface beneath Ryukyu have also found evidence for a contribution from serpentinite [*McCormack et al.*, 2013]. However, other subduction systems exhibit very small delay times due to wedge anisotropy at stations in the forearc (e.g., Central America [*Abt et al.*, 2009]; Indonesia [*Hammond et al.*, 2010]), and small splitting delay times in combination with anisotropic receiver function analysis rule out a major contribution from serpentinite LPO beneath northeastern Japan [*Wirth and Long*, 2010, 2012].

[73] The search for a single unified explanation for the anisotropic signature of the mantle wedge has so far been unsuccessful. *Long and Wirth* [2013] concluded that mantle wedge flow is likely controlled by a host of competing factors in any given subduction system, including downdip

motion of the slab, trench migration, ambient (background) mantle flow, small-scale convection, proximity to slab edges, and slab morphology. The lack of a single global model for wedge anisotropy presents a challenge for the interpretation of data sets in wedge regions, but it also presents an opportunity, in that the pattern of wedge anisotropy likely contains information about a host of subduction-related variables (e.g., wedge viscosity, distribution of hydrous minerals) that are often difficult to constrain observationally.

6. THE TRANSITION ZONE AND THE LOWERMOST MANTLE

[74] The main focus of this review has been to understand the constraints on upper mantle anisotropy in subduction systems. However, the anisotropic signature of slab dynamics in the deeper parts of the mantle—the transition zone, uppermost lower mantle, and the D″ layer in the lowermost mantle—represents a frontier area. Here I discuss recent observations of anisotropy in deep regions of the mantle and explore how continued progress in understanding the potential mechanisms for this anisotropy can lead to insight into deep subduction dynamics.

[75] A key question about the behavior of slabs as they descend into the deep mantle concerns the dynamic interaction between slabs and the mantle transition zone. As slabs descend through the transition zone and impinge on the more viscous lower mantle, they exhibit a range of behaviors, with some slabs easily penetrating the 660 km discontinuity while other slabs lie flat in the transition zone. Numerical simulations have explored the dynamic effect of transition zone discontinuities [e.g., *Tackley et al.*, 1993; *Davies*, 1995] and the viscosity jump at the 660 [e.g., *Bunge et al.*, 1996; *Tackley*, 1996] on mantle convection and the ability of slabs to penetrate to the lower mantle. Some studies have suggested the possibility of episodic slab ponding in the transition zone and subsequent mantle "avalanches" [e.g., *Pysklywec et al.*, 2003; *Pysklywec and Ishii*, 2005; *Capitanio et al.*, 2009]. Tomographic imaging of mantle heterogeneity indicates the presence of so-called "stagnant slabs" that seem to lie flat in the transition zone [e.g., *Fukao et al.*, 2001, 2009] and a variety of models to explain why some slabs (although not all) stagnate in the transition zone have been explored [e.g., *Billen*, 2010]. The two end-member behaviors of slabs in the transition zone—with some slabs easily penetrating the 660 km discontinuity and others flattening at transition zone depths— are likely associated with different patterns of deformation in the transition zone and uppermost mantle. Observations of seismic anisotropy at mid-mantle depths have the potential to resolve some of the outstanding questions relating to the dynamic interaction between slabs and the transition zone.

[76] Observations of seismic anisotropy in the transition zone and uppermost lower mantle are sparse but intriguing. Global surface wave inversions have found evidence for radial anisotropy in the transition zone (that is, a difference in propagation speed for vertically versus horizontally

polarized waves) [e.g., *Montagner and Kennett*, 1996; *Visser et al.*, 2008]. It appears that anisotropy in the uppermost part of the lower mantle may not be required by the data [*Visser et al.*, 2008]. *Trampert and van Heijst* [2002] presented a model of azimuthal anisotropy from surface wave overtones at transition zone depths and argued that this anisotropy is a global feature. More recent work based on surface wave tomography, however, has suggested that transition zone anisotropy is weak in most regions but is regionally strong in the vicinity of subducting slabs, implying that slabs impinging on the lower mantle produce strong deformation in the transition zone [*Montagner et al.*, 2012]. Recent shear wave splitting observations have provided some support for the idea that there is anisotropy in the mid-mantle near the Tonga subduction zone in particular, beginning with *Wookey et al.* [2002]. While there has been some controversy about the source of the splitting documented in that study [*Saul and Vinnik*, 2003], later papers have also documented mid-mantle anisotropy near the Tonga slab [*Chen and Brudzinski*, 2003; *Wookey and Kendall*, 2004; *Foley and Long*, 2011].

[77] The interpretation of mid-mantle anisotropy has been hampered by the lack of robust constraints on elasticity and fabric development in mid-mantle materials, and this represents an important avenue for future progress. For example, *Foley and Long* [2011] identified relatively strong ($\delta t \sim 1$ s) splitting due to mid-mantle anisotropy beneath the Tonga slab, with fast directions roughly parallel to the strike of the slab at depth, but the interpretation of these measurements in terms of mid-mantle deformation processes remains uncertain. Single-crystal elastic constants of transition zone and uppermost lower mantle minerals at the relevant pressure and temperature conditions are imperfectly known, but wadsleyite and perovskite in particular likely have significant intrinsic anisotropy [e.g., *Mainprice*, 2007]. If deformation in the transition zone is accommodated by dislocation creep, then LPO-induced anisotropy should result [e.g., *Tommasi et al.*, 2004]. Little is known, however, about LPO formation in the relevant minerals, and studies of LPO development at transition zone conditions are in a very early stage, with only a few published studies [e.g., *Kawazoe et al.*, 2013]. Anisotropy in the transition zone and uppermost lower mantle may be indicative of mid-mantle flow, likely induced by interaction between the slab and the ambient mantle [e.g., *Nippress et al.*, 2004], or it may reflect anisotropy within the slab itself [e.g., *Mookherjee*, 2011].

[78] The bulk of the lower mantle is generally thought to be isotropic, based on both observational and mineral physics considerations [e.g., *Meade et al.*, 1995], but there is abundant evidence for anisotropy at the base of the mantle in the D'' layer (for a recent review, see *Nowacki et al.* [2011]). The D'' region in the lowermost few hundred kilometers of the mantle exhibits striking seismological properties, including strong lateral heterogeneity in velocity and thermochemical structure [e.g., *Trampert et al.*, 2004], a complex and intermittent seismic discontinuity structure [e.g., *Lay and Garnero*, 2007; *Hernlund et al.*, 2005;

van der Hilst et al., 2007], and localized regions of ultralow velocities [e.g., *Thorne and Garnero*, 2004]. Many studies have found evidence for anisotropy in D'' [e.g., *Kendall and Silver*, 1996; *Lay et al.*, 1998; *Garnero et al.*, 2004; *Panning and Romanowicz*, 2004; *Wookey et al.*, 2005; *Wookey and Kendall*, 2007, 2008; *Long*, 2009; *Nowacki et al.*, 2010; *He and Long*, 2011]. However, as with the mid-mantle, the interpretation of this anisotropy in terms of mantle dynamics is difficult because our understanding of the causative mechanism is incomplete, and we are not yet at the point of being able to reliably relate anisotropy to mantle flow patterns.

[79] Anisotropy in D'' may be produced by LPO of lowermost-mantle minerals, potentially including perovskite [e.g., *Stixrude*, 1998; *Kendall and Silver*, 1998], post-perovskite [e.g., *Oganov et al.*, 2005; *Stackhouse et al.*, 2005; *Mao et al.*, 2010; *Merkel et al.*, 2007; *Miyagi et al.*, 2010], and/or ferropericlase [e.g., *Karato*, 1998; *Yamazaki and Karato*, 2002; *Long et al.*, 2006; *Marquardt et al.*, 2009]. Alternatively, anisotropy could be produced by the SPO of inclusions of downgoing slab materials or partial melt [e.g., *Kendall and Silver*, 1996, 1998], but it is difficult to discriminate among the different mechanisms. This is partially due to the limited raypath coverage in most studies of D'' anisotropy, which means that the geometry of anisotropy can only be loosely constrained, and is partially a function of our imperfect knowledge of single-crystal elastic constants for lowermost minerals and a dearth of experimental studies of LPO development at the relevant temperature and pressure conditions.

[80] Despite these difficulties, however, the delineation and interpretation of D'' anisotropy is crucially important for our understanding of how subducting slabs interact with the CMB and whether (and how) flow patterns in the lowermost mantle are driven by this interaction. There has been debate about whether or not (some) slabs penetrate all the way to the CMB, but many studies based on seismic tomography [e.g., *van der Hilst et al.*, 1997; *Li et al.*, 2008; *van der Meer et al.*, 2010] and geodynamics considerations [e.g., *Kellogg et al.*, 1999; *Steinberger*, 2000; *Tan et al.*, 2002; *Garnero and McNamara*, 2008] have argued that they do. If slabs do indeed routinely impinge on the CMB, then slab-driven flow likely represents one of the most important dynamic processes taking place in D''. Several studies have argued that such slab-driven flow may produce anisotropic signatures [e.g., *McNamara et al.*, 2002, 2003; *Wenk et al.*, 2006, 2011; *Merkel et al.*, 2007] by inducing strong deformation in the dislocation creep regime above the CMB, which in turn produces LPO of lowermost-mantle minerals. A few observational studies have made explicit connections between D'' anisotropy and deformation induced by subducting slabs; for example, *Nowacki et al.* [2010] documented anisotropic structure beneath North America that they linked to horizontal shear induced by the remnant Farallon slab (Figure 15).

[81] Compared to studies of upper mantle anisotropy, our ability to interpret measurements of anisotropy in the transition zone and D'' layer in terms of mantle flow remains
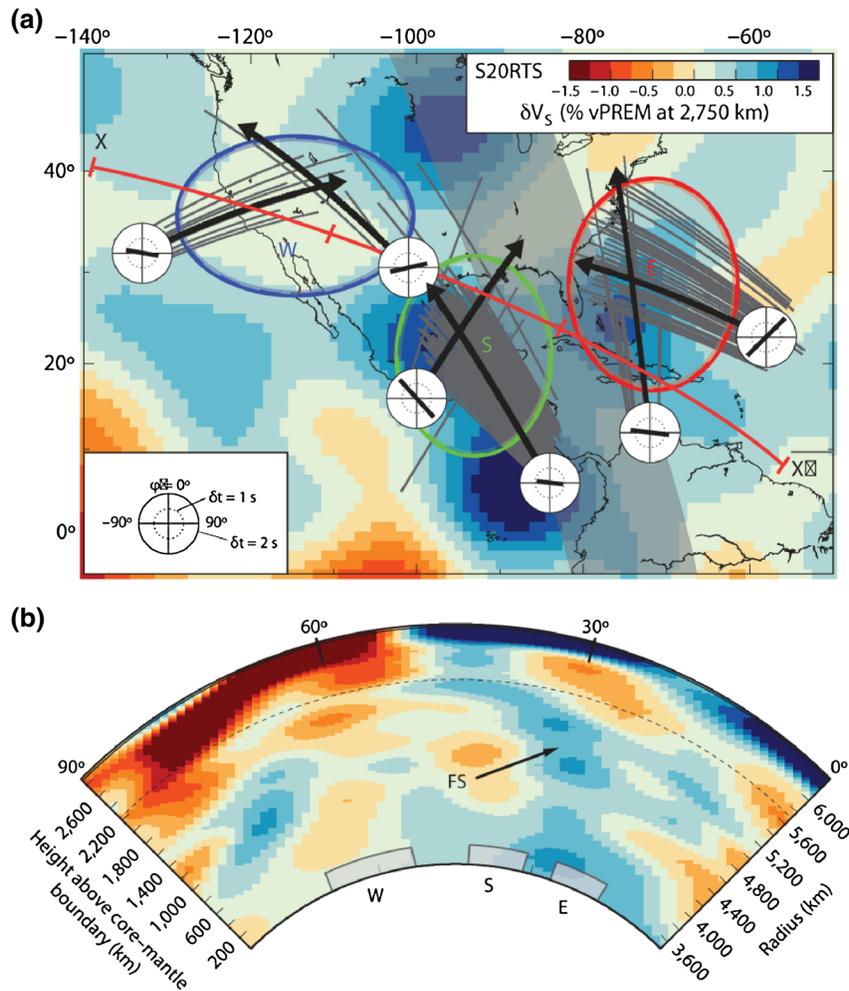
Figure 15. Results of the study of *Nowacki et al.* [2010] of anisotropy in the lowermost mantle beneath North America, inferred to be associated with the subduction of the Farallon slab. (a) Multi-azimuth stacked shear wave splitting results beneath North America. Shown are individual D″ ray paths of *ScS* phases used in stacks (thin gray lines), representative mean ray paths in D″ of stacked measurements (thick black lines, arrows indicate propagation direction), and plots of splitting parameters for each stack (white circles with black bars, bar indicates orientation and delay time). Background colors indicate isotropic *S* wave speed variations at 2750 km depth from *Ritsema et al.* [1999]. Thick red line indicates location of cross-section shown in Figure 15b. (b) Cross-section through the *Ritsema et al.* [1999] *S* wave tomography model in the study region, with colors as in Figure 15a. Gray boxes marked "W," "S," and "E" correspond to the regions marked in Figure 15a. The inferred location of the subducting Farallon slab is marked with "FS." Figure from *Nowacki et al.* [2010].

limited. Despite the challenges, however, the study of how anisotropy in the deep mantle relates to the dynamic behavior of deep subducting slabs represents a frontier area for deep Earth dynamics. Recent progress has been made on understanding the structure and elasticity of deep mantle minerals, particularly the post-perovskite phase, and although consensus has not yet been reached on the most likely mechanisms for mid- and lowermost-mantle anisotropy, future progress is likely. To date only a few regions of the transition zone and D″ have been studied in detail in terms of their anisotropic structure, but future observational studies should be able to place tighter constraints on the geometry of anisotropy in the deep mantle, particularly when innovative techniques such as source-side splitting for deep earthquakes [e.g., *Wookey and Kendall*, 2004; *Foley and Long*, 2011] or

combining phases with different raypath geometries [e.g., *Nowacki et al.*, 2010] are applied. In the transition zone, studies of seismic anisotropy in different subduction systems will allow for comparisons between the deformation behaviors of stagnant versus nonstagnant slabs and will allow for the testing of hypotheses regarding the causes of slab stagnation. For D″, comparing the anisotropic structure in regions where paleoslab material is likely present with regions where it is likely absent will help us to understand whether and how subducting slab remnants drive flow in the lowermost mantle. Comparisons between observations of D″ anisotropy and the predictions of global flow models [e.g., *Walker et al.*, 2011; *He and Long*, 2011] will allow for the testing of the hypothesis that a primary driver of flow at the base of the mantle is the impingement of slabs upon the CMB.

7. MAJOR UNSOLVED PROBLEMS IN SUBDUCTION GEODYNAMICS

[82] Much recent progress has been made in delineating, characterizing, and interpreting seismic anisotropy in the mantle and in elucidating the relationships between anisotropy and deformation in subduction systems. While there are still many unanswered questions relating to the interpretation of anisotropy in terms of mantle processes, we have reached a point in our study of mantle anisotropy at which observations and models of anisotropy can be used to address a host of broad, fundamental questions related to the dynamics of subduction systems and, more generally, to the dynamics of the mantle. Here I highlight some of the major unsolved problems in mantle dynamics that can be addressed by ongoing and future work on seismic anisotropy in subduction systems.

[83] *Is there a component of three-dimensional mantle flow beneath slabs?* The possibility of dominantly trench-parallel flow beneath subducting slabs is a viable hypothesis for the global dominance of trench-parallel sub-slab ϕ. There are, however, plausible alternative explanations for these observations, such as the model of *Song and Kawakatsu* [2012] and models that invoke entrained flow directly beneath the slab along with a deeper component of toroidal flow [*Faccenda and Capitanio*, 2012]. The relative contributions of toroidal and poloidal flow in subduction systems is vitally important for our understanding of mantle circulation. The classical model of entrained flow beneath slabs suggests that slabs entrain large amounts of material with them as they penetrate into the lower mantle. This in turn has implications for the amount of mass transfer between the upper and lower mantle reservoirs; studies of mantle mixing often explicitly assume that slabs do entrain large amounts of material with them [e.g., *Brandenburg et al*., 2008]. If, in fact, the boundary layer of sub-slab entrainment is small and mantle flow beneath most slabs is mostly trench-parallel, then this suggests that there is a partial barrier to entrained flow at depth and the amount of mass transfer between the upper and lower mantle reservoirs may be limited [*Long and Silver*, 2009]. Because of the major implications of possible along-strike sub-slab flow in subduction systems, it is crucial to carry out detailed, quantitative testing of the various hypothesized mechanisms for trench-parallel sub-slab ϕ and come to an understanding of whether a component of along-strike sub-slab flow is required to explain the data. Detailed datasets that sample sub-slab anisotropy using the source-side splitting technique [e.g., *Müller et al*., 2008; *Russo*, 2009; *Foley and Long*, 2011; *Di Leo et al*., 2012a; *Lynner and Long*, 2013] will be necessary to this effort.

[84] *Is there a component of along-strike material transport in the mantle wedge?* Classical 2-D corner flow is very often used in modeling studies that seek to explore, for example, the thermal structure of the wedge [e.g., *Kelemen et al*., 2003], the generation of melt and the location of arc volcanoes [e.g., *Grove et al*., 2009], and the transport of volatiles through the wedge [e.g., *Cagnioncle et al*., 2007].

There is increasing evidence, however, that there may be a strong along-strike component of flow in many mantle wedges, based on both geochemical tracers [e.g., *Turner and Hawkesworth*, 1998; *Hoernle et al*., 2008; *Heyworth et al*., 2011] and seismic anisotropy data. Given that our basic understanding of mantle wedge melting and volcanism is predicated on a two-dimensional flow model—that is, with a fresh supply of asthenospheric material continuously being drawn into the shallow part of the wedge via corner flow and undergoing melting—the possible presence of along-strike flow in the mantle wedge is vitally important to our understanding of wedge processes. There may be alternative explanations for observations of trench-parallel ϕ beneath the arc and backarc such as trench-parallel stretching induced by complex slab morphology [*Kneller and van Keken*, 2007, 2008] or complex wedge flow due to lower crustal foundering [*Behn et al*., 2007]. Future work is necessary to understand precisely what regions of the wedge may be dominated by trench-parallel flow and what the potential drivers are for such flow. For subduction systems with a substantial component of along-strike material transport in the wedge, it will be imperative to explore how this flow affects wedge processes such as melt generation and the transport of melt and volatiles.

[85] *How well are slabs coupled to the mantle around them?* This question is closely related to the idea of trench-parallel flow in the wedge and sub-slab mantle. In the classical model for subduction zone flow, viscous coupling between the slab and the ambient mantle results in 2-D mantle flow. Modeling studies suggest that trench-parallel sub-slab flow is only geodynamically plausible if the coupling between the slab and the subjacent mantle is weak [*Paczkowski*, 2012]; indeed, some models in which slabs are strongly coupled to the mantle around them do not exhibit much toroidal flow [e.g., *Stadler et al*., 2010]. If the hypothesis of widespread trench-parallel mantle flow is correct, then geodynamical models of mantle circulation will need to take into account the possibility that slabs may be imperfectly coupled to the mantle around them, at least in the upper mantle. Additionally, the mechanism for efficient decoupling, if such decoupling actually exists, remains poorly understood. Identifying geodynamically plausible mechanisms for such decoupling may shed light on, for example, the properties of the lithosphere-asthenosphere boundary, as discussed below.

[86] *What is the viscosity of the mantle wedge?* The viscosity of the mantle, particularly in the wedge region where viscosity may be affected by melting and volatiles, is notoriously difficult to constrain observationally. From the point of view of understanding mantle wedge dynamics, however, it is an important parameter to constrain. Some geodynamical studies have suggested that there may be a low-viscosity region in most mantle wedges [e.g., *Billen and Gurnis*, 2001]; low wedge viscosities may make small-scale convection more likely [e.g., *Wirth and Korenaga*, 2012] and may help to create channelized trench-parallel flow in the presence of an along-strike pressure gradient [e.g., *Conder and Wiens*, 2007]. In contrast, investigations of the possible presence of B-type olivine fabric in the

wedge have suggested that a high-viscosity wedge corner dominated by high stresses and sluggish flow is needed for B-type fabric [*Kneller et al.*, 2007, 2008]. Measurements of seismic anisotropy have the potential to shed light on this important question, as the effect of wedge viscosity on seismic anisotropy may be detectable, if subtle [*Long et al.*, 2007]. A promising avenue for constraining wedge viscosity from anisotropy measurements may be to combine geodynamical modeling and observations to understand the range of viscosity values that is consistent with a given data set. For example, the presence of trench-parallel wedge flow likely requires a low-viscosity region of the wedge, so if anisotropy measurements (perhaps in combination with geochemical and other data) can be used to make an airtight case for along-strike flow in a certain region of the wedge, geodynamical models can be used to estimate the viscosity.

[87] *How is water incorporated into subducting slabs and released from the slab into the wedge? How much water is transported to the deep mantle by slabs?* The release of water and other volatiles from downgoing slabs into the mantle wedge above them play a key role in the generation of melt and the solid Earth's overall water budget [e.g., *Wada et al.*, 2012]. Water is transported into the Earth's mantle in hydrous minerals in the downgoing slab and is released as these minerals are subjected to high pressures and temperatures and become unstable [e.g., *Ulmer and Trommsdorff*, 1995; *Schmidt and Poli*, 1998; *Rüpke et al.*, 2004; *Faccenda et al.*, 2012]. While this process is understood in a general sense, the details of how and where slabs are hydrated and precisely how volatiles released from the slab interact with the overlying mantle remain uncertain. Oceanic crust may be hydrated near mid-ocean ridges and may undergo further hydration via hydrothermal circulation [e.g., *Johnson and Prius*, 2003]. Further plate hydration is likely to occur as plates bend at the outer rise before descending into the mantle [e.g., *Ranero et al.*, 2003; *Grevemeyer et al.*, 2007; *Key et al.*, 2012], and there is evidence for serpentinization of minerals along faults that penetrate well into the mantle lithosphere, in the upper 15–20 km of downgoing slabs [e.g., *Faccenda et al.*, 2008, 2009]. Because serpentinite minerals such as antigorite have a unique anisotropic signature, observational studies that can isolate a contribution from the anisotropy of serpentinized minerals can aid our understanding of the distribution of such minerals in subduction systems. In particular, receiver function studies can help to differentiate between hydrous minerals located within the slab itself and serpentinization within the wedge that results from water release from the slab and the subsequent hydration of the overlying wedge mantle. Future studies that aim to constrain the anisotropic signature of hydrous minerals in both the slab and the wedge will therefore be important for increasing our understanding of subduction zone water budgets.

[88] *How does ambient mantle flow affect the morphology of slabs and trenches, and vice versa?* A variety of trench and slab morphologies are observed in nature, with trench geometries ranging from those that are nearly linear (e.g., Tonga-Kermadec, Central America) to those that have high arc curvature (e.g., Scotia, Caribbean) and slab configurations including those that are nearly planar (e.g., Ryukyu), those that are bent or warped at depth (e.g., Honshu-Kurile), those that are steeply dipping (e.g., Marianas, Vanuatu), and those that include a flat-slab segment (e.g., Peru). Some work has been done to explain specific aspects of trench and slab morphologies; for example, it has been explored to what extent arc curvature is controlled by slab width [*Schellart et al.*, 2007] and whether heterogeneities in the downgoing lithosphere and/or feedback between the downgoing slab and the ambient mantle play a primary role in controlling trench morphology [e.g., *Morra et al.*, 2006]. To take another example, flat-slab subduction such as that observed today beneath Peru is often thought to be a consequence of the subduction of buoyant features on the seafloor such as ridges or seamount tracks [e.g., *Cross and Pilger*, 1982; *Gutscher et al.*, 2000], but the global correlation between such features and regions of flat or shallow subduction is relatively poor [*Skinner and Clayton*, 2011], and other factors such as wedge viscosity [*Manea and Gurnis*, 2007] or ambient mantle flow [*Eakin and Long*,] may play a role. A major open problem in subduction dynamics is the extent to which trench and slab morphology are affected by mantle flow above, beneath, and at the edges of subducting slabs. Conversely, slab morphology may play a major role in controlling flow in the vicinity of subducting slabs. Because studies of seismic anisotropy can constrain the flow field around subducting slabs, future studies of mantle flow and anisotropy in subduction sytems with unusual morphologies—including flat-slab segments such as that found beneath Peru—may help us to understand the relationships between mantle flow and slab morphology.

[89] *Does the anisotropic structure of slabs reflect past geodynamic processes such as spreading rates?* Subducting slabs likely have an anisotropic signature that may reflect the "frozen" or relict structure of oceanic lithosphere [*Hess*, 1964; *Shearer and Orcutt*, 1985; *Gaherty et al.*, 2004] or may reflect subsequent modification such as faulting and serpentinization due to bending at the outer rise. Recent work has suggested that there is a global relationship between observed *P* wave azimuthal anisotropy and spreading rate for present-day oceanic spreading centers [*Song and Kim*, 2012b]. If this relationship holds, then observations of anisotropy in subducting slabs, particularly old ones, may be used to shed light on past deformation processes in the oceanic lithosphere and may contain information about plate spreading rates and the style of deformation at ridges. Compared to the mantle wedge and the sub-slab mantle, the slab itself has not received as much attention in observational studies, but future work on delineating the anisotropic structure of downgoing slabs may shed light on past geodynamical processes. Receiver function analysis is probably the best tool to study slab anisotropy [e.g., *Song and Kim*, 2012a, 2012b; *Wirth and Long*, 2012; *Audet*, 2013], so future anisotropic RF studies will be key to addressing this problem.

[90] *What is the nature of the oceanic asthenosphere and the lithosphere-asthenosphere boundary (LAB)?* The concept of the lithosphere-asthenosphere system invokes a cold,

rigid layer (the lithosphere) that moves over a weaker asthenosphere characterized by low viscosity as well as low seismic velocity. This basic concept is fundamental to plate tectonic theory, but the nature of the lithosphere-asthenosphere boundary—and the asthenosphere itself—remain poorly understood [e.g., *Fischer et al.*, 2010]. Recent observational studies have found evidence for a sharp oceanic LAB associated with a velocity drop up to 10% [e.g., *Kawakatsu et al.*, 2009; *Kumar and Kawakatsu*, 2011; *Rychert and Shearer*, 2009, 2011; *Schmerr*, 2012], which may require the presence of partial melt [e.g., *Kawakatsu et al.*, 2009; *Schmerr*, 2012] or a role for grain boundary sliding [e.g., *Karato*, 2012]. Understanding the nature of the asthenosphere and the nature of the LAB is crucial for our understanding of seismic anisotropy and mantle flow beneath slabs. Two of the most plausible hypotheses to explain the global preponderance of trench-parallel sub-slab fast splitting directions are the trench-parallel flow model [*Long and Silver*, 2008, 2009] and the "strong radial anisotropy" model of entrained asthenosphere [*Song and Kawakatsu*, 2012]. If either of these hypotheses is correct, the implications for our understanding of the asthenosphere and LAB are major. If the *Song and Kawakatsu* [2012] model is correct, then it implies that the anisotropic structure of the oceanic asthenosphere is different than previously thought and is controlled not only by olivine LPO [e.g., *Karato et al.*, 2008] but also by the presence of aligned partial melt [*Kawakatsu et al.*, 2009] or unusual LPO geometries [*Song and Kawakatsu*, 2013]. If the *Long and Silver* [2009] model is correct, then it implies that the nature of the oceanic LAB may play a key role in decoupling the downgoing slab from the subjacent mantle. In particular, the asthenosphere model of *Karato* [2012] suggests that there may be a thin, weak layer of frozen gabbroic melt directly beneath the LAB, which may serve as a mechanism to decouple slabs from the mantle beneath them. In any case, it is clear that solving the puzzle of sub-slab anisotropy will lead to new insight into the nature of the oceanic lithosphere-asthenosphere system.

[91] *How do subducting slabs interact with the viscosity jump at the 660 km discontinuity?* The measurement and interpretation of seismic anisotropy in the mid-mantle in the vicinity of subducting slabs may lead to insight into the pattern of deformation and into the nature of the dynamic interaction between slabs and the transition zone discontinuities. In order to address this important scientific problem, several questions will need to be addressed from an observational point of view. Is seismic anisotropy at transition zone depths a ubiquitous feature of subduction zones? Do stagnant slabs exhibit different patterns of mid-mantle deformation than slabs that easily penetrate the 660 km discontinuity? How does the geometry of anisotropy relate to slab morphology? Are there variations along strike and with depth of mid-mantle anisotropy in individual subduction systems that may provide clues to the nature of slab-mantle interactions? Several hypotheses have been proposed to explain why some slabs stagnate

[e.g., *Billen*, 2010], including metastable olivine with positive buoyancy, a temperature-delayed phase transformation from ringwoodite, or a slab that is weakened by intense mid-mantle deformation and is unable to penetrate the high-viscosity lower mantle. These models make testable predictions about the strength of deformation and anisotropy in different subduction systems, so variations in mid-mantle anisotropy may help to discriminate among the many models for stagnant slab dynamics. Of course, there is a great deal of work that must be done from an observational point of view before we are in a position to be able to answer these questions. Recent successful studies of mid-mantle anisotropy from both body waves [e.g., *Wookey and Kendall*, 2004; *Foley and Long*, 2011; *Di Leo et al.*, 2012b] and surface waves [e.g., *Montagner et al.*, 2012] are encouraging, however.

[92] *How do subducting slabs drive and/or interact with mantle flow in the D'' layer?* The structure and dynamics of the lowermost mantle represents one of the major frontier areas in solid Earth science [e.g., *Garnero and McNamara*, 2008]. Slabs that sink to the base of the mantle and impinge upon the CMB may well represent a major driver for flow at the base of the mantle, but an alternative hypothesis is that lowermost-mantle flow is controlled by other mechanisms. This might take the form of a flow pattern anchored by major lower mantle structures such as thermochemical piles [e.g., *McNamara and Zhong*, 2005] or flow affected by processes such as small-scale convection or plume upwellings [e.g., *Russell et al.*, 1998]. In the absence of observational constraints on the style and geometry of deformation at the base of the mantle, it is difficult to evaluate hypotheses about the relationships between subducting slabs and flow. Studies of D'' anisotropy have the potential to provide such observational constraints. In particular, future studies of lowermost-mantle anisotropy that include comparisons between regions where paleoslab material may be present and regions where it is likely absent will shed light on potential differences in deformation regime. Comparisons between observations of D'' anisotropy and the predictions of whole-mantle convection models [e.g., *Walker et al.*, 2011] allow for the testing of the hypothesis that a primary driver of flow at the base of the mantle is the impingement of slabs upon the CMB [e.g., *McNamara et al.*, 2002; *Wenk et al.*, 2006, 2011]. As with the transition zone, limitations remain on our ability to relate observations of D'' anisotropy to flow directions due to uncertainties in the causative mechanism for anisotropy. However, observations of D'' anisotropy are becoming increasingly sophisticated, as studies incorporate multiple raypaths [e.g., *Wookey and Kendall*, 2008; *Nowacki et al.*, 2010] and/or multiple phases [e.g., *He and Long*, 2011] to obtain tighter constraints on anisotropic geometry. Ongoing and future work on D'' anisotropy from both a seismological and a mineral physics point of view should allow us to constrain the mechanism(s) for anisotropy and ultimately to test hypotheses related to the dynamic interactions between subducting slabs and the CMB.

8. OUTLOOK AND SUMMARY

[93] As reviewed in this paper, there has been an enormous amount of progress over the past ~10 years in characterizing seismic anisotropy in subduction systems and in understanding the controls on this anisotropic structure. This progress has come on many fronts, including observational studies, mineral physics experiments, and geodynamic modeling work. It is particularly exciting that we are at the point where truly interdisciplinary studies that integrate constraints from all these disciplines are possible. Nevertheless, major challenges remain in the study of seismic anisotropy as it relates to the dynamics of subduction systems. For example, we still have not converged on first-order explanations for wedge, slab, and sub-slab anisotropy in subduction zones globally, although a large number of conceptual models have been proposed to explain the observed patterns.

[94] There are, fortunately, a number of avenues for future progress. From an observational point of view, the construction of what might be thought of as "next-generation" data sets is key. The ongoing use of innovative source-receiver combinations to isolate anisotropy in different parts of subduction systems should result in tighter constraints on anisotropic geometry and, hopefully, mechanisms. This includes the use of multiple phase types to study shear wave splitting in individual subduction systems [e.g., *Di Leo et al.*, 2012a, 2012b], the use of the source-side splitting technique to characterize sub-slab anisotropy [e.g., *Müller et al.*, 2008; *Russo*, 2009; *Russo et al.*, 2010; *Foley and Long*, 2011; *Lynner and Long*, 2013], and the use of phases originating from both the upper and lower planes of seismicity in systems which exhibit double Wadati-Benioff zones [*Huang et al.*, 2011a]. The use of phases with long path lengths in the subducting slabs (e.g., guided waves from slab earthquakes measured at stations close to the trench) may hold promise for characterizing anisotropy in the slab itself. The construction of detailed datasets with good raypath coverage that sample different parts of the subduction system, particularly in regions that are well instrumented and/or highly seismogenic, should allow for the quantitative testing of predictions made by the many models for subduction zone anisotropy. Geodynamical modeling studies will also be crucial to this effort, as they can supply detailed predictions for anisotropic behavior for different mantle flow scenarios.

[95] There are other observational techniques that can be brought to bear to gain information about the complex anisotropic structures that are likely present in most subduction zones. The measurement of frequency-dependent splitting can yield information about lateral and depth heterogeneity in anisotropy and has been applied in several regions [e.g., *Marson-Pidgeon and Savage*, 1997; *Greve and Savage*, 2009; *Wirth and Long*, 2010; *Huang et al.*, 2011b]. The application of less common measurement strategies such as anisotropic receiver function analysis and anisotropic *P* wave tomography to more subduction systems is also promising, particularly since these techniques can provide information about the depth distribution of anisotropy that is often difficult to obtain from shear wave splitting data sets.

The application, interpretation, and (perhaps) joint inversion of multiple observation techniques in a single subduction zone also hold promise. Finally, a very exciting avenue for future progress lies in the application of techniques for shear wave splitting tomography. While a great deal of work has been done to develop theoretical bases for the tomographic inversion of shear wave splitting measurements [e.g., *Chevrot*, 2006; *Abt and Fischer*, 2008; *Long et al.*, 2008; *Chevrot and Monteiller*, 2009], the application of the technique has been limited to a few regions with excellent raypath coverage [e.g., *Abt et al.*, 2009; *Monteiller and Chevrot*, 2011]. With the increasing availability of high-quality data sets from dense arrays, however, our ability to implement shear wave splitting tomography in complex regions such as subduction systems should expand.

[96] In comparison to our ability to interpret measurements of upper mantle anisotropy in terms of dynamic processes, the study of anisotropy and mantle flow in the deeper parts of the mantle remains in an early stage. However, the investigation of deep mantle anisotropy in the vicinity of subducting slabs represents an extraordinary opportunity to gain new insight into deep subduction dynamics. Studies of mid-mantle and D″ anisotropy, while limited by the large uncertainties remaining about the causative mechanism, are beginning to reach the point where hypotheses about the relationships between slab-driven flow and the resulting anisotropy can be tested. Progress in the study of deep mantle anisotropy will be enabled by ongoing and future studies on the elasticity and deformation mechanisms of mantle materials at deep mantle conditions, so that observations of anisotropy can be more reliably related to mantle flow patterns. The observational study of subduction dynamics in the deep Earth via the study of deep mantle anisotropy is still at an early phase, but this represents a powerful avenue for progress in understanding the behavior of slabs in the deep mantle.

[97] Understanding how seismic anisotropy can yield constraints on mantle flow in different parts of subduction systems remains an important challenge for the observational seismology community, as well as for mineral physicists and geodynamicists. Despite the challenges inherent in this work, there is a long list of important, first-order questions related to subduction geodynamics and to the dynamics of the mantle as a whole that may be addressed, and perhaps resolved, through the study of seismic anisotropy. The delineation, characterization, and interpretation of seismic anisotropy in subduction systems thus represent an important frontier area in the study of the solid Earth.

thoughtful and constructive comments that helped to improve the manuscript. I thank David Abt, James Conder, Manuele Faccenda, Karen Fischer, Margarete Jadamec, Ikuo Katayama, Vadim Levin, Alex Nikulin, Andy Nowacki, Alex Song, You Tian, and Peter van Keken for graciously sharing figures. Figures 3a and 3b and 6 were reprinted from *Geophysical Journal International* with permission from Oxford University Press on behalf of the Royal Astronomical Society and Deutsche Geophysikalische Gesellschaft. Figure 3d was reprinted from *Physics of the Earth and Planetary Interiors* with permission from Elsevier. Figures 8b, 8c, 9, and 11a–11d were reprinted from *Earth and Planetary Science Letters* with permission from Elsevier. Figures 10, 13c, 13d, and 15 were reprinted from *Nature* with permission from MacMillan Publishers Ltd. Figures 13a, 13b, and 14a were reprinted from *Science* with permission from AAAS.

[99] The editor on this paper was Fabio Florindo. He thanks the Associate Editor Kate Chen and two anonymous reviewers for their review assistance on this manuscript.

REFERENCES

Abt, D. L. and K. M. Fischer (2008), Resolving three-dimensional anisotropic structure with shear-wave splitting tomography, *Geophys. J. Int.*, 173, 859–889.

Abt, D. L., K. M. Fischer, G. A. Abers, M. Protti, V. González, and W. Strauch (2010), Constraints on upper mantle anisotropy surrounding the Cocos slab from SK(K)S splitting, *J. Geophys. Res.*, 115, B06316, doi:10.1029/2009JB006710.

Abt, D. L., K. M. Fischer, G. A. Abers, W. Strauch, J. M. Protti, and V. González (2009), Shear wave anisotropy beneath Nicaragua and Costa Rica: Implications for flow in the mantle wedge, *Geochem. Geophys. Geosyst.*, 10, Q05S15, doi:10.1029/2009GC002375.

Anderson, M. L., G. Zandt, E. Triep, M. Fouch, and S. Beck (2004), Anisotropy and mantle flow in the Chile-Argentina subduction zone from shear wave splitting analysis, *Geophys. Res. Lett.*, 31, doi:10.1029/2004GL020906.

Ando, M., Y. Ishikawa, and H. Wada (1980), S-wave anisotropy in the upper mantle under a volcanic area in Japan, *Nature*, 286, 43–46.

Ando, M., Y. Ishikawa, and F. Yamazaki (1983), Shear wave polarization anisotropy in the upper mantle beneath Honshu, Japan, *J. Geophys. Res.*, 88, 5850–5864, doi:10.1029/JB088iB07p05850.

Audet, P. (2013), Seismic anisotropy of subducting oceanic uppermost mantle from fossil spreading, *Geophys. Res. Lett.*, 40, 173–177, doi:10.1029/2012GL054328.

Audoine, E., M. K. Savage, and K. Gledhill (2004), Anisotropic structure under a back arc spreading region, the Taupo Volcanic Zone, New Zealand, *J. Geophys. Res.*, 109, doi:10.1029/2003JB002932.

Baccheschi, P., L. Margheriti, and M. S. Steckler (2007), Seismic anisotropy reveals focused mantle flow around the Calabrian slab (Southern Italy), *Geophys. Res. Lett. 34*, doi:10.1029/2006GL028899.

Becker, T. W., S. Chevrot, V. Schulte-Pelkum, and D. K. Blackman (2006), Statistical properties of seismic anisotropy predicted by upper mantle geodynamic models, *J. Geophys. Res.*, 111, B08309, doi:10.1029/2005JB004095.

Becker, T. W., and C. Faccenna (2009), A review of the role of subduction dynamics for regional and global plate motions. in Subduction Zone Geodynamics, edited by Lallemand, S. and Funiciello, F., pp. 3–34, Springer, Berlin Heidelberg, Germany.

Becker, T. W., J. B. Kellogg, G. Ekström, and R. J. O'Connell (2003), Comparison of azimuthal anisotropy from surface waves and finite strain from global mantle-circulation models, *Geophys. J. Int.*, 155, 696–714.

Becker, T. W., S. Lebedev, and M. D. Long (2012), On the relationship between azimuthal anisotropy from shear wave splitting and surface wave tomography, *J. Geophys. Res.*, 117, B01306, doi:10.1029/2011JB008705.

Behn, M. D., G. Hirth, and P. B. Kelemen (2007), Trench-parallel anisotropy produced by foundering of arc lower crust, *Science*, 317, 108–111.

Ben Ismail, W., and D. Mainprice (1998), An olivine fabric database: An overview of upper mantle fabrics and seismic anisotropy, *Tectonophysics*, 296, 145–158.

Bengtson, A. K., and P. E. van Keken (2012), Three-dimensional thermal structure of subduction zones: Effects of obliquity and curvature, *Solid Earth Discuss.*, 4, 919–941.

Bezacier, L., B. Reynard, J. D. Bass, C. Sanchez-Valle, and B. Van de Moortèle (2010), Elasticity of antigorite, seismic detection of serpentinites, and anisotropy in subduction zones, *Earth Planet. Sci. Lett.*, 289, 198–208.

Billen, M. I. (2008), Modeling the dynamics of subducting slabs, *Annu. Rev. Earth Planet. Sci.*, 36, 325–356.

Billen, M. I. (2010), Slab dynamics in the transition zone, *Phys. Earth Planet. Inter.*, 183, 296–308.

Billen, M. I., and M. Gurnis (2001), A low viscosity wedge in subduction zones, *Earth Planet. Sci. Lett.*, 193, 227–236.

Bostock, M. G. (1998), Mantle stratigraphy and evolution of the Slave province, *J. Geophys. Res.*, 103, 21,183–21,200, doi:10.1029/98JB01069.

Bostock, M. G., R. D. Hyndman, S. Rondenay, and S. M. Peacock (2002), An inverted continental Moho and serpentinization of the forearc mantle, *Nature*, 417, 536–538.

Brandenburg, J. P., E. H. Hauri, P. E. van Keken, and C. J. Ballentine (2008), A multiple-system study of the geochemical evolution of the mantle with force-balanced plates and thermochemical effects, *Earth Planet. Sci. Lett.*, 276, 1–13.

Brudzinski, M. R., C. H. Thurber, B. R. Hacker, and E. R. Engdahl (2007), Global prevalence of double Benioff zones, *Science*, 316, 1472–1474.

Bunge, H.-P., M. A. Richards, and J. R. Baumgardner (1996), Effect of depth-dependent viscosity on the planform of mantle convection, *Nature*, 379, 436–438.

Buttles, J., and P. Olson (1998), A laboratory model of subduction zone anisotropy, *Earth Planet. Sci. Lett.*, 164, 245–262.

Cagnioncle, A.-M., E. M. Parmentier, and L. T. Elkins-Tanton (2007), Effect of solid flow above a subducting slab on water distribution and melting at convergent plate boundaries, *J. Geophys. Res.*, 112, B09402, doi:10.1029/2007JB004934.

Capitanio, F. A., C. Faccenna, and R. Funiciello (2009), The opening of Sirte basin: Result of slab avalanching?, *Earth Planet Sci. Lett.*, 285, 210–216.

Chastel, Y. B., P. R. Dawson, H. R. Wenk, and K. Bennett (1993), Anisotropic convection with implications for the upper mantle, *J. Geophys. Res.*, 98, 17,757–17,771.

Chen, W.-P., and M. R. Brudzinski (2003), Seismic anisotropy in the mantle transition zone beneath Fiji-Tonga, *Geophys. Res. Lett.*, 30, 1682, doi:10.1029/2002GL016330.

Chevrot, S. (2006), Finite-frequency vectorial tomography: A new method for high resolution imaging of upper mantle anisotropy, *Geophys. J. Int.*, 165, 641–657.

Chevrot, S., and V. Monteiller (2009), Principles of vectorial tomography—The effects of model parameterization and regularization in tomographic imaging of seismic anisotropy, *Geophys. J. Int.*, 179, 1726–1736.

Christensen, D. H., and G. A. Abers (2010), Seismic anisotropy under central Alaska from SKS splitting observations, *J. Geophys. Res.*, 115, B04315, doi:10.1029/2009JB006712.

Christensen, D. H., G. A. Abers, and T. L. McKnight (2003), Mantle anisotropy beneath the Alaska range inferred from S-wave splitting observations: Results from BEAAR, *Eos Trans. AGU*, 84, Fall Meet. Suppl., Abstract S31C-0782.

Civello, S., and L. Margheriti (2004), Toroidal mantle flow around the Calabrian slab (Italy) from SKS splitting, *Geophys. Res. Lett.*., *31*, doi:10.1029/2004GL019607.

Conder, J. A., and D. A. Wiens (2007), Rapid mantle flow beneath the Tonga volcanic arc, *Earth Planet. Sci. Lett.*, *264*, 299–307.

Conrad, C. P., M. D. Behn, and P. G. Silver (2007), Global mantle flow and the development of seismic anisotropy: Differences between the oceanic and continental upper mantle, *J. Geophys. Res.*, *112*, B07317, doi:10.1029/2006JB004608.

Couvy, H., D. J. Frost, F. Heidelbach, K. Nyials, T. Ungar, S. J. Mackwell, and P. Cordier (2004), Shear deformation experiments of forsterite at 11 GPa - 1400 °C in the multianvil apparatus, *Eur. J. Mineral.*, *16*, 877–889.

Cross, T. A., and R. H. Pilger (1982), Controls of subduction geometry, location of magmatic arcs, and tectonics of arc and back-arc regions, *Geol Soc. Am. Bull.*, *93*, 545–562.

Currie, C. A., J. F. Cassidy, R. Hyndman, and M. G. Bostock (2004), Shear wave anisotropy beneath the Cascadia subduction zone and western North American craton, *Geophys. J. Int.*, *157*, 341–353.

Davies, G. F. (1995), Penetration of plates and plumes through the mantle transition zone, *Earth Planet. Sci. Lett.*, *133*, 507–516.

Di Leo, J. F., J. Wookey, J. O. S. Hammond, J.-M. Kendall, S. Kaneshima, H. Inoue, T. Yamashina, and P. Harjadi (2012a), Deformation and mantle flow beneath the Sangihe subduction zone from seismic anisotropy, *Phys. Earth Planet. Inter.*, *194–195*, 38–54.

Di Leo, J. F., J. Wookey, J. O. S. Hammond, J.-M. Kendall, S. Kaneshima, H. Inoue, T. Yamashina, and P. Harjadi (2012b), Mantle flow in regions of complex tectonics: Insights from Indonesia, *Geochem. Geophys. Geosyst.*, *13*, Q12008, doi:10.1029/2012GC004417.

Druken, K. A., M. D. Long, and C. Kincaid (2011), Patterns in seismic anisotropy driven by rollback subduction beneath the High Lava Plains, *Geophys. Res. Lett.*, *38*, L13310, doi:10.1029/2011GL047541.

Eakin, C. M., and M. D. Long (in review), Complex anisotropy beneath the Peruvian flat-slab from frequency-dependent, multiple-phase shear wave splitting analysis, *J. Geophys. Res.*, revised manuscript in review.

Eberhart-Phillips, D., and M. Reyners (2009), Three-dimensional distribution of seismic anisotropy in the Hikurangi subduction zone beneath central North Island, New Zealand, *J. Geophys. Res.*, *114*, B06301, doi:10.1029/2008JB005947.

Faccenda, M., L. Burlini, T. V. Gerya, and D. Mainprice (2008), Fault-induced seismic anisotropy by hydration in subducting oceanic plates, *Nature*, *455*, 1097–1100.

Faccenda, M., and F. A. Capitanio (2012), Development of mantle seismic anisotropy during subduction-induced 3-D flow, *Geophys. Res. Lett.*, *39*, L11305, doi:10.1029/2012GL051988.

Faccenda, M., and F. A. Capitanio (2013), Seismic anisotropy around subduction zones: Insights from three-dimensional modeling of upper mantle deformation and SKS splitting calculations, *Geochem. Geophys. Geosyst.*, *14*, 243–262, doi:10.1029/2012GC004451.

Faccenda, M., T. V. Gerya, and L. Burlini (2009), Deep slab hydration induced by bending-related variations in tectonic pressure, *Nat. Geosci.*, *2*, 790–793.

Faccenda, M., T. V. Gerya, N. S. Mancktelow, and L. Moresi (2012), Fluid flow during slab unbending and dehydration: Implications for intermediate-depth seismicity, slab weakening and deep water recycling, *Geochem. Geophys. Geosyst.*, *13*, Q01010, doi:10.1029/2011GC003860.

Favier, N., and S. Chevrot (2003), Sensitivity kernels for shear wave splitting in transverse isotropic media, *Geophys. J. Int.*, *153*, 213–228.

Fischer, K. M., H. A. Ford, D. L. Abt, and C. A. Rychert (2010), The lithosphere-asthenosphere boundary, *Annu. Rev. Earth Planet. Sci.*, *38*, 551–575.

Fischer, K. M., A. Li, D. W. Forsyth, and S.-H. Hung (2005), Imaging three-dimensional anisotropy with broadband seismic arrays, in Seismic Earth: Array Analysis of Broadband Seismograms, Geophys. Monogr. Ser. 157, edited by A. Levander and G. Nolet, pp. 99–116, AGU, Washington, DC.

Fischer, K. M., E. M. Parmentier, A. R. Stine, and E. R. Wolf (2000), Modeling anisotropy and plate-driven flow in the Tonga subduction zone back arc, *J. Geophys. Res.*, *105*, 16,181-16,191.

Foley, B., and M. D. Long (2011), Upper and mid-mantle anisotropy beneath the Tonga slab, *Geophys. Res. Lett.*, *38*, L02303, doi:10.1029/2010GL046021.

Forsyth, D. W. (1975), The early structural evolution and anisotropy of the oceanic upper mantle, *Geophys. J. Roy. Astron. Soc.*, *43*, 103–162.

Fouch, M. J., and K. M. Fischer (1998), Shear wave anisotropy in the Mariana subduction zone, *Geophys. Res. Lett.*, *25*, 1221–1224.

Fukao, Y., S. Widiyantoro, and M. Obayashi (2001), Stagnant slabs in the upper and lower mantle transition region, *Rev. Geophys.* *39*, 291–323.

Fukao, Y., M. Obayashi, T. Nakakuki, and the Deep Slab Project Group (2009), Stagnant slab: A review, *Annu. Rev. Earth Planet. Sci.*, *37*, 19–46.

Funiciello, F., C. Faccenna, and D. Giardini (2004), Role of lateral mantle flow in the evolution of subduction system: Insights from 3-D laboratory experiments, *Geophys. J. Int.*, *157*, 1393–1406.

Funiciello, F., M. Moroni, C. Piromallo, C. Faccenna, A. Cenedese, and H. A. Bui (2006), Mapping mantle flow during retreating subduction: Laboratory models analyzed by feature tracking, *J. Geophys. Res.*, *111*, B03402, doi:10.1029/2005JB003792.

Gaherty, J. B., D. Lizarralde, J. A. Collins, G. Hirth, and S. Kim (2004), Mantle deformation during slow seafloor spreading constrained by observations of seismic anisotropy in the western Atlantic. *Earth Planet. Sci. Lett.*, *228*, 255–265.

Garnero, E. J., V. Maupin, T. Lay, and M. J. Fouch (2004), Variable azimuthal anisotropy in Earth's lowermost mantle, *Science*, *306*, 259–262.

Garnero, E. J., and A. K. McNamara (2008), Structure and dynamics of the Earth's lower mantle, *Science*, *320*, 626–628.

Gerya, T. (2011), Future directions in subduction modeling, *J. Geodyn.*, *52*, 344–378.

Greve, S. M., M. K. Savage, and S. D. Hofmann (2008), Strong variations in seismic anisotropy across the Hikurangi subduction zone, North Island, New Zealand, *Tectonophysics*, *462*, 7–21.

Greve, S. M., and M. K. Savage (2009), Modelling seismic anisotropy variations across the Hikurangi subduction margin, New Zealand, *Earth Planet. Sci. Lett.*, *285*, 16–26.

Grevemeyer, I., C. R. Ranero, E. R. Flueh, D. Kläschen, and J. Bialas (2007), Passive and active seismological study of bending-related faulting and mantle serpentinization at the Middle America trench, *Earth Planet. Sci. Lett.*, *258*, 528–542.

Grove, T. L., C. B. Till, E. Lev, N. Chatterjee, and E. Médard (2009), Kinematic variables and water transport control the formation and location of arc volcanoes, *Nature*, *459*, 694–679.

Gudmundsson, O., and M. Sambridge (1998), A regionalized upper mantle (RUM) seismic model, *J. Geophys. Res.*, *103*, 7121–7136,

Gutscher, M. A., W. Spakman, H. Bijward, and E. R. Engdahl (2000), Geodynamics of flat subduction: Seismicity and tomographic constraints from the Andean margin, *Tectonics*, *19*, 814–833.

Hall, C., K. M. Fischer, E. M. Parmentier, and D. K. Blackman (2000), The influence of plate motions on three-dimensional back arc mantle flow and shear wave splitting, *J. Geophys. Res.*, *105*, 28,009–28,033.

Hammond, J. O. S., J. Wookey, S. Kaneshima, H. Inoue, T. Yamashina, and P. Harjadi (2010), Systematic variation in anisotropy beneath the mantle wedge in the Java-Sumatra subduction system from shear wave splitting, *Phys. Earth Planet. Inter.*, *178*, 189–201.

Hanna, J., and M. D. Long (2012). SKS splitting beneath Alaska: Regional variability and implications for subduction processes at a slab edge, *Tectonophysics*, *530–531*, 272–285.

He, X., and M. D. Long (2011), Lowermost mantle anisotropy beneath the northwestern Pacific: Evidence from PcS, ScS, SKS, and SKKS phases, *Geochem. Geophys. Geosyst.*, *12*, Q12012, doi:10.1029/2011GC003779.

Hess, H. (1964), Seismic anisotropy of the uppermost mantle under oceans, *Nature*, *203*, 629–631.

Healy, D., S. M. Reddy, N. E. Timms, E. M. Gray, and A. V. Brovarone (2009), Trench-parallel fast axes of seismic anisotropy due to fluid-filled cracks in subducting slabs, *Earth Planet. Sci. Lett.*, *238*, 75–86.

Hernlund, J. W., C. Thomas, and P. J. Tackley (2005), A doubling of the post-perovskite phase boundary and structure of the Earth's lowermost mantle, *Nature*, *434*, 882–886.

Heyworth, Z., K. M. Knesel, S. P. Turner, and R. J. Arculus (2011), Pb-isotopic evidence for rapid trench-parallel mantle flow beneath Vanuatu, *J. Geol. Soc.*, *168*, 265–271.

Hilairet, N., and B. Reynard (2008), Stability and dynamics of serpentinite layer in subduction zone, *Tectonophyscs*, *465*, 24–29.

Hoernle, K., et al. (2008), Geochemical and geophysical evidence for arc-parallel flow in the mantle wedge beneath Costa Rica and Nicaragua, *Nature*, *451*, 1094–1098.

Holtzman, B. K., and J.-M. Kendall (2010), Organized melt, seismic anisotropy, and plate boundary lubrication, *Geochem. Geophys. Geosyst.*, *11*, Q0AB06, doi:10.1029/2010GC003296.

Holtzman, B. K., D. L. Kohlstedt, M. E. Zimmerman, F. Heidelbach, T. Hiraga, and J. Hustoft, (2003), Melt segregation and strain partitioning: Implications for seismic anisotropy and mantle flow, *Science*, *301*, 1227–1230.

Honda, S. (2011), Planform of small-scale convection under the island arc, *Geochem. Geophys. Geosyst.*, *12*, Q11005, doi:10.1029/2011GC003827.

Honda, S., and T. Yoshida (2005), Application of the model of small-scale convection under the island arc to the NE Honshu subduction zone, *Geochem. Geophys. Geosyst.*, *6*, Q01002, doi:10.1029/2004GC000785.

Huang, Z., D. Zhao, and L. Wang (2011a), Shear wave anisotropy in the crust, mantle wedge, and subducting Pacific slab under northeast Japan, *Geochem. Geophys. Geosyst.*, *12*, Q01002, doi:10.1029/2010GC003343.

Huang, Z., D. Zhao, and L. Wang (2011b), Frequency-dependent shear-wave splitting and multilayer anisotropy in northeast Japan, *Geophys. Res. Lett.*, *38*, L08302, doi:10.1029/2011GL046804.

Hyndman, R. D., and S. M. Peacock (2003), Serpentinization of the forearc mantle, *Earth Planet. Sci. Lett.*, *212*, 417–432.

Jadamec, M. A., and M. I. Billen (2010), Reconciling surface plate motions with rapid three-dimensional mantle flow around a slab edge, *Nature*, *465*, 338–341.

Jadamec, M. A., and M. I. Billen (2012), The role of rheology and slab shape on rapid mantle flow: Three dimensional numerical models of the Alaska slab edge, *J. Geophys. Res.*, *117*, B02304, doi:10.1029/2011JB008563.

Johnson, H. P., and M. J. Prius (2003), Fluxes of fluid and heat from the oceanic crustal reservoir, *Earth Planet. Sci. Lett.*, *216*, 565–574.

Jung, H. (2009), Deformation fabrics of olivine in Val Malenco peridotites found in Italy and implications for seismic anisotropy in the upper mantle, *Lithos*, *109*, 341–349.

Jung, H. (2011), Seismic anisotropy produced by serpentine in mantle wedge, *Earth Planet. Sci. Lett.*, *307*, 535–543.

Jung, H., and S.-i. Karato (2001), Water-induced fabric transitions in olivine, *Science*, *293*, 1460–1463.

Jung, H., I. Katayama, Z. Jiang, T. Hiraga, and S. Karato (2006), Effect of water and stress on the lattice preferred orientation (LPO) of olivine, *Tectonophysics*, *421*, 1–22.

Jung, H., W. Mo, and H. W. Green (2009), Upper mantle seismic anisotropy resulting from pressure-induced slip transition in olivine, *Nature Geosci.*, *2*, 73–77.

Kaminski, É., and N. M. Ribe (2002), Timescales for the evolution of seismic anisotropy in mantle flow, *Geochem. Geophys. Geosyst.*, *3*, 1051, doi:10.1029/2001GC000222.

Kaminski, É., N. M. Ribe, and J. T. Browaeys (2004), D-Rex, a program for calculation of seismic anisotropy due to crystal lattice preferred orientation in the convective upper mantle, *Geophys. J. Int.*, *158*, 744–752.

Karato, S. (1998), Some remarks on the origin of seismic anisotropy in the D″ layer, *Earth Planets Space 50*, 1019–1028.

Karato, S.-i. (2012), On the origin of the asthenosphere, *Earth Planet. Sci. Lett.*, *321–322*, 95–103.

Karato, S.-i., H. Jung, I. Katayama, and P. Skemer (2008), Geodynamic significance of seismic anisotropy of the upper mantle: New insights from laboratory studies, *Annu. Rev. Earth Planet. Sci.*, *36*, 59–95.

Katayama, I., K.-i. Hirauchi, K. Michibayashi, and J.-i. Ando (2009), Trench-parallel anisotropy produced by serpentine deformation in the hydrated mantle wedge, *Nature*, *461*, 1114–1117.

Katayama, I., H. Jung, and S. Karato (2004), New type of olivine fabric at modest water content and low stress, *Geology*, *32*, 1045–1048.

Katayama, I., and S.-i. Karato (2006), Effect of temperature on the B- to C-type olivine fabric transition and implication for flow pattern in subduction zones, *Phys. Earth Planet. Inter.*, *157*, 33–45.

Kaviani, A., G. Rümpker, M. Weber, and G. Asch (2011), Short-scale variations of shear-wave splitting across the Dead Sea basin: Evidence for the effects of sedimentary fill, *Geophys. Res. Lett.*, *38*, L04308, doi:10.1029/2010GL046464.

Kawakatsu, H., P. Kumar, Y. Takei, M. Shinohara, T. Kanazawa, E. Araki, and K. Suyehiro (2009), Seismic evidence for sharp lithosphere-asthenosphere boundaries of oceanic plates, *Science*, *324*, 499–502.

Kawazoe, T., T. Ohuchi, Y. Nishihara, N. Nishiyama, K. Fujino, and T. Irifune (2013), Seismic anisotropy in the mantle transition zone induced by shear deformation of wadsleyite, *Phys. Earth Planet. Inter.*, *216*, 91–98.

Kelemen, P. B., J. L. Rilling, E. M. Parmentier, L. Mehl, and B. R. Hacker (2003), Thermal structure due to solid-state flow in the mantle wedge beneath arcs, in Inside the Subduction Factory, pp. 293–311, edited by J. Eiler, American Geophysical Union, Washington, DC.

Kellogg, L. H., B. H. Hager, and R. D. van der Hilst (1999), Compositional stratification in the deep mantle, *Science*, *283*, 1881–1884.

Kendall, J.-M., and P. G. Silver (1996), Constraints from seismic anisotropy on the nature of the lowermost mantle, *Nature*, *381*, 409–412.

Kendall, J.-M., and P. G. Silver (1998), Investigating causes of D″ anisotropy, In: The Core-Mantle Boundary Region, edited by M. Gurnis et al., pp. 97–118, AGU, Washington, DC.

Kern, H. (1993), *P*- and *S*-wave anisotropy and shear-wave splitting at pressure and temperature in possible mantle rocks and their relation to the rock fabric, *Phys. Earth Planet. Inter.*, *78*, 245–256.

Key, K., S. Constable, T. Matsuno, R. L. Evans, and D. Myer (2012), Electromagnetic detection of plate hydration due to bending faults at the Middle America Trench, *Earth Planet. Sci. Lett.*, *351–352*, 45–53.

Kincaid, C., and R. W. Griffiths (2003), Laboratory models of the thermal evolution of the mantle during rollback subduction, *Nature*, *425*, 58–62.

Kincaid, C., and R. W. Griffiths (2004), Variability in flow and temperatures within mantle subduction zones, *Geochem. Geophys. Geosyst.*, *5*, Q06002, doi:10.1029/2003GC000666.

Király, E., I. Bianchi, and G. Bokelmann (2012), Seismic anisotropy in the south western Pacific region from shear wave splitting, *Geophys. Res. Lett.*, *39*, L05302, doi:10.1029/2011GL050407.

Kneller, E. A., M. D. Long, and P. E. van Keken (2008), Olivine fabric transitions and shear-wave anisotropy in the Ryukyu subduction system, *Earth Planet. Sci. Lett.*, *268*, 268–282.

Kneller, E. A., and P. E. van Keken (2007), Trench-parallel flow and seismic anisotropy in the Marianas and Andean subduction systems, *Nature*, *450*, 1222–1225.

Kneller, E. A., and P. E. van Keken (2008), The effects of three-dimensional slab geometry on deformation in the mantle wedge: Implications for shear wave anisotropy, *Geochem. Geophys. Geosyst.*, 9, doi:10.1029/2007GC001677.

Kneller, E. A., P. E. van Keken, S. Karato, and J. Park (2005), B-type olivine fabric in the mantle wedge: Insights from high-resolution non-Newtonian subduction zone models. *Earth Planet, Sci. Lett.*, 237, 781–797.

Kneller, E. A., P. E. van Keken, I. Katayama, and S. Karato (2007), Stress, strain, and B-type olivine fabric in the fore-arc mantle: Sensitivity tests using high-resolution steady-state subduction zone models, *J. Geophys. Res.*, 112, B04406, doi:10.1029/2006JB004544.

Koulakov, I., A. Jakovlev, and B. G. Luehr (2009), Anisotropic structure beneath central Java from local earthquake tomography, *Geochem. Geophys. Geosyst.*, 10, Q02011, doi:10.1029/2008GC002109.

Kumar, P., and H. Kawakatsu (2011), Imaging the seismic lithosphere-asthenosphere boundary of the oceanic plate, *Geochem. Geophys. Geosyst.*, 12, Q01006, doi:10.1029/2010GC003358.

Lay, T., and E. J. Garnero (2007), Reconciling the post-perovskite phase with seismological observations of lowermost mantle structure, in Post-Perovskite, the Last Mantle Phase Transition, edited by K. Hirose et al., pp. 129–154, AGU, Washington, DC.

Lay, T., Q. Williams, and E. J. Garnero (1998), The core-mantle boundary layer and deep Earth dynamics, *Nature*, 392, 461–468, 1998.

Lassak, T. M., M. J. Fouch, C. E. Hall, and E. Kaminski (2006), Seismic characterization of mantle flow in subduction systems: Can we resolve a hydrated mantle wedge?, *Earth Planet. Sci. Lett.*, 243, 632–649.

Léon Soto, G., J. F. Ni, S. P. Grand, E. Sandvol, R. W. Valenzuela, M. Guzmán Speziale, J. M. Gómez González, and T. Domínguez Reyes (2009), Mantle flow in the Rivera-Cocos subduction zone. *Geophys. J. Int.*, 179, 1004–1012.

Lev, E., and B. H. Hager (2008), Prediction of anisotropy from flow models: A comparison of three methods, *Geochem. Geophys. Geosyst.*, 9, Q07014, doi:10.1029/2008GC002032.

Levin, V., D. Droznin, J. Park, and E. Gordeev (2004), Detailed mapping of seismic anisotropy with local shear waves in south-eastern Kamchatka, *Geophys. J. Int.*, 158, 1009–1023.

Levin, V., D. Okaya, and J. Park (2007), Shear wave birefringence in wedge-shaped anisotropic regions, *Geophys. J. Int.*, 168, 275–286.

Levin, V., and J. Park (1998), P-SH conversions in layered media with hexagonally symmetric anisotropy: a cookbook, *Pure Appl. Geophys.*, 151, 669–697.

Li, C., R. D. van der Hilst, E. R. Engdahl, and S. Burdick (2008), A new global model for P wave speed variations in Earth's mantle, *Geochem. Geophys. Geosyst.*, 9, Q05018, doi:10.1029/2007GC001806.

Liu, K. H. (2009), NA-SWS-1.1: A uniform database of teleseismic shear-wave splitting measurements for North America, *Geochem. Geophys. Geosyst.*, 10, Q05011, doi:10.1029/2009GC002440.

Long, M. D., 2009. Complex anisotropy in D″ beneath the eastern Pacific from SKS-SKKS splitting discrepancies, *Earth Planet. Sci. Lett.*, 283, 181–189.

Long, M. D., and T. W. Becker (2010), Mantle dynamics and seismic anisotropy, *Earth Planet. Sci. Lett.*, 297, 341–354.

Long, M. D., M. V. de Hoop, and R. D. van der Hilst (2008), Wave-equation shear wave splitting tomography, *Geophys. J. Int.*, 172, 311–330.

Long, M. D., B. H. Hager, M. V. de Hoop, and R. D. van der Hilst (2007), Two-dimensional modeling of subduction zone anisotropy and application to southwestern Japan, *Geophys. J. Int.*, 170, 839–856.

Long, M. D., and P. G. Silver (2008), The subduction zone flow field from seismic anisotropy: A global view, *Science*, 319, 315–318.

Long, M. D., and P. G. Silver (2009), Mantle flow in subduction systems: The sub-slab flow field and implications for mantle dynamics, *J. Geophys. Res.*, 114, B10312, doi:10.1029/2008JB006200.

Long, M. D., and R. D. van der Hilst (2005), Upper mantle anisotropy beneath Japan from shear wave splitting, *Phys. Earth Planet. Inter.*, 151, 206–222.

Long, M. D., and R. D. van der Hilst, (2006), Shear wave splitting from local events beneath the Ryukyu arc: Trench-parallel anisotropy in the mantle wedge, *Phys. Earth Planet. Inter.*, 155, 300–312.

Long, M. D., and E. A. Wirth (2013), Mantle flow in subduction systems: The wedge flow field and implications for wedge processes, *J. Geophys. Res.*, 118, 1–24, doi:10.1002/jgrb.50063..

Long, M. D., X. Xiao, Z. Jiang, B. Evans, and S.-i. Karato (2006), Lattice preferred orientation in deformed polycrystalline (Mg,Fe) O and implications for seismic anisotropy in D″, *Phys. Earth Planet. Inter.*, 156, 75–88.

Lynner, C., and M. D. Long (2012), Evaluating contributions to SK(K)S splitting from lower mantle anisotropy: A case study from station DBIC, Côte D'Ivoire, *Bull. Seism. Soc. Am.*, 102, 1030–1040.

Lynner, C., and M. D. Long (2013), Sub-slab seismic anisotropy and mantle flow beneath the Caribbean and Scotia subduction zones: Effects of slab morphology and kinematics, *Earth Planet. Sci. Lett.*, 361, 367–378.

Mainprice, D. (2007), Seismic anisotropy of the deep Earth from a mineral and rock physics perspective, in *Treatise on Geophysics*, edited by Schubert, G., v. 2, pp. 437–492, Elsevier, Amsterdam, The Netherlands.

Mainprice, D., and B. Ildefonse (2009), Seismic anisotropy of subduction zone minerals—Contribution of hydrous phases, in *Subduction Zone Geodynamics*, pp. 63–84, edited by S. Lallemand and F. Funiciello, Springer-Verlag, Berlin Heidelberg.

Mainprice, D., A. Tommasi, H. Couvy, P. Cordier, and D. J. Frost (2005), Pressure sensitivity of olivine slip systems and seismic anisotropy of Earth's upper mantle, *Nature*, 433, 731–733.

Mao, W. L., Y. Meng, and H.-K. Mao (2010), Elastic anisotropy of ferromagnesian post-perovskite in Earth's D″ layer, *Phys. Earth Planet. Inter.*, 180, 203–208.

Manea, V., and M. Gurnis (2007), Subduction zone evolution and low viscosity wedges and channels, *Earth Planet. Sci. Lett.*, 264, 22–45.

Marquardt, H., S. Speziale, H. J. Reichmann, D. J. Frost, F. R. Schilling, and E. J. Garnero (2009), Elastic shear anisotropy of ferropericlase in Earth's lower mantle, *Science*, 324, 224–226.

Marson-Pidgeon K., and M. K. Savage (1997), Frequency-dependent anisotropy in Wellington, New Zealand, *Geophys. Res. Lett.*, 24, 3297–3300.

McCormack, K., E. A. Wirth, and M. D. Long (2013), B-type olivine fabric and mantle wedge serpentinization beneath the Ryukyu arc, *Geophys. Res. Lett.*, in press, doi:10.1002/grl.50369.

McKenzie, D. (1979), Finite deformation during fluid flow, *Geophys. J. Roy. Astron. Soc.*, 58, 689–715.

McKenzie, D. P. (1969), Speculations on the consequences and causes of plate motions, *Geophys. J. Roy. Astron. Soc.*, 18, 1–32.

McNamara, A. K., P. E. van Keken, and S. Karato (2002), Development of anisotropic structure by solid-state convection in the Earth's lower mantle, *Nature*, 416, 310–314.

McNamara, A. K., P. E. van Keken, and S. Karato (2003), Development of finite strain in the convecting lower mantle and its implications for seismic anisotropy, *J. Geophys. Res.*, 108 (B5), 2230, doi:10.1029/2002JB001970.

McNamara, A. K., and S. Zhong (2005), Thermochemical structures beneath Africa and the Pacific Ocean, *Nature*, 437, 1136–1139.

Meade, C., P. G. Silver, and S. Kaneshima (1995), Laboratory and seismological observations of lower mantle isotropy, *Geophys. Res. Lett.*, 22, 1293–1296.

Mehl, L., B. R. Hacker, G. Hirth, and P. B. Kelemen (2003), Arc-parallel flow within the mantle wedge: Evidence from the accreted Talkeetna arc, south central Alaska, *J. Geophys. Res.*, 108, 2375, doi:10.1029/2002JB002233.

Merkel, S., A. K. McNamara, A. Kubo, S. Speziale, L. Miyagi, Y. Meng, T. S. Duffy, and H.-R. Wenk (2007), Deformation of (Mg,Fe)SiO3 post-perovskite and D″ anisotropy, *Science*, *316*, 1729–1732.

Michibayashi, K., N. Abe, A. Okamoto, T. Satsukawa, and K. Michikura (2006), Seismic anisotropy in the uppermost mantle, back-arc region of the northeast Japan arc: Petrophysical analyses of Ichinomegata peridotite xenoliths, *Geophys. Res. Lett.*, *33*, L10312, doi:10.1029/2006GL025812.

Miyagi L., W. Kanitpanyacharoen, P. Kaercher, K. K. M. Lee, and H.-R. Wenk (2010), Slip systems in MgSiO3 post-perovskite: Implications for D″ anisotropy, *Science*, *329*, 1639–1641.

Mizukami, T., S. R. Wallis, and J. Yamamoto (2004), Natural examples of olivine lattice preferred orientation patterns with a flow-normal a-axis maximum, *Nature*, *427*, 432–436.

Montagner, J.-P., G. Burgos, M. Drilleau, E. Beucler, Y. Capdeville, A. Mocquet, and J. Trampert (2012), Seismic anisotropy in the transition zone of the mantle. *Geophysical Research Abstracts*, *14*, EGU2012–9951.

Montagner, J.-P., and B. L. N. Kennett (1996), How to reconcile body-wave and normal-mode reference Earth models, *Geophys. J. Int.*, *125*, 229–248.

Monteiller, V., and S. Chevrot (2010), How to make robust splitting measurements for single-station analysis and three-dimensional imaging of seismic anisotropy, *Geophys. J. Int.*, *182*, 311–328.

Monteiller, V., and S. Chevrot (2011), High resolution imaging of the deep anisotropic structure of the San Andreas Fault system beneath southern California, *Geophys. J. Int.*, *186*, 418–446.

Mookherjee, M., 2011. Mid-mantle anisotropy: Elasticity of aluminous phases in subducted MORB. *Geophys. Res. Lett.*, *38*, L14302, doi:10.1029/2011GL047923.

Mookherjee, M., and G. C. Capitani (2011), Trench parallel anisotropy and large delay times: Elasticity and anisotropy of antigorite at high pressures, *Geophys. Res. Lett.*, *38*, L09315, doi:10.1029/2011GL047160.

Morishige, M., and S. Honda (2011), Three-dimensional structure of P-wave anisotropy in the presence of small-scale convection in the mantle wedge, *Geochem. Geophys. Geosyst.*, *12*, Q12010, doi:10.1029/2011GC003866.

Morley, A. M., G. W. Stuart, J.-M. Kendall, and M. Reyners (2006), Mantle wedge anisotropy in the Hikurangi subduction zone, central North Island, New Zealand, *Geophys. Res. Lett.*, *33*, L05301, doi:10.1029/2005GL024569.

Morra, G., K. Regenauer-Lieb, and D. Giardini (2006), Curvature of oceanic arcs, *Geology*, *34*, 877–880.

Müller, C. (2001), Upper mantle seismic anisotropy beneath Antarctica and the Scotia Sea region, *Geophys. J. Int.*, *147*, 105–122.

Müller, C., B. Bayer, A. Eckstaller, and H. Miller (2008), Mantle flow in the South Sandwich subduction environment from source-side shear wave splitting, *Geophys. Res. Lett.*, *35*, doi:10.1029/2007GL032411.

Nakajima, J., and A. Hasegawa (2004), Shear-wave polarization anisotropy and subduction-induced flow in the mantle wedge of northern Japan, *Earth Planet. Sci. Lett.*, *225*, 365–377.

Nakajima, J., J. Shimizu, S. Hori, and A. Hasegawa (2006), Shear-wave splitting beneath the southwestern Kurile arc and northeastern Japan arc: A new insight into mantle return flow, *Geophys. Res. Lett.*, *33*, doi:10.1029/2005GL025053.

Nikulin, A., V. Levin, and J. Park (2009), Receiver function study of the Cascadia megathrust: Evidence for localized serpentinization, *Geochem. Geophys. Geosyst.*, *10*, Q07004, doi:10.1029/2009GC002376.

Nippress, S. E. J., N. J. Kusznir, and J.-M. Kendall (2004), Modeling of lower mantle seismic anisotropy beneath subduction zones, *Geophys. Res. Lett.*, *31*, L19612, doi:10.1029/2004GL020701.

Nishamura, C. E., and D. W. Forsyth (1989), The anisotropic structure of the upper mantle in the Pacific, *Geophys. J.*, *96*, 203–229.

Nishii, A., S. R. Wallis, T. Mizukami, and K. Michibayashi (2011), Subduction related antigorite CPO patterns from forearc mantle in the Sanbagawa belt, southwest Japan, *J. Struct. Geol.*, *33*, 1436–1445.

Niu, F., and A. M. Perez, (2004), Seismic anisotropy in the lower mantle: A comparison of waveform splitting of SKS and SKKS, *Geophys. Res. Lett.*, *31*, L24612, doi:10.1029/2004GL021196.

Nowacki, A., J. Wookey, and J.-M. Kendall (2010), Deformation of the lowermost mantle from seismic anisotropy, *Nature*, *467*, 1091–1094.

Nowacki, A., J. Wookey, and J.-M. Kendall (2011), New advances in using seismic anisotropy, mineral physics and geodynamics to understand deformation in the lowermost mantle, *J. Geodyn.*, *52*, 205–228.

Oganov, A., R. Martonak, A. Laio, P. Paiteri, and M. Parrinello (2005), Anisotropy of Earth's D″ layer and stacking faults in the MgSiO3 post-perovskite phase, *Nature*, *438*, 1142–1144.

Olive, J. A., S. Rondenay, and F. Pearce (2011), Evidence for trench-normal flow beneath the Western Hellenic slab from shear-wave splitting analysis, Abstract DI41A-2067 presented at the AGU Fall Meeting.

Paczkowski, K., (2012), Dynamic analysis of modifications to simple plate tectonics theory. Ph.D. Thesis, Yale University, 185 pp.

Panning, M., and B. Romanowicz (2004), Inferences on flow at the base of Earth's mantle based on seismic anisotropy, *Science*, *303*, 351–353.

Park, J., H. Yuan, and V. Levin (2004), Subduction zone anisotropy beneath Corvallis, Oregon: A serpentinite skid mark of trench-parallel terrane migration?, *J. Geophys. Res.*, *109*, B10306, doi:10.1029/2003JB002718.

Peyton, V., V. Levin, J. Park, M. Brandon, J. Lees, E. Gordeev, and A. Ozerov (2001), Mantle flow at a slab edge: Seismic anisotropy in the Kamchatka region, *Geophys. Res. Lett.*, *28*, 379–382.

Piñero-Felicangeli, L., and J.-M. Kendall (2008), Sub-slab mantle flow parallel to the Caribbean plate boundaries: Inferences from SKS splitting, *Tectonophysics*, *462*, 22–34.

Piromallo, C., T. W. Becker, F. Funiciello, and C. Faccenna (2006), Three-dimensional instantaneous mantle flow induced by subduction, *Geophys. Res. Lett.*, *33*, L08304, doi:10.1029/2005GL025390.

Polet, J., P. G. Silver, S. Beck, T. Wallace, G. Zandt, S. Ruppert, R. Kind, and A. Rudloff (2000), Shear wave anisotropy beneath the Andes from the BANJO, SEDA, and PISCO experiments, *J. Geophys. Res.*, *105*, 6287–6304.

Pozgay, S. H., D. A. Wiens, J. A., Conder, H. Shiobara, and H. Sugioka (2007), Complex mantle flow in the Mariana subduction system: Evidence from shear wave splitting, *Geophys. J. Int.*, *170*, 371–386.

Pysklywec, R. N., and M. Ishii (2005), Time dependent subduction dynamics driven by the instability of stagnant slabs in the transition zone, *Phys. Earth Planet. Inter. 149*, 115–132.

Pysklywec, R. N., J. X. Mitrovica, and M. Ishii (2003), Mantle avalanche as a driving force for tectonic reorganization in the southwest Pacific, *Earth Planet. Sci. Lett.*, *209*, 29–38.

Ranero, C. R., J. Phipps Morgan, K. McIntish, and C. Reichert (2003), Bending-related faulting and mantle serpentinization at the Middle America trench, *Nature*, *425*, 367–373.

Raterron, P., J. Chen, L. Li, D. J. Weidner, and P. Cordier (2007), Pressure-induced slip system transition in forsterite: Single-crystal rheological properties and mantle pressure and temperature, *Am. Mineral.*, *92*, 1436–1445.

Restivo, A., and G. Helffrich (2006), Core-mantle boundary structure investigated using *SKS* and *SKKS* polarization anomalies, *Geophys. J. Int.*, *165*, 288–302.

Reynard, B., N. Hilairet, E. Balan, and M. Lazzeri (2007), Elasticity of serpentines and extensive serpentinization in subduction zones, *Geophys. Res. Lett.*, *34*, L13307, doi:10.1029/2007GL030176.

Ritsema, J., H. J. van Heijst, and J. H. Woodhouse, (1999), Complex shear velocity structure imaged beneath Africa and Iceland, *Science*, *286*, 1925–1928.

Rokosky, J. M., T. Lay, and E. J. Garnero (2006), Small-scale lateral variations in azimuthally anisotropic D″ structure beneath the Cocos Plate, *Earth Planet. Sci. Lett.*, *248*, 411–425.

Rüpke, L. H., J. Phipps Morgan, M. Hort, and J. A. D. Connolly (2004), Serpentine and the subduction zone water cycle, *Earth Planet. Sci. Lett.*, *223*, 17–34.

Russell, S. A., T. Lay, and E. J. Garnero (1998), Seismic evidence for small-scale dynamics in the lowermost mantle at the root of the Hawaiian hotspot, *Nature*, *396*, 255–258.

Russo, R. M. (2009), Subducted oceanic asthenosphere and upper mantle flow beneath the Juan de Fuca slab, *Lithosphere*, *1*, 195–205.

Russo, R. M., A. Gallego, D. Comte, V. I. Mocanu, R. E. Murdie, and J. C. VanDecar (2010), Source-side shear wave splitting and upper mantle flow in the Chile Ridge subduction zone, *Geology*, *38*, 707–710.

Russo, R. M., and P. G. Silver (1994), Trench-parallel flow beneath the Nazca plate from seismic anisotropy, *Science*, *263*, 1105–1111.

Rychert, C. A., and P. M. Shearer (2009), A global view of the lithosphere-asthenosphere boundary, *Science*, *324*, 495–498.

Rychert, C. A., and P. M. Shearer (2011), Imaging the lithosphere-asthenosphere boundary beneath the Pacific using SS waveform modeling, *J. Geophys. Res.*, *116*, B07307, doi:10.1029/2010JB008070.

Saul, J., and L. Vinnik (2003), Mantle deformation or processing artefact?, *Nature*, *422*, 136.

Savage, M. K. (1998), Lower crustal anisotropy or dipping boundaries? Effects on receiver functions and a case study in New Zealand, *J. Geophys. Res.*, *103*, 15,069–15,087.

Savage, M. K. (1999), Seismic anisotropy and mantle deformation: What have we learned from shear wave splitting?, *Rev. Geophys.*, *37*, 65–106.

Savage, M. K., J. Park, and H. Todd (2007), Velocity and anisotropy structure at the Hikurangi subduction margin, New Zealand, from receiver functions, *Geophys. J. Int.*, *168*, 1034–1050.

Schellart, W. P. (2004), Kinematics of subduction and subduction-induced flow in the upper mantle, *J. Geophys. Res.*, *109*, B07401, doi:10.1029/2004JB002970.

Schellart, W. P., J. Freeman, D. R. Stegman, L. Moresi, and D. May (2007), Evolution and diversity of subduction zones controlled by slab width, *Nature*, *446*, 308–311.

Schmerr, N. (2012), The Gutenberg discontinuity: Melt at the lithosphere-asthenosphere boundary, *Science*, *335*, 1480–1483.

Schmidt, M. W., and S. Poli (1998), Experimentally based water budgets for dehydrating slabs and consequences for arc magma generation, *Earth Planet. Sci. Lett.*, *163*, 361–379.

Shearer, P. M., and J. A. Orcutt (1985), Anisotropy in the oceanic lithosphere—Theory and observations from the Ngendei seismic refraction experiment in the south-west Pacific, *Geophys. J. Roy. Astron. Soc.*, *80*, 493–526.

Silver, P. G. (1996), Seismic anisotropy beneath the continents: Probing the depths of geology, *Annu. Rev. Earth Planet. Sci.*, *24*, 385–432.

Silver, P. G., and W. W. Chan (1991), Shear wave splitting and subcontinental mantle deformation, *J. Geophys. Res.*, *96*, 16,429–16,454.

Silver, P. G., and M. K. Savage (1994), The interpretation of shear-wave splitting parameters in the presence of two anisotropic layers, *Geophys. J. Int.*, *119*, 949–963.

Skemer, P. A., I. Katayama, and S. Karato (2006), Deformation fabrics of a peridotites from Cima di Gagnone, central Alps, Switzerland: Evidence of deformation under water-rich conditions at low temperatures, *Contrib. Mineral. Petrol.*, *152*, 43–51.

Skemer, P., J. M. Warren, and G. Hirth (2012), The influence of deformation history on the interpretation of seismic anisotropy, *Geochem. Geophys. Geosyst.*, *13*, Q03006, doi:10.1029/2011GC003988.

Skinner, S. M., and R. W. Clayton (2011), An evaluation of proposed mechanisms of slab flattening in central Mexico, *Pure Appl. Geophys.*, *168*, 1461–1474.

Smith, G. P., D. A. Wiens, K. M. Fischer, L. M. Dorman, S. C. Webb, and J. A. Hildebrand, (2001), A complex pattern of mantle flow in the Lau Backarc, *Science*, *292*, 713–716.

Song, T.-R. A., and H. Kawakatsu (2012), Subduction of oceanic asthenosphere: Evidence from sub-slab seismic anisotropy, *Geophys. Res. Lett.*, *39*, L17301, doi:10.1029/2012GL052639.

Song, T.-R. A., and Y. Kim (2012a), Localized seismic anisotropy associated with long-term slow-slip events beneath southern Mexico, *Geophys. Res. Lett.*, *39*, L09308, doi:10.1029/2012GL051324.

Song, T.-R. A., and Y. Kim (2012b), Anisotropic uppermost mantle in young subducted slab underplating Central Mexico, *Nat. Geosci.*, *5*, 55–59.

Song, T.-R. A., and H. Kawakatsu (2013), Subduction of oceanic asthenosphere: A critical appraisal in central Alaska, *Earth Planet. Sci. Lett.*, *367*, 82–94.

Stackhouse, S., J. P. Brodholt, J. Wookey, J.-M. Kendall, and G. D. Price (2005), The effect of temperature on the seismic anisotropy of the perovskite and post-perovskite polymorphs of $MgSiO_3$, *Earth Planet. Sci. Lett.*, *230*, 1–10.

Stadler, G., M. Gurnis, C. Burstedde, L. C. Wilcox, L. Alisic, and O. Ghattas (2010), The dynamics of plate tectonics and mantle flow: From local to global scales, *Science*, *329*, 1033–1038.

Stegman, D. R., J. Freeman, W. P. Schellart, L. Moresi, and D. May (2006), Influence of trench width on subduction hinge retreat rates in 3-D models of slab rollback, *Geochem. Geophys. Geosyst.*, *7*, Q03012, doi:10.1029/2005GC001056.

Steinberger, B. (2000), Slabs in the lower mantle—Results of dynamic modeling compared with tomographic images and the geoid, *Phys. Earth Planet. Inter.*, *118*, 241–257.

Stixrude, L. (1998), Elastic constants and anisotropy of MgSiO3 perovskite, periclase, and SiO2 at high pressure, in The Core-Mantle Boundary Region, edited by M. Gurnis et al., AGU, Washington, DC, pp. 83–96.

Tackley, P. J. (1996), On the ability of phase transitions and viscosity layering to induce long wavelength heteroegeneity in the mantle, *Geophys. Res. Lett.*, *23*, 1985–1988.

Tackley, P. J., D. J. Stevenson, G. A. Glatzmeier, and G. Schubert (1993), Effects of an endothermic phase transition at 670 k depth in a spherical model of convection in the Earth's mantle, *Nature*, *361*, 699–704.

Tan, E., M. Gurnis, and L. Han (2002), Slabs in the lower mantle and their modulation of plume formation, *Geochem. Geophys. Geosyst.*, *3*, 1067, doi:10.1029/2001GC000238.

Tasaka, M., K. Michibayashi, and D. Mainprice (2008), B-type olivine fabrics developed in the fore-arc side of the mantle wedge along a subducting slab, *Earth Planet. Sci. Lett.*, *272*, 747–757.

Thorne, M. S., and E. J. Garnero (2004), Inferences on ultra-low-velocity zone structure from a global analysis of SPdKS waves, *J. Geophys. Res.*, *109*, B08301, doi:10.1029/2004JB003010.

Tian, Y., and D. Zhao (2012), Seismic anisotropy and heterogeneity in the Alaska subduction zone, *Geophys. J. Int.*, *190*, 629–649.

Tommasi, A., D. Maniprice, P. Cordier, C. Thoraval, and H. Couvy (2004), Strain-induced seismic anisotropy of wadsleyite polycrystals: Constraints on flow patterns in the mantle transition zone, *J. Geophys. Res.*, *109*, B12405, doi:10.1029/2004JB003158.

Tommasi, A., A. Vauchez, M. Godard, and F. Belley (2006), Deformation and melt transport in a highly depleted perdotite massif from the Canadian Cordillera: Implications to seismic anisotropy above subduction zones, *Earth Planet. Sci. Lett.*, *252*, 245–259.

Tono, Y., Y. Fukao, T. Kunugi, and S. Tsuboi (2009), Seismic anisotropy of the Pacific slab and mantle wedge beneath the Japanese islands, *J. Geophys. Res.*, *114*, B07307, doi:10.1029/2009JB006290.

Trampert, J., F. Deschamps, J. Resovsky, and D. Yuen (2004), Probabilistic tomography maps chemical heterogeneities throughout the lower mantle, *Science*, *306*, 853–856.

Trampert, J., and H. J. van Heijst (2002), Global azimuthal anisotropy in the transition zone, *Science*, *296*, 1297–1300.

Turner, S., and C. Hawkesworth (1998), Using geochemistry to map mantle flow beneath the Lau Basin, *Geology*, *26*, 1019–1022.

Ulmer, P., and V. Trommsdorff (1995), Serpentine stability to mantle depths and subduction-related magmatism, *Science*, *268*, 858–861.

van de Moortèle, B., L. Bezacier, G. Trullenque, and B. Reynard (2010), Electron backscattering diffraction (EBSD) measurements of antigorite lattice-preferred orientation (LPO), *J. Microscopy*, *239*, 245–248.

van der Hilst, R. D., M. V. de Hoop, P. Wang, S.-H. Shim, P. Ma, and L. Tenorio (2007), Seismostratigraphy and thermal structure of Earth's core-mantle boundary region, *Science*, *315*, 1813–1817.

van der Hilst, R. D., S. Widiyantoro, and E. R. Engdahl (1997), Evidence for deep mantle circulation from global tomography, *Nature*, *386*, 578–584.

van der Meer, D. G., W. Spakman, D. J. J. van Hinsbergen, M. L. Amaru, and T. H. Torsvik (2010), Towards absolute plate motions constrained by lower-mantle slab remnants, *Nature Geosci.*, *3*, 36–40.

Vauchez, A., A. Tommasi, G. Barruol, and J. Maumus (2000), Upper mantle deformation and seismic anisotropy in continental rifts, *Phys. Chem. Earth A*, *25*, 111–117.

Vecsey, L., J. Plomerová, and V. Babuska (2008), Shear-wave splitting measurements—Problems and solutions, *Tectonophysics*, *462*, 178–196.

Vinnik, L., R. Kind, G. L. Kosarev, and L. Makeyeva (1989), Azimuthal anisotropy in the lithosphere from observations of long-period *S*-waves, *Geophys. J. Int.*, *99*, 549–559.

Visser, K., J. Trampert, S. Lebedev, and B. L. N. Kennett (2008), Probability of radial anisotropy in the deep mantle, *Earth Planet. Sci. Lett.*, *270*, 241–250.

Wada, I., M. D. Behn, and A. Shaw (2012), Effects of heterogeneous hydration in the incoming plate, slab rehydration, and mantle wedge hydration on slab-derived H_2O flux in subduction zones, *Earth Planet. Sci. Lett.*, *353–354*, 60–71.

Walker, A. M., A. M. Forte, J. Wookey, A. Nowacki, and J.-M. Kendall (2011), Elastic anisotropy of D″ predicted from global models of mantle flow, *Geochem. Geophys. Geosyst.*, *12*, Q10006, doi:10.1029/2011GC003732.

Wang, J., and D. Zhao (2008), P wave anisotropic tomography beneath Northeast Japan, *Phys. Earth Planet. Inter.*, *170*, 115–133.

Wang, J., and D. Zhao (2012), P wave anisotropic tomography of the Nankai subduction zone in Southwest Japan, *Geochem. Geophys. Geosyst.*, *13*, Q05017, doi:10.1029/2012GC004081.

Wenk, H.-R., S. Speziale, A. K. McNamara, and E. J. Garnero (2006), Modeling lower mantle anisotropy development in a subducting slab, *Earth Planet Sci. Lett.*, *245*, 302–314.

Wenk, H.-R., S. Cottaar, C. T. Tome, B. Romanowicz, and A. K. McNamara (2011), Deformation in the lowermost mantle: From polycrystal plasticity to seismic anisotropy, *Earth Planet. Sci. Lett.*, *306*, 33–45.

Wirth, E. A., and J. Korenaga (2012), Small-scale convection in the subduction zone mantle wedge, *Earth Planet. Sci. Lett.*, *357–358*, 111–118.

Wirth, E., and M. D. Long (2010), Frequency dependent shear wave splitting beneath the Japan and Izu-Bonin subduction zones. *Phys. Earth Planet. Inter.*, *181*, 141–154.

Wirth, E. A., and M. D. Long (2012), Multiple layers of seismic anisotropy and a low-velocity layer in the mantle wedge beneath Japan: Evidence from teleseismic receiver functions, *Geochem. Geophys. Geosyst.*, in press, doi:10.1029/2012GC004180.

Wookey, J., J.-M. Kendall, and G. Barruol (2002), Mid-mantle deformation inferred from seismic anisotropy, *Nature*, *415*, 777–780.

Wookey, J., and J.-M. Kendall (2004), Evidence of midmantle anisotropy from shear wave splitting and the influence of shear-coupled *P* waves, *J. Geophys. Res.*, *109*, B07309, doi:10.1029/2003JB002871.

Wookey, J., and J.-M. Kendall (2007), Seismic anisotropy of post-perovskite and the lowermost mantle, In: Post-Perovskite, the Last Mantle Phase Transition, edited by K. Hirose et al., pp. 171–189, AGU, Washington, DC.

Wookey, J., and J.-M. Kendall (2008), Constraints on lowermost mantle mineralogy and fabric beneath Siberia from seismic anisotropy, *Earth Planet. Sci. Lett.*, *275*, 32–42.

Wookey, J., J.-M. Kendall, and G. Rumpker (2005), Lowermost mantle anisotropy beneath the north Pacific from differential S-ScS splitting, *Geophys. J. Int.*, *161*, 829–838.

Wüstefeld, A., G. H. R. Bokelmann, G. Barruol, and J.-P. Montagner (2009), Identifying global seismic anisotropy patterns by correlating shear-wave splitting and surface waves data, *Phys. Earth Planet. Inter.*, *176*, 198–212.

Wüstefeld, A., G. H. R. Bokelmann, G. Barruol, and C. Zaroli (2008), SplitLab: A shear wave splitting environment in Matlab, *Comp. Geosci.*, *34*, 515–528.

Yamazaki, D., and S.-i. Karato (2002), Fabric development in (Mg,Fe)O during large strain, shear deformation: Implications for seismic anisotropy in Earth's lower mantle, *Phys. Earth Planet. Inter.*, *131*, 251–267.

Zhang, S., and S.-I. Karato (1995), Lattice preferred orientation of olivine aggregates deformed in simple shear, *Nature*, *375*, 774–777.

Zimmerman, M. E., S. Zhang, D. L. Kohlstedt, and S. Karato (1999), Melt distribution in mantle rocks deformed in simple shear, *Geophys. Res. Lett.*, *26*, 1505–1508.